School of Chemical and Petroleum Engineering
Department of Chemical Engineering

Multi-Scale Modelling of Gibbsite Calcination in a Fluidized Bed Reactor

Amirpiran Amiri

This thesis is presented for the Degree of
Doctor of Philosophy
of
Curtin University

February 2013

Publications

1. Journal Papers

- Amiri A, Bekker A, Ingram G, Maynard N, Livk I; 2013. A 1-D non-isothermal dynamic model for the thermal decomposition of a gibbsite particle. *Chemical Engineering Research and Design,* 91, 485–496.

- Amiri A, Ingram G, Bekker A, Livk I, Maynard N; 2013. A multi-stage, multi-reaction shrinking core model for self-inhibiting gas-solid reactions. *Advanced Powder Technology,* 24, 728–736.

- Amiri A, Ingram G, Bekker A, Livk I, Maynard N; 2012. An unreacted shrinking core model for calcination and similar solid-to-gas reactions. Accepted subject to revision, *Chemical Engineering Communications*.

- Amiri A, Ingram G, Bekker A, Livk I, Maynard N; 2012. A multi-scale model for gibbsite calcination in a fluidized bed reactor (in preparation).

2. Peer-Reviewed Conference Papers

- Amiri A, Ingram G, Bekker A, Livk I, Maynard N; 2012. A multi-stage shrinking core model for thermal decomposition reactions with a self-inhibiting nature. *Chemeca 2012,* Wellington, New Zealand, September 23–26, 2012.

- Amiri A, Ingram G, Maynard N, Livk I, Bekker A; 2010. A multiscale modelling outlook for gibbsite calcination. *Chemeca 2010*, Adelaide, South Australia, September 26–29, 2010.

Awards

- Awarded the **John A Brodie Medal** in 2012 for the paper selected by the Board of Engineers Australia Chemical College as the best chemical engineering paper presented at that year's Chemeca Conference or published in Chemical Engineering in Australia in the last 12 months.
  (*http://www.engineersaustralia.org.au/sites/default/files/shado/cea_-_december.pdf*; *http://www.chemeca2012.com/highlights.asp?Awards)*

- Awarded the **Chemeca 2012 Prize for Best Student Paper**, sponsored by Fell Consulting Pty Ltd.
  (*http://www.chemeca2012.com/highlights.asp?Awards*)

Abstract

The alumina industry provides the feedstock for aluminium metal production and contributes to around A$6 billion of Australian exports annually. One of the most energy-intensive parts of alumina production, with a strong effect on final product quality, is calcination or thermal decomposition, in which gibbsite powder is converted into alumina. Industrially, gibbsite calcination is conducted in bubbling or circulating fluidized beds. Better modelling of fluid bed calciners is needed to improve process design, control and operations. Multi-scale models, which account for phenomena interacting across different length and time scales, are increasingly being used to describe complex, multidisciplinary, nonlinear, non-equilibrium processes, including fluidized bed reactors. In order to attain more insight into the gibbsite calciner, from a multi-scale viewpoint, this investigation has been conducted in five steps as follows.

Firstly, the possibilities for developing a multi-scale model for the fluidized bed calcination of gibbsite are investigated, followed by recommendations on promising directions. The key elements of the multi-scale approach that is considered were: (i) identification of the relevant scales of interest for bubbling and circulating fluidized bed reactors; (ii) characterisation of the dominant phenomena, modelling approaches and available data at each scale; (iii) an integrated communication framework to link the scales of interest, and briefly (iv) experiment design and model validation for multi-scale models. A conceptual model having three scales (particle, volume element / cluster, and vessel) was proposed and the information flows between the scales were outlined. There are several possibilities for the sub-models used at each scale, and these have been noted.

Secondly, as a part of the particle scale modelling efforts, a 1-D mathematical model describing the calcination of a single gibbsite particle to alumina has been developed and validated against literature data. A dynamic, spatially-distributed, mass and energy balance model enables the prediction of the evolution of chemical composition and temperature as a function of radial position inside a particle. In the thermal decomposition of gibbsite, water vapour is formed and the internal water vapour pressure plays a significant role in determining the rate of gibbsite dehydration. A thermal decomposition rate equation was developed by closely matching experimental data reported previously in the literature. Estimated values of the transformation kinetic parameters are reported. The reaction order with respect to water vapour concentration was negative, meaning that the water vapour that is produced impedes further gibbsite calcination, which is in agreement with previous kinetic studies. Using these kinetic parameters, the gibbsite particle model is solved numerically to predict the evolution of the internal water vapour pressure, temperature and gibbsite concentration. The model prediction is shown to be very sensitive to the values of heat transfer coefficient, effective diffusivity, particle size and external pressure, but relatively less sensitive to the mass transfer coefficient and particle thermal conductivity. The predicted profile of the water vapour pressure inside the particle helps explain some phenomena observed in practice, including particle breakage and formation of a boehmite phase.

Thirdly, a new variation on the unreacted shrinking core model has been developed for calcination and similar non-catalytic thermal solid-to-gas decomposition reactions in which there is no gaseous reactant involved and the reaction rate decreases with increasing product gas concentration. The numerical solution of the developed model has been verified against an analytical solution for the isothermal case. The model parameters have been tuned using literature data for the calcination of gibbsite to alumina over a wide range of temperatures. The model results for gibbsite conversion are found to agree well with the published experimental data. Predictions of the non-isothermal unreacted shrinking core model compare well with the more complex, distributed model developed in the previous step.

Fourthly, a multi-stage, multi-reaction, shrinking core model is proposed for the simulation of solid-to-gas reactions with self-inhibiting behaviour and in which the build-up of internal pressure caused by the product gas may alter the reaction pathway in a way that favours one pathway over others. This model emphasises the role of the produced gas, not only in mass transfer, but also in the reaction kinetics. It includes parallel and series reactions, allowing for the formation of an intermediate species. The model has been applied to the conversion of gibbsite to alumina, including the formation of intermediate boehmite. Modelling results for gibbsite conversion, boehmite formation and its subsequent consumption, as well as alumina formation, agree well with literature data; the corresponding kinetic parameters are estimated for all reactions. Significantly, the experimentally-observed plateaux in the particle’s temperature history are predicted by the model. The role of heating rate and particle size on boehmite formation is also evaluated using the model, and is in agreement with observation.

Fifthly, a simplified version of the multi-scale model proposed in the first step has been developed. Particle scale models are valuable for analysing kinetics, understanding behaviour and some experimental design of gas-solid reactions. However, engineers are always interested in practical, equipment-scale models that can predict the performance of operating units in different scenarios. In this part of the research, some fluid bed reactor phenomena are described along with their modelling methodologies, and then a two-scale model combining one of the particle scale models with a simple reactor scale model is described. The simple reactor model consists of a collection of ideal mixed volumes connected in series. In each volume element, the reaction rate from the particle scale is linked into material and energy balances at the reactor scale. The number of volume elements is variable and thus able to simulate reactor behaviour from an ideal CSTR to a near-ideal PFR, and also for flow regimes in between them. In spite of the simplicity, the solid residence time distribution and gas flow rate variation are accounted for at the reactor scale. Even though a general discussion of fluid bed reactors is presented, gibbsite calcination is again considered for the case study, the same as for the other steps in the project. The developed two-scale model predicts the gas and solid temperature profiles, trends in overall gas flow rate and water vapour pressure, and alumina and gibbsite concentration profiles through the reactor. Sensitivity analyses are conducted into the number of volume elements and the solid throughput rate.

Finally, potential research opportunities for multi-scale modelling of fluidized bed reactors are outlined.

Acknowledgements

I would like to thank many individuals. The accomplishment of this work would not be possible without their kind technical and emotional support. In particular, I would like to acknowledge the following people.

To my supervisor, Dr Gordon Ingram, thank you for all you have done over the last four years, starting from my PhD application until its completion, and the support beyond my academic life. Especially, I appreciate your viewpoints and control on the quality of the work, along with opportunities I had under your supervision.

To my co-supervisors, A/Prof Nicoleta Maynard, Dr Iztok Livk, and Dr Andrey Bekker, I appreciate your attention, support and advice for my research commitments. I was fortunate to have you as my supervisory panel. Life and work were given perspective using Nicoleta’s advice, made balanced by Iztok’s guidance, and made more authentic by passing Andrey’s challenges.

I would like to express my gratitude to Professor Moses Tade and Professor Ming Ang, who kindly supported me during this research, and also Curtin University, the Parker Centre, and CSIRO for the financial support.

Finally my special thanks will go to my parents who were very patient and kindly supportive during my studies overseas.

There are many more who deserve my gratitude. I sincerely apologise to those whose names are not mentioned here but played a role in my achievements so far.

Table of contents

Chapter 1: Introduction 1

Chapter 2: A multi-scale modelling outlook for gibbsite calcination 11

Chapter 3: A 1-D non-isothermal dynamic model for the thermal decomposition of a gibbsite particle 26

Chapter 4: An unreacted shrinking core model for calcination and similar solid-to-gas reactions *60*

Chapter 5: A multi-stage, multi-reaction shrinking core model for self-inhibiting gas-solid reactions *98*

List of figures

List of tables

1

Introduction

Particle technology is central to minerals processing and to Australia's current resources boom. It spans applications to other industries, such as food, building products, pharmaceuticals, and agriculture. The alumina industry alone, which provides the feedstock for aluminium metal production, contributes around A$6 billion to Australian exports annually. Although a technologically mature industry, it strives for continual advancements in the process to stay competitive in the global market, while at the same time meeting increasingly high expectations from the community. One of the most energy intensive processes in alumina production, with a strong effect on final product quality, is calcination, which is conducted in fluidized bed reactors (FBRs). An improved quantitative understanding of this operation will lead to significant benefits to the alumina industry. Modelling as an engineering tool makes it feasible to optimize the process productivity and energy consumption.

Further, product design is increasingly receiving attention, which makes modelling endeavours more valuable and necessary. With regards to alumina as a strategic product that has application in other industries and also in high-tech composite materials, both process intensification and product quality control are of importance.

Accordingly, much research effort has been undertaken to address the requirements of this industry. However, the majority of these works are experimental studies with especial attention to reaction behaviour. Little modelling work on gibbsite calcination has been done due to the complex nature of this process, particularly when conducted in a full-scale fluidized bed reactor. Different mechanisms and interactions come in to play in fluidized bed reactor systems, causing difficulties in developing a simple and accurate predictive model. In addition, the calcination of gibbsite, in itself, has inherent complexity in its reaction kinetics, as several parallel and series reactions are involved and the reaction orders are considerably different.

As a novel and promising methodology, multi-scale models are under development to address some of difficulties in describing FBR systems. Actually, the main concept behind multi-scale models, which potentially could reduce the ambiguities of FBR systems, is that they are built using different layers of information derived at different scales of interest. In other words, data and concepts at different time and length scales are combined into an integrated model, which should offer enhanced predictions and interpretations of the system. Process control and optimization, along with product design, are realised not only at one time-length scale, but also potentially through manipulation of parameters at different scales.

Development of different particle scale models for solid-to-gas reactions with negative order reactions and subsequent application of these models at the reactor scale is the main focus of this research, with particular attention to the gibbsite calcination process. Comparable solid-to-gas processes include lime calcination, sodium bicarbonate calcination, pyrolysis of carbonaceous materials, and the thermal decomposition of other organic and inorganic compounds. The gibbsite calcination process possesses considerable ambiguities in terms of scale identification, sub-model formulation, the selection of the most appropriate multi-scale modelling framework and model validation. Therefore, the key elements of a comprehensive multi-scale modelling approach that should be considered are: (i) identification of the relevant scales of interest for bubbling and circulating fluidized bed reactors; (ii) characterisation of the dominant phenomena, modelling approaches and available data at each scale; and (iii) integrated communication frameworks to link the scales of interest. Since this scope of work is broad, care has been taken to limit the work undertaken, where necessary, to those aspects that are most relevant to gibbsite calcination.

1.1. Background

Dense, gas-particle, two-phase flows are always aggregative, resulting in considerable heterogeneity over a wide spectrum of spatio-temporal scales. Some researchers analyse them at three scales of observation, termed micro-scale, meso-scale and macro-scale. Regarding the micro-scale, the difference between the gas and solid phases forms a natural heterogeneity in the system. For example, the density difference between gas and solid phase causes such heterogeneity. Furthermore, solid particles are usually irregular in shape and may be porous. The particle-particle effects can be divided in two main groups, including contact effects (friction forces for instance) and non-contact effects (Van der Waals forces for instance). In the riser of a circulating fluidized bed, the meso-scale consists of dynamic dense clusters in contact with a dilute phase system, and these clusters deform, interact, break up and re-form continuously. In bubbling fluidized beds, the meso-scale consists of rising bubbles and the surrounding emulsion phase. As a consequence of this dynamic behaviour, the transport and reaction properties could be strongly affected. On the macro-scale, which is of high importance to process engineers, a wide range of flow regimes exists and macro-scale behaviour changes in time and location because of boundary, inlet and outlet conditions. The aforementioned heterogeneous flow regime and phase interactions are challenging in terms of their explanation and interpretation, and have been a focus in the investigation of multi-phase flow.

In order to address the difficulties caused by the multi-scale nature of gas-particle flows, many methods have been introduced in various domains of interest. A reasonably accurate simulation of gas and solid flows should be based on micro-scale (individual particle) behaviour. However, direct, naive utilization of this method seems unacceptable for practical (industrial) systems because of the very large number of particles in a typical vessel, but micro-scale information can be linked to macro-scale behaviour through a multi-scale modelling approach.

A coarse-grid methodology utilizing the two-fluid model (TFM) from computational fluid dynamics (CFD) and a hybrid approach, which mixes the continuum description for the gas and the discrete particle method (DPM) or discrete element method (DEM) for particles, are the current available approaches for reactor scale simulation from the industrial viewpoint. Finding ways of enhancing the available simulations by their improvement or combination, so that industrial scale models are able to use insights into micro-scale behaviour, is a crucial task for researchers in multi-phase systems, and in particular for fluidized bed reactor specialists.

A literature search on multi-scale modelling aspects and applications in the chemical engineering field has revealed four main categories of research areas, which are as follows:

- Qualitative (descriptive) research on the definition, application and importance of multi-scale modelling;
- Hydrodynamics of fluidized beds;
- Multi-scale modelling of mass and heat transfer and reaction;
- Quantitative research and publications on specific chemical engineering issues.

The research work on fluidized beds in these four categories has some shortcomings, a few of which are addressed in this study and some of which are presented in the last chapter of this thesis as possibilities for future work.

1.2. Significance

As mentioned earlier, the production of alumina and aluminium in Australia alone is a multi-billion dollar industry. During calcination, which is a very energy-intensive part of the Bayer process, gibbsite powder is converted into alumina. Calcination also has a strong impact on product quality because it is essentially the last processing step. Industrially, the calcination is conducted in bubbling or circulating fluidized beds. From an industrial viewpoint, the following areas are of particular interest:

- Energy consumption minimization;
- Temperature distribution and control;
- Transition reaction pathway prediction;
- Product quality control;
- Particle breakage minimization.

Better modelling of fluid bed calciners is needed to improve process design, control and operations, leading in turn to cost, safety and environmental benefits for the industry. Current modelling approaches do not strongly link micro-scale product quality characteristics, such as chemical composition, microstructure and mechanical strength, to vessel-scale operating conditions and design details.

1.3. Project aims

This project aims to

1. Investigate and outline potential research opportunities in the

    i. Multi-scale nature of fluidized bed reactors;
    ii. Gibbsite calcination–related fundamentals.
2. Develop a multi-scale modelling framework for gibbsite calcination in fluidized bed reactors.
3. Develop particle scale models for solid-to-gas reactions that possess a self-inhibiting nature due to the gas produced, with an especial focus on gibbsite calcination as the case study.
4. Investigate dominant mechanisms and parameters in the gibbsite calcination process using predictive and descriptive models at the particle scale.
5. Exemplify employment of the particle scale model at the reactor scale through a simplified multi-scale modelling endeavour.

1.4. Research method

Multi-scale models are composite mathematical models that combine two or more component models that describe phenomena at different characteristic length and time scales. In contrast to single-scale models, in multi-scale modelling there are four tasks that need special attention:

- Identifying and selecting the time and length scales to include in the model;
- Choosing the order of model construction in terms of scale;
- Adopting or developing appropriate models at each scale of interest;
- Linking the single-scale models into a coherent multi-scale model.

The tools and techniques developed in this project focus on addressing the above four topics for modelling the fluid bed calcination of gibbsite. The multi-scale model is developed by following several steps.

Firstly, a comprehensive literature review is done on topics including multi-scale modelling, alumina production and the calcination process. Each chapter of this thesis reflects a part of the literature review in its own Introduction section.

Secondly, the possibilities for fluidized bed reactor modelling for gibbsite calcination from a multi-scale point of view are outlined. This sets out a “modelling map”.

Thirdly, the identification of scales of interest is accomplished. For each scale it is necessary to characterise the boundaries and define the specifications that will be considered during this investigation. In addition, the wide range of current modelling approaches is explored, and decisions made to adopt them or develop new models for the processes on each scale. Mass and energy balances as well as reaction-related issues are studied on each scale at this stage (Figure 1.1). Three candidate scales have been identified as:

1. *Micro-scale* (particle size): on this scale a single particle should be considered in terms of mass and heat transfer and reaction to develop a predictive model for reaction conversion. Therefore this part includes a deep focus on reaction kinetics as well as possible reaction pathways to provide constitutive equations needed for mass and heat balance equations.

2. *Meso-scale* (bed volume element size): by importing information from the particle scale (e.g., water vapour production rate, particle composition), this scale will account for phenomena such as particle-particle interactions, and overall energy and mass balances. The meso-scale is large with respect to individual particles, but small with respect to the whole reactor. Although hydrodynamics, as the dominant phenomenon on this scale, can be estimated more accurately using CFD modelling, ideal flow and mixing regimes result in a simpler model. In particular, combinations of plug flow and well mixed regimes for both gas and solids phases can be considered. Temperature and concentration profiles are the main outputs of this scale's model. The meso-scale is an interface between micro- and macro-scales.

3. *Macro-scale* (reactor size): overall performance of a real-life reactor in terms of product quality and spatial profiles will be the modelling outputs on this scale. Similar to the meso-scale, we need a good approximation of the hydrodynamics at the macro-scale.

However, in this thesis two scales are considered, micro- and macro-scale, as discussed later.

Fourthly, the particle scale modelling has been done through different approaches. This part of the work mainly consists of fundamental modelling, and numerical and analytical solution of the models, along with the model validation against experimental data. The developed models include distributed, shrinking core and multi-stage, multi-reaction shrinking core models for a single reacting particle. MATLAB coding is utilized for numerical calculations.

Fifthly, application of particle scale models at the reactor scale is illustrated through a simplified FBR model. At the reactor scale, diversity of the particle sizes and residence time distributions are accounted for. In addition, different possibilities for reactor modelling are explored.

1.5. Thesis structure

This thesis is arranged in seven chapters. In all chapters a relatively short literature review on the main subject of the chapter is presented in the *Introduction* section. In addition, all modelling work starts with a general development, followed by validation and analysis using the gibbsite calcination process as a case study.

Chapter 2 includes the conceptual multi-scale modelling framework proposed for the gibbsite calcination process inside a FBR. The chapter illustrates the main concerns on modelling of FBRs at each scale, along with a discussion of research and modelling possibilities. Finally, a general framework is suggested for the case study. The following chapters present work that goes part of the way to realising the proposed framework.

Chapter 3 presents the development steps of a spatially-distributed model of single reacting particle experiencing a thermal decomposition reaction. In this chapter, a simple reaction is simulated to attain valuable and useful insight into intra-particle parameters including the gas and solid concentrations, temperature and gas pressure. Further, kinetic parameters are extracted from literature data and justified for the case study. Subsequently, several sensitivity analyses on gibbsite calcination are conducted using the validated model.

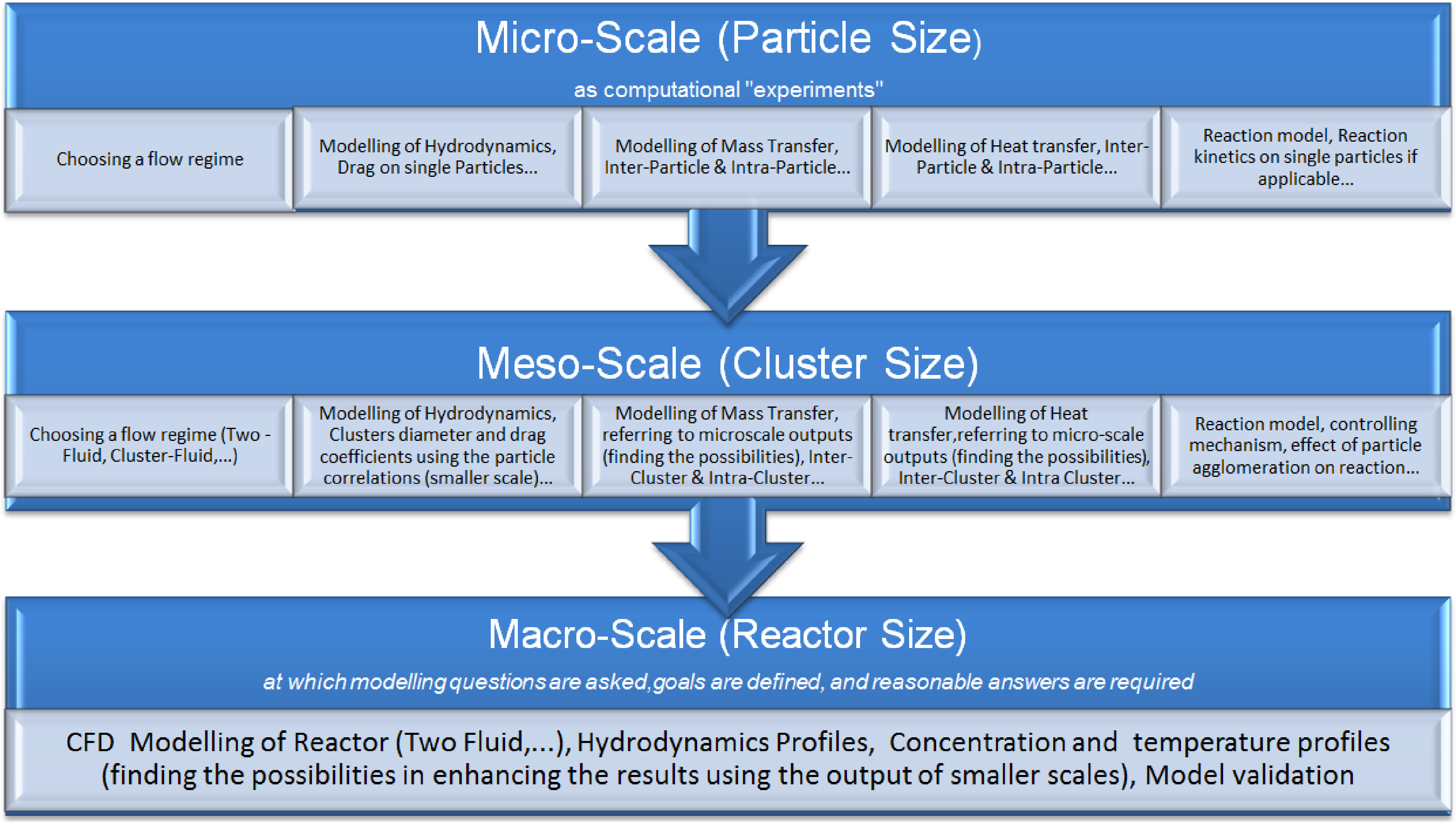

Figure 1.1 – Flowchart showing potential multi-scale topics to investigate.

Chapter 4 involves a different modelling approach to the same reacting system as in Chapter 3. A new variation of the shrinking core model is proposed and developed for solid-to-gas reactions in which the product gas negatively influences the reaction progress. The role of the gas is accounted for in both the intrinsic reaction rate and the mass transfer rate inside the particle. Similar to the previous chapter, the model is validated for gibbsite calcination through comparison to experimental data and also to the results of the distributed model of Chapter 3.

In Chapter 5, some complex features of solid-to-gas reactions with negative reaction orders with respect to gas species are addressed. A multi-stage, multi-reaction shrinking core model is developed and examined for a combination of series and parallel reactions. Prediction of reaction progress through different pathways was the main goal of this modelling study. A practical application of this model is to capture the formation of the intermediate species boehmite during gibbsite calcination. However, the model is general enough to be implemented for similar reacting systems.

Use of particle scale modelling at the reactor scale is shown via a simplified reactor model in Chapter 6. Even though different modelling strategies and considerations are described in this chapter, a pseudo-single-phase FBR is simulated using ideal flow regimes, from well-mixed to near plug-flow. Two-way information transfer occurs between particle and reactor scales. This chapter aims to illustrate multi-scale modelling practice.

Chapter 7 presents the conclusions and future work recommendations.

Figure 1.2 shows how the individual chapters are interconnected.

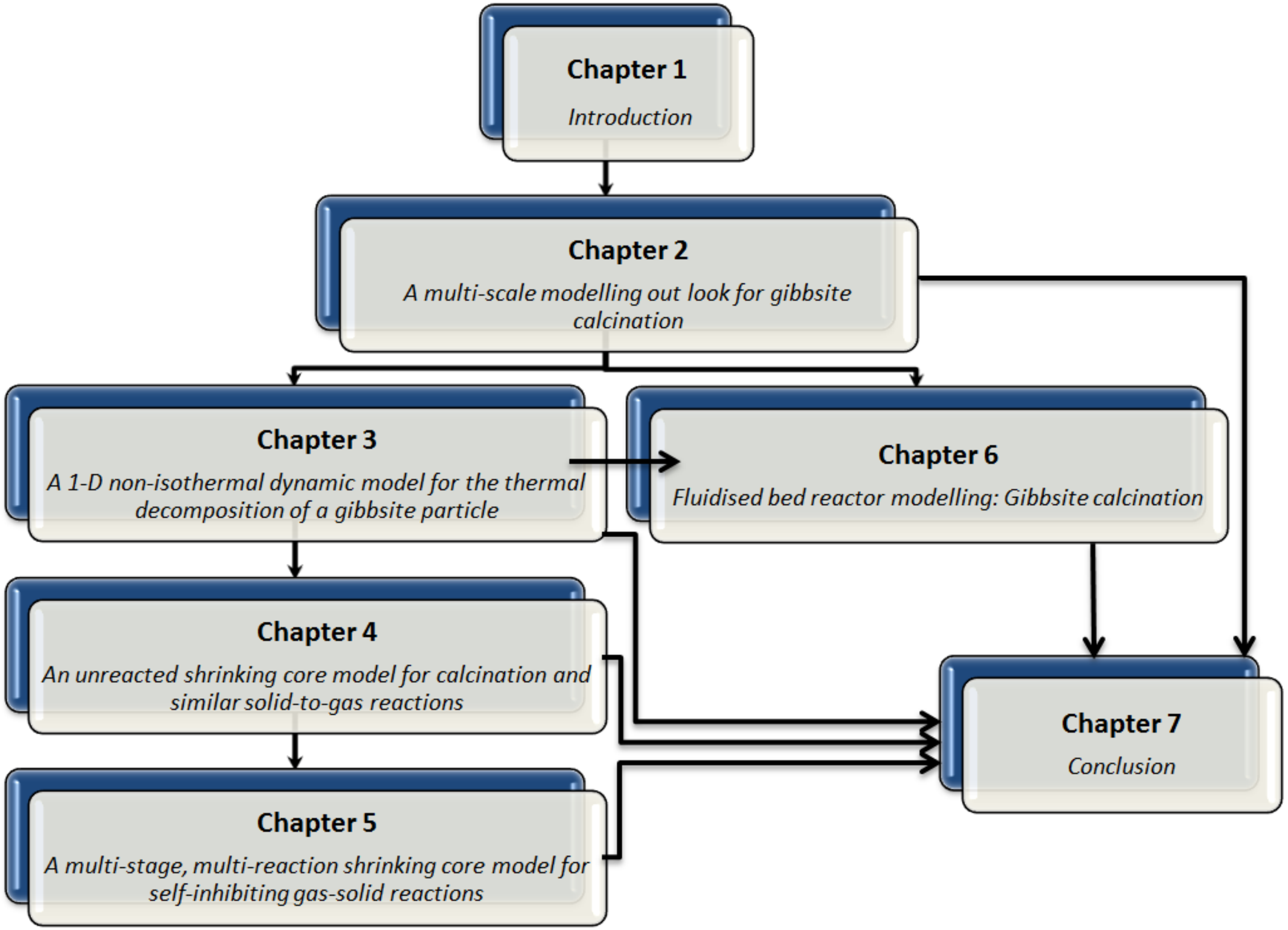

Figure 1.2 – Overall structure of the thesis.

2

A multi-scale modelling outlook for gibbsite calcination

Multi-scale models, which account for phenomena interacting across different length and time scales, are increasingly being used to describe complex multidisciplinary, nonlinear, non-equilibrium processes. The main objective of this chapter is to explore the possibilities for developing a multi-scale model for the fluidized bed calcination of gibbsite, and to make recommendations on promising directions. The suggested framework in this chapter serves as a roadmap for the tasks that need to be accomplished in other parts of the thesis. The key elements of the multi-scale approach that were considered are (i) identification of the relevant scales of interest for bubbling and circulating fluidized bed reactors; (ii) characterisation of the dominant phenomena, modelling approaches and available data at each scale; (iii) an integrated communication framework to link the scales of interest, and briefly (iv) experiment design and model validation for multi-scale models. A conceptual model having three scales (particle, volume element / cluster, and vessel) is proposed and the information flows between the scales are outlined. There are several possibilities for the sub-models used at each scale, and these have been noted.

2.1 Introduction

The aluminium industry relies on the Bayer process to produce alumina (Al_2O_3) from bauxite, the main aluminium ore, which consists mostly of gibbsite, boehmite and diaspore. Despite being over 120 years old, the Bayer process remains the most economical approach for obtaining alumina powder, which may then be converted into aluminium metal (Hudson et al., 2005). In the Bayer process, bauxite is washed, ground and dissolved in sodium hydroxide at high pressure and temperature. The resulting liquor consists of sodium aluminate solution, along with undissolved bauxite residues containing iron, silicon and titanium. These residues, known as “red mud”, sink to the bottom of the processing vessel and are removed (International Aluminium Institute, 2010). Aluminium hydrate ($Al(OH)_3$) is precipitated from the solution by cooling. The final stage of the Bayer process is calcination, or thermal dehydration, which is conducted approximately at 1100°C to remove the chemically-bound water. The dehydration reaction involves several solid phase transitions, but these can be approximated as (Gan et al., 2009):

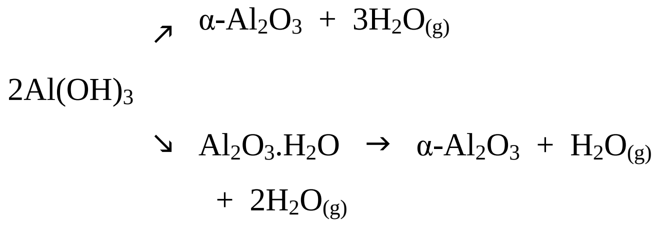

$$
\begin{array}{lll}
 & \nearrow & \alpha\text{-}Al_2O_3 \;+\; 3H_2O_{(g)} \\
2Al(OH)_3 & & \\
 & \searrow & Al_2O_3.H_2O \;\rightarrow\; \alpha\text{-}Al_2O_3 \;+\; H_2O_{(g)} \\
 & & \;+\; 2H_2O_{(g)}
\end{array}
\qquad (2.1)
$$

The end product is white α-alumina powder.

In current practice, the Bayer process hydrate is calcined into alumina in a fluidized bed reactor (FBR), either a bubbling fluidized bed (BFB) or a circulating fluidized bed (CFB). In older alumina refineries, calcination was carried out in rotary kilns, but today all new capacity is installed as fluidized bed calciners (Outotec, 2008). In a CFB calciner (Figure 2.1), the energy is supplied through direct combustion of hydrocarbon fuels, oil and gas, as well as energy recovery from downstream processes.

The key component of a CFB reactor is the riser, which is where the reaction takes place. A relatively high fluidizing gas velocity is used that causes the solids and gas to flow cocurrently upwards in the riser. At the top of the riser, the solids are separated from the gas using cyclones and other equipment, and then they are recycled to the base of the riser, thus forming a circulating flow of solids. On the other hand, BFBs consist of a vessel with a semi-porous base that allows the upwards flow of gas, but prevents solids flow through. Lower gas velocities are used compared to CFBs, and the solids are more or less confined to the processing vessel.

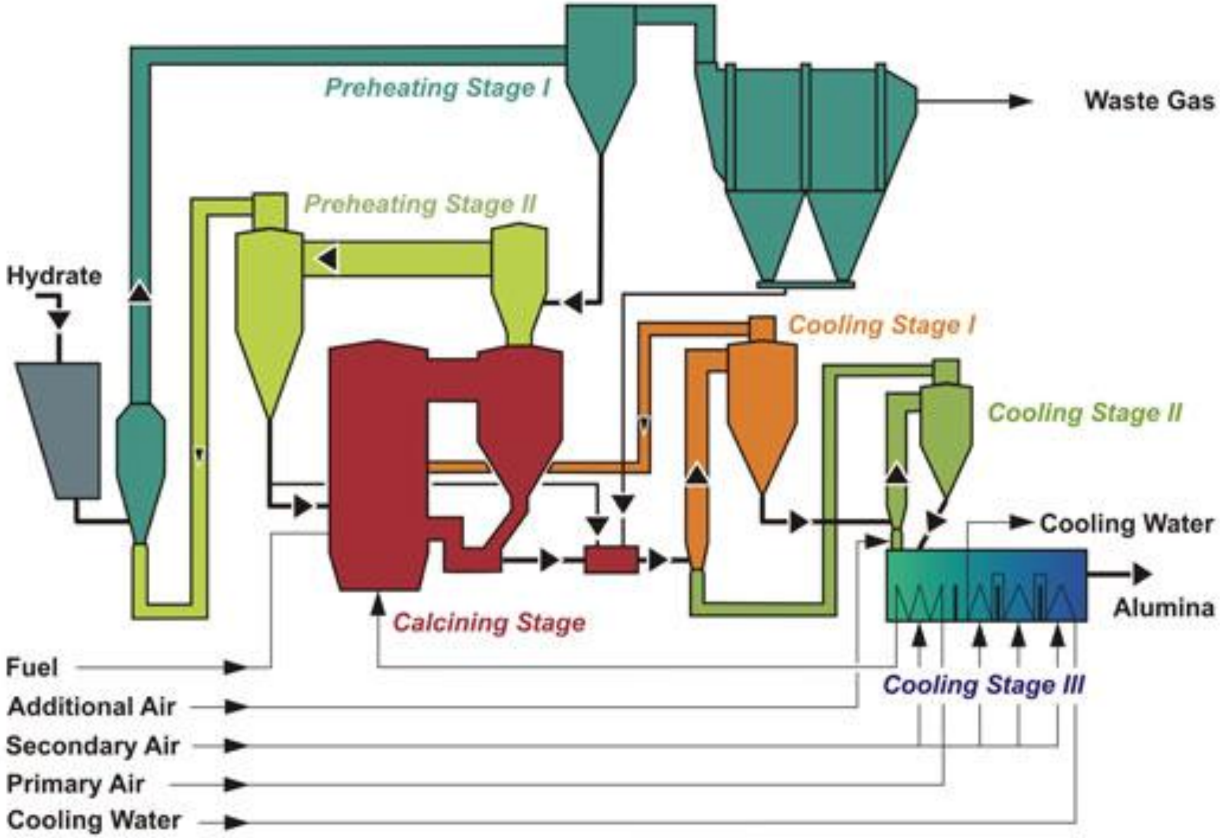

Figure 2.1 – Alumina calcination in a CFB (Outotec, 2008).

Over many years CFB and BFB reactors have been proven to be highly effective reactors for gas–solid and solid-catalysed gas reactions. Their successful applications include catalytic cracking, calcination, coal and wood pyrolysis, biomass gasification, polyethylene production and combustion of a variety of fuels (Ściążko and Zieliński, 1995; Nemtsov and Zabaniotou, 2008). They offer advantages such as high throughput rates and thorough gas–solid contacting, leading to excellent heat and mass transfer (Bolkan et al., 2003). The near-homogeneous temperatures in FBRs assist in producing high-quality products. Low maintenance cost, no moving mechanical parts in the hot zone, high availability, uniform product quality, stability and ease of control are further advantages of CFB reactors (Karches et al., 2004).

The availability of accurate, validated models will assist in the design, control and optimization of FBRs. In the Bayer process, better modelling of fluid bed calciners should lead to cost, safety and environmental benefits for the industry. Developing an accurate, comprehensive model of an alumina calciner is, however, difficult because of the wide range of physical and chemical processes occurring together. These include:

- Hydrodynamics, essentially the gas and particle flows inside the CFB or BFB;
- If the calciner is fired with heavy fuel oil, then liquid droplet dispersion amongst the bed solids, and droplet evaporation are also important; however, these processes are absent for calciners operating on natural gas;
- High-temperature heat transfer – inside the solids, between solids and gas, and between the gas-solid suspension and the vessel walls;
- The fuel combustion reaction;
- The calcination reaction itself, including intrinsic reaction kinetics, diffusional resistances, solid phase transitions and microstructure evolution in the solid.

All these phenomena are interdependent and must be considered in an integrated model if it is to produce meaningful results (Marsh, 2009).

2.2 Review of current models

2.2.1 Fluidized bed reactors

Many authors have reported on the modelling of FBRs, especially the hydrodynamics (Gungor and Eskin, 2007; Behjat et al., 2008). Hydrodynamics plays a crucial role in the performance of fluidized beds as it can strongly affect the other processes taking place: heat transfer, mass transfer and reaction. Computational fluid dynamics (CFD) and discrete particle modelling (DPM) are key techniques used to describe the details of gas-solid hydrodynamics. Coupling CFD and reaction kinetics in fluid beds is a challenging but promising area of investigation (Bi and Li, 2004).

FBR modelling can also be considered from a multi-scale perspective, which may help develop more accurate and reliable models. Some investigators have reported on multi-scale modelling of FBRs in general or its application to specific fluid bed processes (Bauer and Eigenberger, 2001; Raimondeau and Vlachos, 2002; Balaji et al., 2010).

2.2.2 Alumina calcination

Very few publications report specifically on the calcination of aluminium ores in FBRs. Guardani et al. (1989) presented experimental work on thermal transformation of aluminium phosphate rock in a FBR. Marsh (2009) reported CFD modelling of a gibbsite calciner. The majority of publications related to gibbsite calcination have focused on the detailed reaction kinetics and phase transitions (Whittington and Ilievski, 2004; Wang et al., 2006; Gan et al., 2009). Little work has been published on coupling reaction kinetics and hydrodynamics, and no work specifically on multi-scale modelling of alumina calciners appears to be available.

Based on the open literature, one can summarise a number of deficiencies in current gibbsite calcination models:

- Alternative pathways for gibbsite calcination exist, as seen in reaction (2.1), but it is not currently possible to predict the extent to which each path is followed (Gan et al., 2009).
- There is no comprehensive model for a gibbsite particle undergoing calcination, in particular to predict chemical composition, essentially α-

alumina content, and physical properties, such as porosity and specific surface area.

- There is a lack of coupling of processes at different scales, such as particle and vessel scales, in current models.
- In general, the design of experiments for multi-scale systems, which is needed for model calibration and validation, needs further study.

Multi-scale modelling holds the promise of relating vessel scale measures, like energy efficiency and throughput, to the particle-scale factors that determine product quality: chemical composition and microstructure. Before discussing multi-scale modelling of gibbsite calcination, a general explanation of the multi-scale approach is given below.

2.2.3 Multi-scale modelling

Due to increasing market demands and environmental regulations along with increases in computing power, chemical engineers are turning to multi-scale approaches to improve model accuracy and detail (Ingram et al., 2004). Multi-scale modelling comes in many forms, some of them relatively new, and the methodology continues to evolve.

The aim of a multi-scale model is to transfer process information from one length or time scale to other scales. Utilizing molecular-scale (micro) information on larger (macro) scales was the initial approach in multi-scale modelling. This approach has been employed, for instance, in the design of nano-structured materials, like catalysts (Nily, 2009). More recent multi-scale models use a wide range of configurations.

One view of the procedure for developing a multi-scale model is given below:

1. Identifying the relevant scales, phenomena and variables of interest in the system under study;
2. Surveying the modelling approaches and available data at each scale;
3. Implementing an integrated communication framework to link the scales of interest; and
4. Developing experimental designs and undertaking validation for the candidate multi-scale model.

This chapter discusses the conceptual implementation of this strategy for fluidized bed gibbsite calcination, and presents a synthesis of the state of the art. More details on the multi-scale approach in chemical engineering are available (Ingram et al., 2004; Li et al., 2004, 2005; Reis, 2009; Charpentier, 2010).

2.3 Elements of a multi-scale modelling approach

The following sections use the modelling procedure above to flesh out the components of a possible multi-scale model for CFB and BFB reactors used in gibbsite calcination.

2.3.1 Identification of scales, phenomena and key variables

Gibbsite calcination involves a wide range of size and time scales. On the micro-scale, gibbsite particles undergo reaction and consequent structural deformation because of the loss of chemically-bound water molecules. This process is driven by heating, and several types of intermediates may form depending on the process conditions and physico-chemical properties of the gibbsite particle (Gan et al., 2009).

On the macroscopic scale, calcination is conducted at high throughputs during industrial alumina production, and it is at this scale that the process is influenced through equipment design and process control. The mass production of high-quality alumina is challenging because microscopic processes affect the macro-scale production in terms of the end product’s physical and chemical properties. The micro-scale and macro-scale processes are tied together by the meso-scale of cluster (CFB) and bubble (BFB) dynamics. Traditional reactor models used for alumina processing are not accurate enough to establish the relationship between end product properties and microscopic processes (Marsh, 2009). Other scales of interest can be identified (Li and Kwauk, 2001), for example the nano-scale that considers reactions at the atomistic level, and the mega-scale of the flowsheet or factory, in which process efficiency and profitability are considered. Models that help to bridge the gap between scales should lead to productivity and quality improvements.

It is proposed to concentrate on the micro, meso and macro scales, since these should be sufficient to relate product quality to calciner design and operation. Table 2.1 summarises some possibilities for relevant scales, active mechanisms and modelling approaches. The key phenomena and process variables at the scales of interest are discussed below:

2.3.1.1. Micro-scale: This involves gibbsite calcination at the particle scale, including thermal dehydration of a single particle and its consequent change in structure. Many characteristics of alumina particles—chemical composition, porosity, pore diameter, specific surface area, particle size and so on—are determined at this scale. While intrinsic reaction kinetics are important, intra-particle diffusion and heat transfer also need attention in the particle-scale model.

2.3.1.2. Meso-scale: Here we are concerned with gas and many-particle interactions, and the transient structures that form: particle clusters in CFBs and gas bubbles in BFBs. Cluster and bubble formation and breakage rates, and size distribution; effective drag coefficients; heat and mass transfer; and ways to control these parameters are considered at this scale. The meso-scale will be referred to as the "cluster scale" and "volume element" scale for CFBs and BFBs, respectively. Temperature control is important during calcination, and prediction of vessel and particle temperature distributions needs to consider meso-scale phenomena.

2.3.1.3. Macro-scale: The third scale considered is the vessel scale. Variables of interest include production capacity, energy consumption, vessel design parameters, and bulk product quality measures, such as particle size distribution. Most available models and practical data are related to this scale.

Having identified the relevant scales and key variables, the next step to consider is the available models and method of connecting the smaller scales with the vessel scale.

Table 2.1 – Scale identification and characteristics of gibbsite calcination using BFB and CFB reactors.

FBR type	***Scale***	***Character-istic size & time scale***	***Phenomena / Mechanisms***					
			Hydrodynamics		***Heat and mass transfer***		***Reaction***	
			Issues	***Current model(s)***	***Issues***	***Current model(s)***	***Issues***	***Current model(s)***
BFB & CFB	Particle	10^{-5}–10^{-3} m 10^{-6}–2000 s	Interaction between individual particles, wall & gas; Flow around individual particle	Direct numerical simulation (DNS); Discrete particle modelling (DPM)	Intra-particle mass diffusion & heat conduction; Thermal shock; Particle-gas heat transfer	Fick's law; Knudsen diffusion equation; Fourier's law	Reaction pathway & kinetics; Conversion; Breakage	Un-reacted & reacted core model; Homogeneous reaction model
BFB	Volume element	10^{-3}–0.1 m 10^{-3}–100 s	Bubble size, bubble-bubble & bubble-solid interaction & mixing; Flows corresponding to volume elements	Two-fluid model (TFM); Computational fluid dynamics; Local averaging; Zonal models	Bubble phase & emulsion phase heat and mass transfer	Gridding or meshing methodology; Computational fluid dynamics	Reaction progress through a calculation cell; Reaction kinetics & void fraction	Two-phase approach
CFB	Particle cluster		Particle-particle collision; Mixing; Cluster size; Cluster-cluster, cluster-wall & cluster-gas interaction; Inter- & intra-cluster flows		Inter- & intra-cluster heat & mass transfer			Core-annulus model
BFB & CFB	Reactor	0.1–30 m 1–4000 s	Bulk solid motion; Bulk gas motion; Solids fraction distribution; Elutriation	Continuum zero & one dimensional models for gas & solid flows	Overall mass & energy balances; Temperature distribution profile	Core-annulus model; Two-zone model	Overall reaction conversion; Residence time distribution	Plug flow reactor; Well-mixed reactor; Core-annulus reactor model; Population balance model (to describe particle size changes)

2.3.2 Models and inter-scale communication framework

For transferring information among the various models at different scales, the concept of a “multi-scale integration framework” is helpful. However, only the models to use at each scale and the variables used to transfer information between them are suggested—a formal communication framework in the sense of Ingram et al. (2004) is not considered here.

The hydrodynamics at the meso-scale might be modelled using CFD, or a simplified method, such as the network of zones or compartment approach (for example, Bauer and Eigenberger, 2001; Lim et al., 2001). In this thesis, the latter approximate approach is favoured, which should be adequate for calciners heated with natural gas. Water vapour is produced as calcination proceeds, and should be included as a source term in the meso-scale model. The profiles of particle conversion, gas phase concentration and temperature are inputs to the reactor scale model, to help calculate the overall process productivity and efficiency.

The initial temperature, size and other particle characteristics, and the environmental temperature and water vapour pressure are typical outputs of a simplified reactor model that should be passed to a particle scale model. A single-particle reaction model can predict particle diameter, temperature and water vapour production rate for use in the meso-scale model. In addition, the micro-scale model can also provide particle morphological and structural information to larger scales to help assess product quality.

Heat and mass transfer coefficients used in particle reaction modelling are information that the meso-scale provides to the micro-scale. Figure 2.2 depicts the proposed multi-scale modelling framework applicable for the gibbsite calcination process.

Figure 2.2 shows that two-way communication between the models at each scale is needed. Non-overlapping size scales for the sub-models have been identified (Table 2.1); hence, inter-scale communication via the “embedded” multi-scale integration framework (Ingram et al., 2004) could be suitable for this model. However, the time scales for the sub-models do overlap (Figure 2.3), which can lead to hysteresis and memory effects in the variables.

The "model spectrum" at each scale in Figure 2.2 needs some explanation. Depending on the modelling goal, and possibly sensitivity analyses, a simplified or rigorous model may be used at each scale, for example, a lumped model compared to a distributed-parameter model. On the macro-scale, I consider only one aspect of control-relevant modelling: "hard-sensor control" refers to measuring all variables using sensors, while in "soft-sensor control" un-measured variables are inferred by combining sensor outputs using a neural network or similar.

2.3.3 Multi-scale design of experiments

The design of experiments (DOE) is a tool used in model building and validation. Various approaches to DOE have been used in the past, but recent work favours model-based, and particularly multi-scale model-based, approaches (Vlachos et al., 2006; Franceschini and Macchietto, 2008). Prasad et al. (2010) published a new methodology for multi-scale, model-based DOE, using the production of hydrogen from ammonia as a case study. DOE and validation for multi-scale models remain open research topics. Multi-scale, model-based DOE is out of the scope of this thesis.

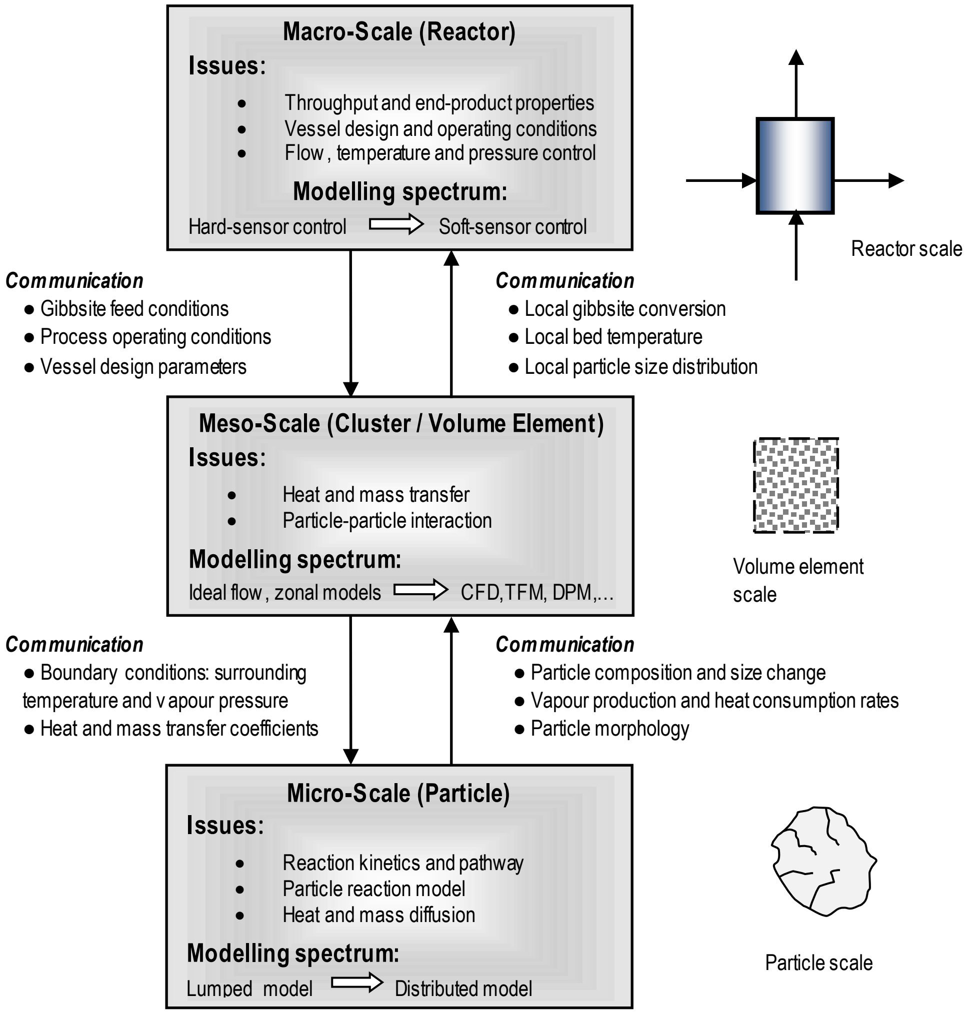

Figure 2.2 – Proposed multi-scale modelling framework for gibbsite calcination in a FBR.

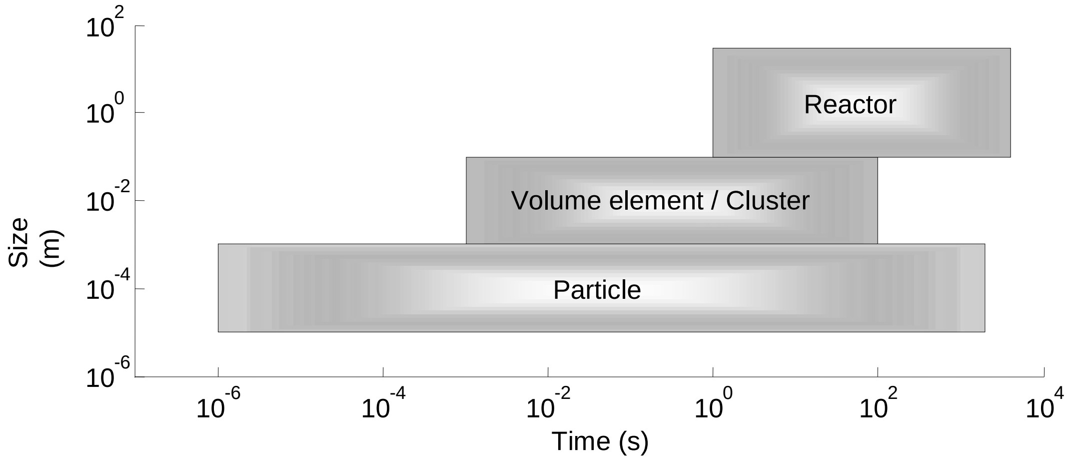

Figure 2.3 – Scale distribution of sub-models in fluid bed gibbsite calcination.

2.4 Summary

A conceptual framework has been proposed for a multi-scale model to predict the performance of fluidized bed reactors used for gibbsite calcination. The aim of the conceptual model is to relate product quality parameters, such as particle size and chemical composition, with calciner design and operating conditions. It links a single-particle reaction model, a meso-scale model describing fluidized bed hydrodynamics, and a vessel-scale model. This framework depicts the scales, mechanisms and potential models needed, as well as commenting on the important variables at each scale.

With regards to the conceptual framework described in this chapter, the development of the elements of the proposed framework is the subject of the following chapters, starting with a detailed investigation of the particle scale.

References

Balaji, S., Du, J., White, C.M. & Ydstie, B.E. 2010. Multi-scale modeling and control of fluidized beds for the production of solar grade silicon. *Powder Technology*, 199**,** 23-31.

Bauer, M. & Eigenberger, G. 2001. Multiscale modeling of hydrodynamics, mass transfer and reaction in bubble column reactors. *Chemical Engineering Science,* 56**,** 1067-1074.

Behjat, Y., Shahhosseini, S. & Hashemabadi, S.H. 2008. CFD modeling of hydrodynamic and heat transfer in fluidized bed reactors. *International Communications in Heat and Mass Transfer,* 35**,** 357-368.

Bi, H.T. & Li, J. 2004. Multiscale analysis and modeling of multiphase chemical reactors. *Advanced Powder Technology,* 15**,** 607-627.

Bolkan, Y., Berruti, F., Zhu, J. & Milne, B. 2003. Modeling circulating fluidized bed downers. *Powder Technology,* 132**,** 85-100.

Charpentier, J.-C. 2010. Among the trends for a modern chemical engineering, the third paradigm: The time and length multiscale approach as an efficient tool for process intensification and product design and engineering. *Chemical Engineering Research and Design,* 88**,** 248-254.

Franceschini, G. & Macchietto, S. 2008. Model-based design of experiments for parameter precision: State of the art. *Chemical Engineering Science*, 63, 4846-4872.

Gan, B., Madsen, I.C., Hockridge, J.G., 2009. *In situ* X-ray diffraction of the transformation of gibbsite to α-alumina through calcination: effect of particle size and heating rate. *Journal of Applied Crystallography,* 42**,** 697-705.

Guardani, R., Drahos, J., Giulietti, M. & Schügerl, K. 1989. Studies on calcination of aluminium phosphate rock in fluidized bed reactors. *Nutrient Cycling in Agroecosystems,* 20**,** 181-191.

Gungor, A. & Eskin, N. 2007. Hydrodynamic modeling of a circulating fluidized bed. *Powder Technology,* 172**,** 1-13.

Hudson, L.K., Misra, C., Perrotta, A. J., Wefers, K., Williams, F. S. 2005. Aluminum oxide, in *Ullmann's Encyclopedia of Industrial Chemistry*, Wiley-VCH, Weinheim.

Ingram, G.D., Cameron, I.T. & Hangos, K.M. 2004. Classification and analysis of integrating frameworks in multiscale modelling. *Chemical Engineering Science,* 59**,** 2171-2187.

International Aluminium Institute. 2010. *Alumina refining*, viewed 11 June 2010, <http://www.world-aluminium.org>.

Karches, M., Takashima, H. & Kanno, Y. 2004. Development of a circulating fluidized-bed reactor for microwave-activated catalysis. *Industrial & Engineering Chemistry Research*, 43**,** 8200-8206.

Li, J., Ge, W., Zhang, J. & Kwauk, M. 2005. Multi-scale compromise and multi-level correlation in complex systems. *Chemical Engineering Research and Design,* 83**,** 574-582.

Li, J. & Kwauk, M. 2001. Multiscale nature of complex fluid–particle systems. *Industrial and Engineering Chemistry Research,* 40, 4227-4237.

Li, J., Zhang, J., Ge, W. & Liu, X. 2004. Multi-scale methodology for complex systems. *Chemical Engineering Science,* 59**,** 1687-1700.

Lim, K.S., Peeler, P. & Schwarz, P. 2001. Comparison of solids residence time distributions from fluidized bed and kiln processes. *6th World Congress of Chemical Engineering*, Melbourne, 23-27 September, 2001.

Marsh, C., 2009. CFD Modelling of alumina calciner furnaces. In: *Seventh International Conference on CFD in the Minerals and Process Industries*, Melbourne, Australia, 9–11 December 2009.

Nemtsov, D.A. & Zabaniotou, A. 2008. Mathematical modelling and simulation approaches of agricultural residues air gasification in a bubbling fluidized bed reactor. *Chemical Engineering Journal*, 143**,** 10-31.

Nily, D. 2009. New developments in multiscale modeling. *Current Opinion in Colloid & Interface Science*, 15, 1-1.

Outotec. 2008. *Alumina and aluminium technologies*, viewed 11 June, 2010, <http://www.outotec.com/36972.epibrw>.

Prasad, V., Karim, A.M., Ulissi, Z., Zagrobelny, M. & Vlachos, D.G. 2010. High throughput multiscale modeling for design of experiments, catalysts, and reactors: Application to hydrogen production from ammonia. *Chemical Engineering Science,* 65, 240-246.

Raimondeau, S. & Vlachos, D.G. 2002. Recent developments on multiscale, hierarchical modeling of chemical reactors. *Chemical Engineering Journal,* 90**,** 3-23.

Reis, M.S. 2009. A multiscale empirical modeling framework for system identification. *Journal of Process Control*, 19**,** 1546-1557.

Ściążko, M., & Zieliński, H. 1995. Circulating fluid-bed reactor for coal pyrolysis. *Chemical Engineering & Technology*, 18**,** 343-348.

Vlachos, D.G., Mhadeshwar, A.B. & Kaisare, N.S. 2006. Hierarchical multiscale model-based design of experiments, catalysts, and reactors for fuel processing. *Computers & Chemical Engineering,* 30, 1712-1724.

Wang, H., Xu, B., Smith, P., Davies, M., Desilva, L. & Wingate, C. 2006. Kinetic modelling of gibbsite dehydration/amorphization in the temperature range 823-923 K. *Journal of Physics and Chemistry of Solids*, 67**,** 2567-2582.

Whittington, B. & Ilievski, D. 2004. Determination of the gibbsite dehydration reaction pathway at conditions relevant to Bayer refineries. *Chemical Engineering Journal,* 98**,** 89-97.

3

A 1-D non-isothermal dynamic model for the thermal decomposition of a gibbsite particle

As the first stage of the single reacting-particle modelling, a 1-D mathematical model describing the thermal decomposition, or calcination, of a single gibbsite particle to alumina has been developed and validated against literature data. A dynamic, spatially-distributed, mass and energy balance model enables the prediction of the evolution of chemical composition and temperature as a function of radial position inside a particle. In the thermal decomposition of gibbsite, water vapour is formed and the internal water vapour pressure plays a significant role in determining the rate of gibbsite dehydration. A thermal decomposition rate equation, developed by closely matching experimental data reported previously in the literature, assumes a reaction order of 1 with respect to gibbsite concentration, and an order of –1 with respect to water vapour pressure. Estimated values of the transformation kinetic parameters were $k_0=2.5\times10^{13}$ *mol/m*^{3} *s for the pre-exponential factor, and* $E_a=131$ *kJ/mol for the activation energy. Using these kinetic parameters, the gibbsite particle model is solved numerically to predict the evolution of the internal water vapour pressure, temperature and gibbsite concentration. The model prediction was shown to be very sensitive to the values of heat transfer coefficient, effective diffusivity, particle size and external pressure, but relatively less sensitive to the mass transfer coefficient and particle thermal conductivity. The predicted profile of the water vapour pressure inside the particle helps explain some phenomena observed in practice, including potential particle breakage and the formation of a boehmite phase. The results of this chapter are utilized for validation purposes in Chapter 4 and also in conjunction with a reactor scale model in Chapter 6.*

3.1. Introduction

Gibbsite, known as aluminium tri-hydroxide, undergoes calcination to convert it into alumina in the final stage of the Bayer process. Final product physical properties are significantly affected by the process conditions experienced in the calcination stage. In current industrial practice, gibbsite calcination is conducted at atmospheric pressure at approximately 1100°C. Replacing rotary kilns with stationary calciners, either bubbling or circulating fluidized beds, has resulted in reductions in the energy consumption from 4.5 GJ/t Al_2O_3 to lower than 3.0 GJ/t Al_2O_3 (Williams and Misra, 2011) for gibbsite calcination under atmospheric pressure (Wind et al., 2011).

Further reductions in energy consumption may result from the commercialisation of a high pressure (4–30 atm) continuous pilot-scale unit, which achieved an energy consumption of only 1.55 GJ/t Al_2O_3, and produced better quality alumina (Sucech and Misra, 1986). Because alumina and its partial hydrates are of high importance, not only for aluminium production, but also for other applications, such as catalysts, absorbents and catalyst supports, gibbsite calcination has been the subject of investigation for decades.

The modelling of thermal dehydration is central to the prediction of gibbsite transformation in calciners. Moreover, by using a predictive process model, it may be possible to develop effective methods for process troubleshooting, optimization and product design. In this area, experimental studies are much more common in the literature than mathematical modelling, particularly modelling at the particle scale. Most research into gibbsite calcination has focused on the details of dehydration kinetics and phase transitions (Gan et al., 2009; Wang et al., 2006; Whittington and Ilievski, 2004). Further, the amount of work published on coupling kinetics with hydrodynamics in a calciner is limited (Marsh, 2009), and no specific work on the simulation of a gibbsite particle undergoing calcination appears to be available. A combination of dehydration, mass and heat transfer processes needs to be investigated to understand the controlling mechanisms, as well as to explore the effects of different operational parameters. Several important questions could be answered by modelling gibbsite calcination at the particle scale, for instance, the extent of particle breakage due to the build-up of internal water vapour pressure, the effect of external pressure on the decomposition rate, and the conditions favouring different thermal decomposition pathways. The aim of this chapter is to develop a dynamic model that can predict the distribution of temperature, gibbsite concentration and internal water vapour pressure in a single gibbsite particle as a function of calcination conditions in a range that is relevant to industrial practice.

There are several mathematical modelling approaches that are commonly used for describing the characteristics of a reacting particle that undergoes changes in physical structure and chemical composition. Typical modelling methodologies that are widely used for gas-solid reactions include homogeneous, unreacted core, grain, random pore and volumetric models (Chang and Kuo, 1999; Homma et al., 2005; Kasaoka et al., 1985; Molina and Mondragón, 1998; Silcox et al., 1989). In this chapter, the term “distributed model” will be used to denote a model in which the state variables are functions of particle radius. Generally, the selection of the modelling approach depends on the properties of the specific reactants and products, as well as on the modelling goals. These models and their selection criteria are reviewed by Molina and Mondragón (1998). The distributed model is particularly suitable for describing thermal decomposition involving porous and relatively porous solids. Mathematical simplicity, incorporation of meaningful physical and chemical parameters, and insight into the distribution profiles inside the particle are the main advantages of a 1-D distributed dehydration model. In this model, it is assumed that thermal decomposition proceeds in all parts of the particle; however, the dehydration rate varies spatially due to concentration and possibly temperature gradients.

Unlike common gas-solid reactions that have a gas-phase species as one of the reactants, in dehydration, as considered in this study, gaseous species are reaction products only and they may inhibit the reaction. No previous work has been reported on particle-scale modelling that combines dehydration kinetics and transport phenomena for gibbsite calcination. In addition, while the influence of external water vapour pressure has been studied before at relatively low temperatures, the effects of internal vapour pressure at elevated temperatures have not been explored. The model developed in this chapter allows for the inhibiting role of water vapour that is produced during gibbsite calcination. Internal and external mass and heat transfer resistances are combined with the dehydration rate expression in a distributed model, which can predict, for the first time, the characteristic heating behaviour and the internal vapour pressure build up in a gibbsite particle. Both these processes are relevant to the understanding of particle breakage and dehydration pathways. The model is validated against literature laboratory data at 873–923 K. While it is known that external water vapour pressure has a significant effect on gibbsite thermal transformation at low temperatures (Stacey, 1987; Candela and Perlmutter, 1986), our study extends the prediction to elevated temperatures. Sensitivity studies are conducted into the effects of particle size, heat and mass transfer coefficients, effective diffusivity and external water vapour pressure.

In the first part of this chapter, literature on the dehydration kinetics of gibbsite is briefly discussed, particularly the modelling of the effect of water vapour pressure and the estimated value of the activation energy. The model’s governing conservation and constitutive equations are then presented. Subsequently, the numerical approach employed for model solution is explained. Finally, model validation and sensitivity analyses are reported.

3.2. Mathematical model

3.2.1. Gibbsite dehydration kinetics

Depending on processing conditions, the calcination or thermal dehydration of gibbsite to alumina mainly takes place via two well-known dehydration and phase transition pathways. Heating rate, particle size distribution and water vapour pressure inside and around the particles are the dominant parameters that affect the dehydration pathway. Disregarding some additional intermediate chemical species, the two gibbsite dehydration pathways may be summarized as follows (Whittington and Ilievski, 2004):

1. Gibbsite transformation directly to alumina.
2. Gibbsite transformation to boehmite and then to alumina.

According to Whittington and Ilievski (2004) and Candela and Perlmutter (1992), boehmite formation is more likely to happen in high water vapour pressure environments and in coarse particles. However, even at high vapour pressures and for large particle sizes (> 50 µm), the majority (~70%) of gibbsite dehydrates directly to alumina via the first pathway. In this development of a model for gibbsite calcination, both dehydration pathways are effectively lumped into one and consider the reactant to be gibbsite and the product to be alumina. Determination of the distribution of intermediate chemical species, such as boehmite, and different alumina phases, is not a goal of this study, but is partly addressed in Chapter 5.

Gibbsite calcination is complicated in terms of its dehydration kinetics and dominant mechanisms. Different kinetic correlations have been presented in the literature for the thermal decomposition of gibbsite; some involve an activation energy that apparently changes with temperature and dehydration extent. In general for gas-solid reactions, in order to use a model such as the distributed model or shrinking core model to predict conversion (Levenspiel, 1999), a reaction rate based on solid and gas species concentration has been used widely in the literature. The majority of these investigations have been focused on gas-solid reactions that generally have the form: $aA_{(g)} + bB_{(s)} \rightarrow cC_{(g)} + dD_{(s)}$. Subsequently, a first order reaction based on gas (*A*) and solids (*B*) concentrations makes it possible to proceed using established results from the literature; these ignore the presence of reaction products. However, in calcination and dehydration cases, the water vapour component is a product, appearing on the right hand side of the reaction equation and causing a barrier to the dehydration progress. For example, in gibbsite calcination:

$$\underset{Gibbsite}{2Al(OH)_3} \rightarrow 3H_2O + \underset{Alumina}{Al_2O_3} \tag{3.1}$$

The effect of water vapour pressure (concentration) on gibbsite calcination has been reported by a number of investigators (Candela and Perlmutter, 1986, 1992; Stacey, 1987). This influence may be considered through the rate equation for gibbsite consumption:

$$(-r_G) = k_0 e^{-E_a/(RT)} C_W^{n_1} C_G^{n_2} \tag{3.2}$$

where C_W and C_G represent the water vapour and gibbsite concentrations, respectively, and n_1 and n_2 denote the corresponding orders of reaction. In the definition of molar concentrations, the particle volume was chosen as the basis for both solid and gas species. The dehydration reaction is assumed to be irreversible and to obey the Arrhenius law, as shown above. The calcination of 75 µm gibbsite particles at 473 K and different water vapour pressures (100–3200 Pa) was studied by Stacey (1987) who determined n_1 values of –1.3 and –0.4 for gibbsite to alumina and boehmite to alumina dehydration reactions, respectively. Candela and Perlmutter (1986) estimated the value of n_1 as –2. Their investigation was done under a controlled, pure water vapour atmosphere at pressures from 50 to 3000 Pa over a temperature range from 458 to 508 K. The negative value of n_1 means that increasing the water vapour concentration reduces the rate of gibbsite conversion, although the precise value of n_1 remains uncertain as seen above. More experimental investigations are needed into dehydration kinetics at conditions relevant to industrial calcination, which operates at temperatures and pressures much higher than those investigated by Stacey (1987) or Candela and Perlmutter (1986). In the absence of high temperature and high pressure data, and for simplicity of the model, in this study $n_1 = -1$ was considered. The value of the dehydration order with respect to gibbsite concentration is also uncertain for high temperature and pressure. The use of a fixed value of $n_2 = 1$ was selected, which is consistent with the few data that are available.

Regarding the activation energy, several kinetic studies have been published by different authors, but substantial uncertainty exists over the value for E_a. Candela and Perlmutter (1986) report E_a = 260±20 kJ/mol as the activation energy for gibbsite decomposition, which is reasonably consistent with the value of 272±12 kJ/mol presented by Stacey (1987). The E_a value estimated by Lopushan et al. (2007) was 150±12 kJ/mol, obviously not in agreement with either previous study. These three studies were mainly conducted at low and moderate temperatures. Jovanović et al. (1992) and Wang et al. (2006) report a change in the dominant dehydration mechanism at elevated temperatures. According to Jovanović et al. (1992) at 883 K, the mechanism of gibbsite thermal decomposition changes and this causes a decrease in the activation energy from 141 to 53 kJ/mol. Wang et al. (2006) confirm the low activation energies at elevated temperatures (823–923 K) and they estimated the E_a value for the thermal transformation of gibbsite to alumina as only 14 kJ/mol. Table 3.1 shows a summary of kinetic parameters reported in the literature.

In summary, the activation energy reported for gibbsite calcination appears to vary considerably with operational conditions. In this study, average k_0 and E_a values are estimated from dehydration rate constants fitted to literature conversion data.

Table 3.1 – Kinetic parameters for the calcination of gibbsite to alumina as reported by different authors.

Reference	Temperature range (K)	k_0	E_a (kJ/mol)	n_1	n_2
Stacey (1987)	473–623	$4.7 \pm 0.7 \times 10^{27}$ ($Pa^{1.3}/s$)	272±12	–1.3	-
Wang et al. (2006)	823–923	-	14	-	1
Lopushan et al. (2007)	443–783	-	150±12	-	-
Jovanović et al. (1992)	823–923	-	141 to 53	-	-
Candela and Perlmutter (1986)	458–508	-	260±20	–2	-
Rožić et al. (2001)	883–943	$8.85 \pm 0.7 \times 10^{-3}$ (1/s)	66.5	-	-

3.2.2. Model assumptions

The assumptions of the model are as follows:

- The particle is initially pure gibbsite.
- A dehydration reaction of the form of Eq. (3.1) takes place throughout the particle to produce water vapour and porous alumina. The rate of the dehydration reaction, which is given by Eq. (3.2), may vary through the particle.
- The particle is spherical with constant shape and constant outer diameter during the dehydration reaction. Possible changes due to particle breakage, aggregation and shrinkage processes have been neglected in the model.
- The particle porosity is assumed constant, with a value in between the very low porosity of gibbsite and the relatively high porosity of alumina.
- Convective heat and mass transfer processes take place between the particle and the environment; radiation heat transfer may also take place between the particle and the environment.
- All physical properties are assumed to be constant during dehydration. In particular, the effects of any structural changes on the diffusion coefficient are ignored. The effect of the diffusion coefficient is explored in Section 3.4.8.
- Heat and mass transfer fluxes inside the particle are modelled using an effective thermal conductivity and an effective diffusion coefficient, respectively, following the practice of Bird et al. (2002).

3.2.3. A 1-D, non-isothermal dehydration model for a single particle

A distributed single-particle dehydration model should take into account three interdependent processes: heat transfer in the particle and the surrounding gas film, the dehydration reaction, and mass transfer of water vapour in the particle and the gas film. A 1-D, spherically symmetrical, dynamic dehydration model that incorporates distributed water vapour and gibbsite mass balances and a distributed energy balance may be developed as follows.

The equation of continuity for the water vapour in terms of concentration, $C_W(r,t)$, over the domain $r \in (0, R_p)$, $t \in (0, t_{end}]$ is

$$\varepsilon \frac{\partial C_W}{\partial t} = \frac{1}{r^2} \frac{\partial}{\partial r} (D_e r^2 \frac{\partial C_W}{\partial r}) + \alpha(-r_G) \tag{3.3}$$

where ε is the particle porosity, t is time, r is radial position, D_e is the effective diffusion coefficient, α is the ratio of the stoichiometric coefficients of water vapour production to gibbsite consumption in Eq. (3.1) and r_G is the gibbsite dehydration rate defined in Eq. (3.2). Initially, the water vapour concentration inside the particle is assumed to be the same as the environment:

$$C_W(r,0) = C_{Wb} \tag{3.4}$$

At the centre of the particle, the water vapour profile is symmetric:

$$\left.\frac{\partial C_W}{\partial r}\right|_{r=0} = 0 \tag{3.5}$$

while at the surface of the particle, convective mass transfer takes place:

$$-D_e \left.\frac{\partial C_W}{\partial r}\right|_{r=R_p} = K(C_W|_{r=R_p} - C_{Wb}) \tag{3.6}$$

Here, R_p is the particle radius, K is the mass transfer coefficient and C_{Wb} is the water vapour concentration in the environment.

The gibbsite concentration at any point in the particle is deduced from the dehydration rate:

$$\frac{\partial C_G}{\partial t} = r_G \tag{3.7}$$

The initial concentration of gibbsite is considered to be the same in all parts of the particle:

$$C_G(r,0) = C_{G0} \tag{3.8}$$

The energy balance equation for the reacting gibbsite particle during dehydration may be written as:

$$\rho C_p \frac{\partial T}{\partial t} = \frac{1}{r^2}\frac{\partial}{\partial r}(\lambda_e r^2 \frac{\partial T}{\partial r}) - \Delta H(-r_G) \tag{3.9}$$

where ρ, C_p and λ_e are, respectively, the molar density, molar heat capacity and effective thermal conductivity of the gibbsite particle, and ΔH is the dehydration enthalpy of gibbsite. Initially, the particle temperature is uniform at the ambient temperature:

$$T(r,0) = T_0 \tag{3.10}$$

Due to symmetry the heat flux at the particle centre is zero:

$$\left.\frac{\partial T}{\partial r}\right|_{r=0} = 0 \tag{3.11}$$

The particle receives the majority of the required energy for calcination from the surroundings via convection and radiation at the particle surface. The radiation contribution has been linearised around environmental temperature T_b and lumped with the convection term:

$$-\lambda_e \left.\frac{\partial T}{\partial r}\right|_{r=R_p} = h(T|_{r=R_p} - T_b) \tag{3.12}$$

where h is a combined convective / radiative heat transfer coefficient.

Finally, the gibbsite conversion X and gibbsite mass fraction W_G, averaged through the particle, at any time of interest can be calculated by

$$X = 1 - \frac{3\int_0^{R_p} r^2 C_G(r)\,dr}{R_P^3\, C_{G0}} \tag{3.13}$$

and

$$W_G = \frac{(1-X)M_G}{(1-X)M_G + X\beta M_A} \tag{3.14}$$

where M_G and M_A are the molecular weights of gibbsite and alumina, respectively, and β is the ratio of stoichiometric coefficients of alumina to gibbsite in Eq. (3.1).

The ideal gas law is used to relate the concentration of water vapour to its partial pressure in the bulk gas: $C_{Wb} = P_{Wb}/RT_b$. At higher pressures, other equations of state, for example Peng-Robinson or Soave-Redlich-Kwong, may be used.

3.2.4. Model solution

Time and radial position are the independent variables, and the main dependent variables in this modelling study are T, C_G and C_W. The last variable is of high importance for the interpretation of the role of water vapour pressure in gibbsite calcination. The governing equations of the distributed model, Eqs. (3.2)–(3.12), were solved simultaneously along with corresponding initial and boundary conditions to find the values of the dependent variables as functions of time and radial position. The numerical solution was obtained by applying the *MATLAB*® (2010b) *pdepe* algorithm, which uses the method of Skeel and Berzins (1990) for spatial discretisation, and performs time integration with a variable-order, multi-step solver. Eqs. (3.13) and (3.14) were evaluated through post-processing, with the integral in Eq. (3.13) being calculated by trapezoidal integration using *MATLAB*'s *trapz* routine. The parameter values used in the simulations are shown in Table 3.2.

The *MATLAB* Optimization Toolbox was used to fit the model kinetic parameters to the experimental data of Wang et al. (2006) via nonlinear regression calculations, as discussed in the next section.

3.3. Estimation of kinetic parameters and sensitivity study

Wang et al. (2006) performed calcination experiments at elevated temperatures (823 to 923 K) in an autoclave. The particle size ranged from 20 nm to 2000 µm, with the mean particle size being approximately 100 µm. They measured the average gibbsite mass fraction in the particles as a function of time and estimated dehydration rate constants with regression analysis without considering any internal or external resistances to mass or heat transfer. However, heat transfer on the particle boundary and mass transfer inside the particle play a significant role in controlling the progress of gibbsite dehydration. In this study, kinetic parameters are estimated based on the particle dehydration model developed in Section 3.2. Two sets of experimental data (at 873 and 923 K) reported by Wang et al. (2006) were used for parameter estimation and one set (at 898 K) was used to validate the model.

In order to find the best values of the parameters k_0 and E_a, the following objective function was minimised:

$$f(k_0, E_a) = \sum_{T_b=\{873,923\mathrm{K}\}} \sum_{i=1}^{N_{Tb}} (W_{G,i} - W_{G,exp,i})^2 \tag{3.15}$$

where N_{Tb} is the number of temporal data points i from Wang et al. (2006) at temperature T_b, $W_{G,i}$ is the mass fraction of gibbsite predicted by the model via Eq. (3.14) and $W_{G,exp,i}$ is the experimental gibbsite mass fraction measured by Wang et al. (2006).

Since the regression problem and model are nonlinear, an isothermal analysis was first performed by setting $T(r,t) \approx T_b$ to estimate the dehydration constant $k = k_0 e^{-E_a/(RT)}$ at 873 and 923 K. The approximate activation energy and pre-exponential coefficient were obtained from the slope and intercept of the straight line produced by plotting ln(k) against $1/T_b$. These values were used as initial guesses in the full non-isothermal numerical analysis. The constant temperature reported by Wang et al. (2006) was used as the external temperature, T_b. More precise kinetic values for k_0 and E_a obtained by non-isothermal analysis were 2.5×10^{13} mol/m^3 s and 131 kJ/mol, respectively. Figure 3.1 presents a comparison of experimental results (Wang et al., 2006) and the results of the fitted model at 873 and 923 K for the evolution of the gibbsite mass fraction.

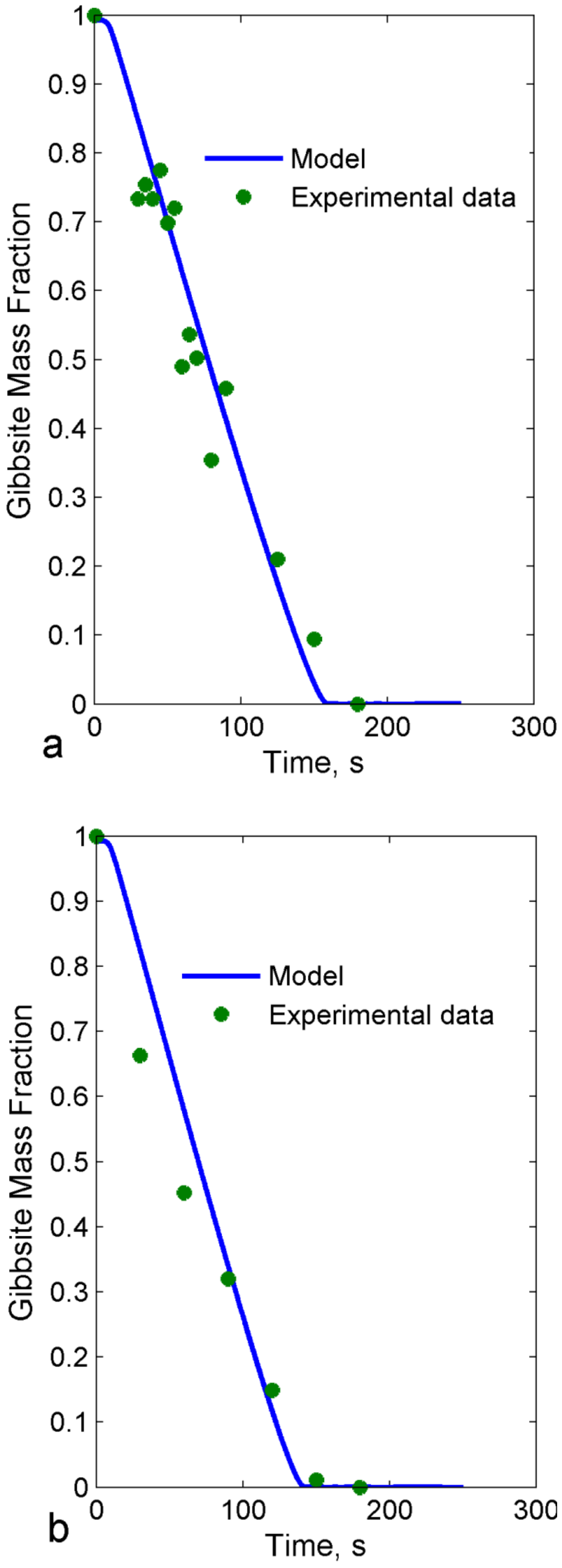

Figure 3.1 – Evolution of gibbsite mass fraction predicted by the model using fitted kinetic parameters and original experimental data (Wang et al., 2006) at (a) 873 K and (b) 923 K.

Table 3.2 – Model parameters used for validation and in all sensitivity studies unless noted otherwise.

Parameter	Value	Reference / comment
C_{G0} (mol/m^3)	3.1×10^4	Wefers and Misra (1987)
C_p (J/mol K)	80	Wefers and Misra (1987)
D_e (m^2/s)	7×10^{-10}	Value for alumina; Fowler et al. (1977)
D_p (μm)	100	Experimental conditions of Wang et al. (2006); $R_p = D_p/2 = 50$ μm
E_a (kJ/mol)	131	Found by parameter estimation – see Section 3.3.
h (W/m^2 K)	1.5	Combines radiation and convection; Incropera et al. (2007)
ΔH (kJ/mol)	147	Beyer et al. (1989)
k_0 (mol/m^3 s)	2.5×10^{13}	Found by parameter estimation – see Section 3.3.
K (m/s)	0.1	Estimated based on minimum Sherwood number (Sh = 2)
M_A (g/mol)	102	-
M_G (g/mol)	80	-
n_1	–1	Discussed in Section 3.2.1
n_2	1	Wang et al. (2006)
P_{Wb} (kPa)	3	Typical environmental water vapour pressure
R (J/mol K)	8.314	Ideal gas constant
T_b (K)	873, 893, 923	Experimental conditions of Wang et al. (2006)
T_0 (K)	298	Particle initially at ambient temperature
α	1.5	From Eq. (3.1)
β	0.5	From Eq. (3.1)
ε	0.3	Altundoğan and Tümen (2003)
λ_e (W/m K)	19	Wefers and Misra (1987)
ρ (mol/m^3)	3.1×10^4	Wefers and Misra (1987)

Model predictions for the concentration distribution of water vapour inside the gibbsite particle are found to be sensitive to the effective diffusion coefficient. For water vapour diffusion in alumina, a wide range of diffusivities are reported in the literature (Doremus, 2006; Fowler et al., 1977). Ideally, D_e should be a function of temperature and dehydration extent or composition, since the particle porosity changes during dehydration. Due to the lack of such a function, in most of this study the constant porosity value ε and constant D_e reported by Fowler et al. (1977) for alumina were used; however, Section 3.4.8 examines the effect of different D_e values.

3.3.1. Validation of the model

A set of the experimental data of Wang et al. (2006) at 898 K was used to independently validate the model, as presented in Figure 3.2. The model prediction, using kinetic parameters estimated from the 873 K and 923 K data, are in good agreement with Wang et al.'s data at 898 K.

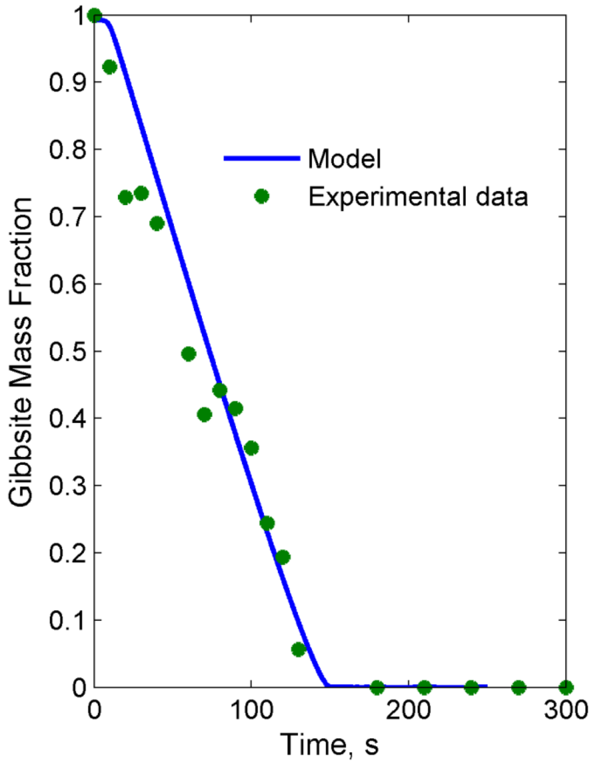

Figure 3.2 – Validation of the model against independent experimental data (Wang et al., 2006) at 898 K.

3.4. Model analysis

This section reports temperature and composition profiles inside the particle predicted by the model, and it also presents sensitivity studies for the model parameters. The conditions for each study are those given in Table 3.2, except where otherwise noted.

3.4.1 Temperature profile inside the particle

Figure 3.3 shows the predicted temporal and spatial temperature distribution in a reacting 100 µm diameter gibbsite particle at 898 K. At any time, the temperature is almost uniform throughout the particle cross-section. This result is consistent with a lumped capacity model for the particle energy balance. The Biot number criterion, Bi = $hD_p/\lambda_e < 0.1$, has been used to confirm particle isothermality, even in the presence of a solid-phase reaction, such as pyrolysis (Chern and Hayhurst, 2010). For particles 100 µm in diameter fluidized by air at 400 K, the heat transfer coefficient between the gas and the particles would be around 420 W/m^2 K according to Kunii and Levenspiel (1991). A combination of the above parameters with a conservative particle thermal conductivity of 16 W/m K for alumina at 400 K (Shackelford and Alexander, 2001), yields Bi = 0.0026 << 0.1, which confirms that it is reasonable to assume isothermal conditions inside the particle. Smaller particles, lower heat transfer coefficients and higher particle thermal conductivities would satisfy the isothermality criterion even more easily. Conversely, in the work of Wang et al. (2006), the gibbsite-alumina particle size ranged up to 2000 µm, and at high temperatures the effective gas-particle heat transfer coefficient can increase further due to a significant radiative contribution. For these conditions, it would be possible that gibbsite particles could exhibit Bi numbers larger than 0.1, leading to a non-uniform spatial temperature profile.

The finding of uniform temperature inside the particle suggests that the distributed energy balance, Eqs. (3.9)–(3.12), could be replaced with a lumped capacity energy balance:

$$\rho C_p \frac{4}{3}\pi R_p^3 \frac{dT}{dt} = -\Delta H \int_0^{R_p} 4\pi r^2 (-r_G) dr - h 4\pi R_p^2 (T - T_b) \tag{3.16}$$

which has the initial condition:

$$T(0) = T_0 \tag{3.17}$$

It should be noted, however, that while the reacting particle has a spatially uniform temperature, it is not temporally isothermal. The particle internal temperature is unsteady, increasing over time as dehydration progresses as seen in Figure 3.3. In the first few seconds, the particle temperature shows a very rapid rise. This shock is damped by the demand for energy as the endothermic calcination reaction begins.

From about 10 to 130 s, the temperature rises slowly as approximately 90% of the particle reacts. At ~130 s, the dehydration reaction slows down due to depletion of fresh reactant and the mass diffusion resistance. After ~130 s, the temperature again increases quickly since little heat is consumed by the calcination reaction, and the particle finally reaches the environmental temperature. It is a significant achievement of the model that the predicted temperature history reproduces well the shape and temperature plateau during gibbsite thermal decomposition found in the independent experimental work of Stacey (1987). In contrast to the uniform temperature field inside the particle, the dehydration reaction takes place at a greater rate at the particle surface compared to its interior due to the high internal mass diffusion resistance and the effect of water vapour concentration on the dehydration rate, as discussed in the next section.

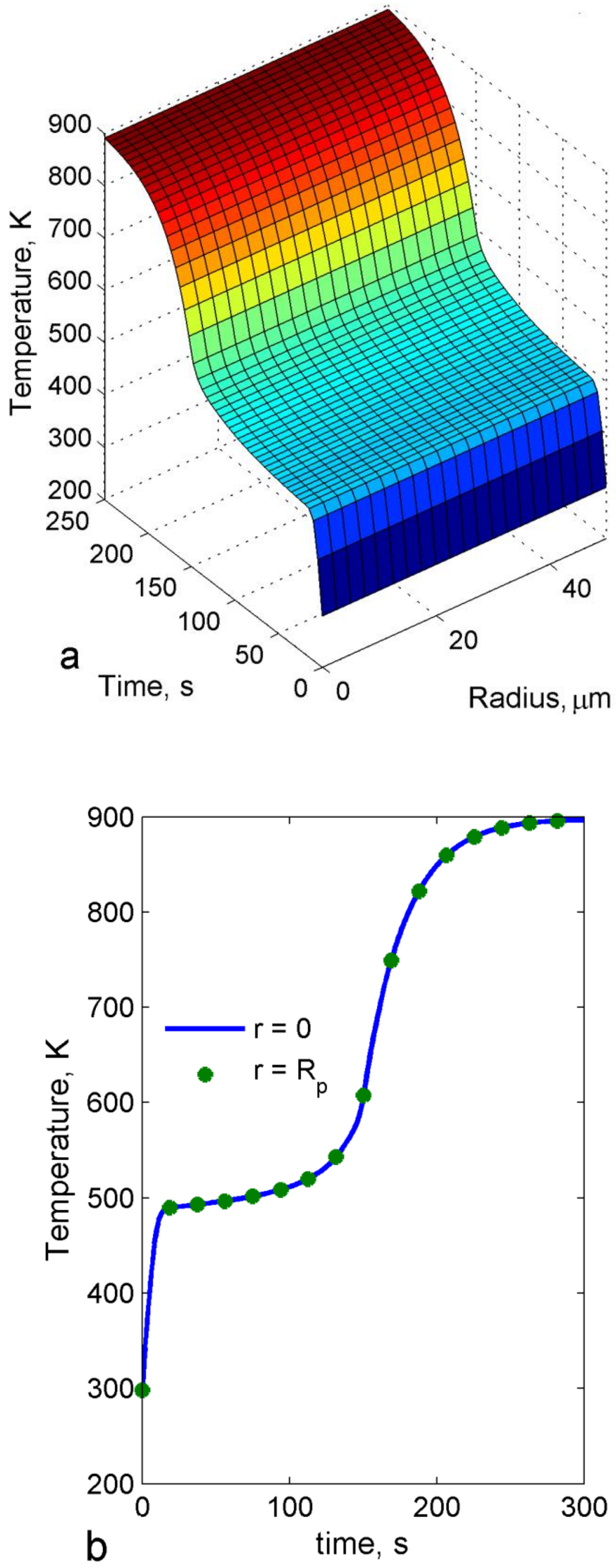

Figure 3.3 – Temperature evolution as a function of time and particle radius (a), and temperature evolution at the particle centre and outer boundary (b); both for T_b=898 K.

3.4.2 Water vapour profile inside the particle

Several aspects of gibbsite thermal decomposition may be attributed to the water vapour pressure inside and around the reacting particle. As water vapour pressure affects the dehydration and phase transformation reaction pathways and subsequently the formation of different alumina phases, having some knowledge of this distributed parameter will help to explain experimental and industrial observations. In addition, particle breakage, which is frequently reported for high temperature calcination, could potentially be monitored and controlled using model predictions of the pressure increase inside the particle over its calcination period.

Figure 3.4 shows the predicted spatial and temporal distribution of water vapour pressure inside a gibbsite particle reacting at 898 K. Note that the surrounding vapour pressure is 3 kPa, or 0.03 atm. A significant increase in internal vapour pressure over time can be seen in Figure 3.4(b). The pressure build up is a maximum at the particle centre and is predicted to be very high at elevated temperatures. This pressure could contribute to particle fracturing under flash calcination conditions, which involve high temperatures and a short calcination time, especially for large particles. When the dehydration is complete, the vapour pressure inside the particle quickly decreases due to diffusion of the remaining vapour to the particle surface. Finally, the internal vapour pressure will become uniform at the bulk gas pressure.

Since higher vapour pressure favours boehmite formation (Candela and Perlmutter, 1992; Wang et al., 2006; Whittington and Ilievski, 2004) it can be concluded that the outer layer of a particle is more likely to convert directly to the final product (alumina), while intermediate boehmite formation is more probable at the particle centre where the vapour pressure is higher.

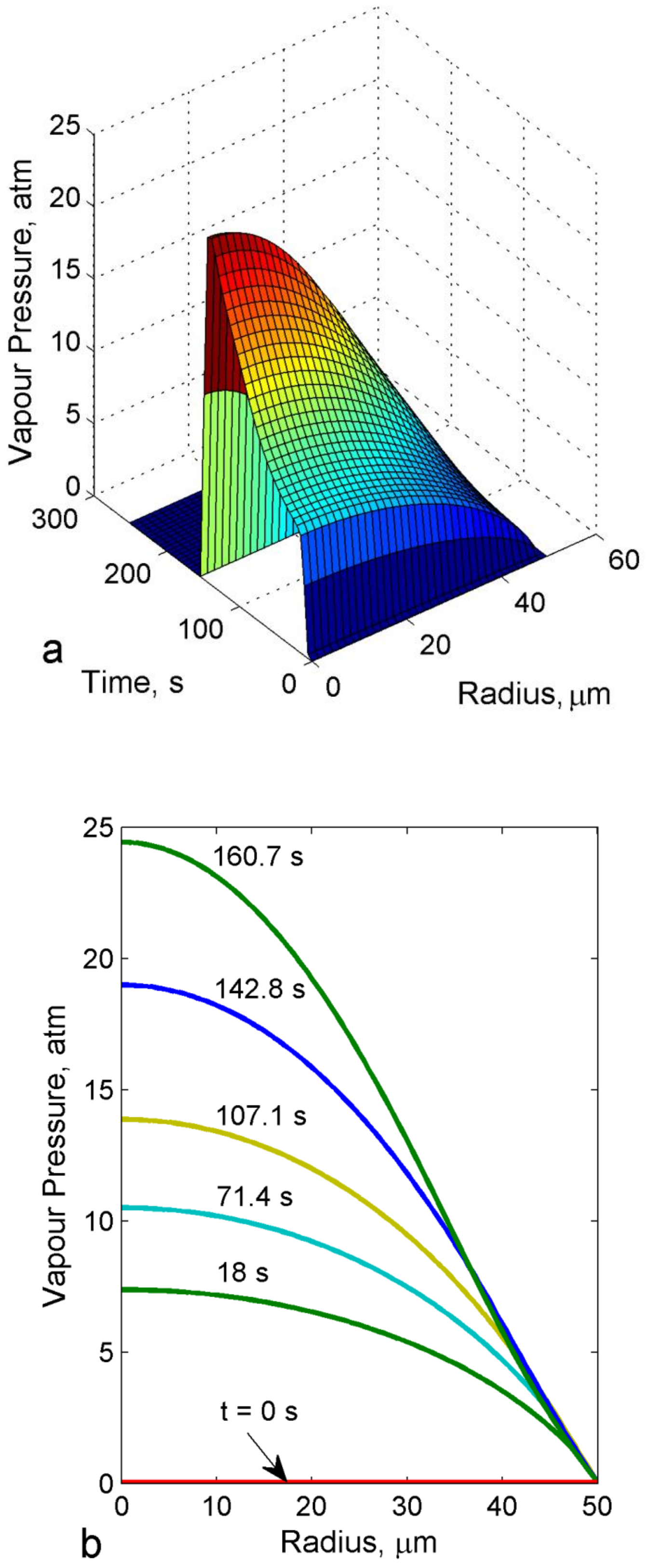

Figure 3.4 – Evolution of water vapour pressure as a function of time and particle radius (a), and water vapour pressure as a function of particle radius at selected times (b); both for T_b=898 K.

3.4.3 Gibbsite concentration profile inside the particle

Figure 3.5 shows the gibbsite concentration as a function of radial position at several times during calcination. Near the particle centre, the gibbsite concentration is reasonably uniform, particularly in the early stages of dehydration. In the outer layers of the particle, however, a considerable difference in gibbsite concentration develops. A difference between the behaviour of the central and outer regions of the particle shown in Figure 3.5 is supported by the experimental results of Perlander (2010).

In gibbsite calcination, temperature and water vapour pressure are the dominant parameters controlling dehydration progress. While the temperature is the same at all points in the particle cross-section at a given time, the water vapour pressure is not. As can be seen in Figure 3.4(b), the vapour gradient is steeper near the particle surface in comparison to the centre, particularly at the beginning of dehydration. Thus, different dehydration rates at the outer surface and particle centre may be reasonably attributed to the water vapour pressure profile.

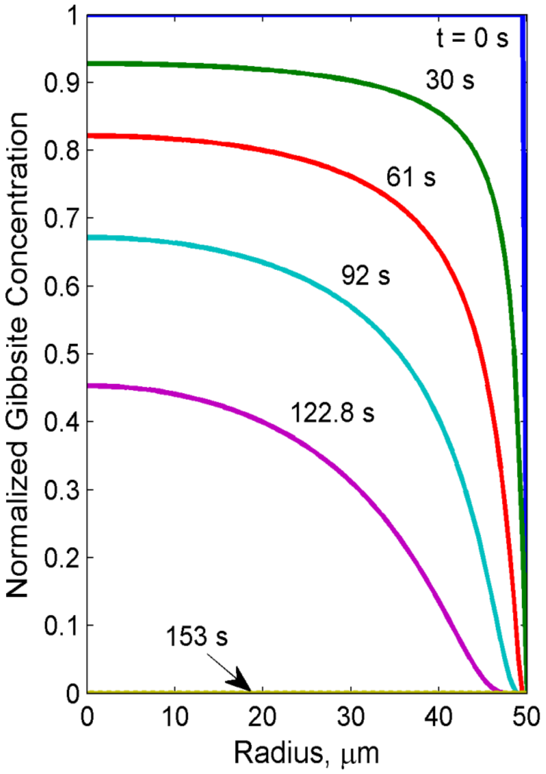

Figure 3.5 – Normalized gibbsite concentration (C_G/C_{G0}) as a function of particle radius at different times; T_b=898 K.

3.4.4 Effect of particle size

Gibbsite calcination behaviour is a strong function of particle size. Temperature history, internal water vapour pressure and gibbsite concentration are all affected by particle size as can be seen in Figures 3.6 and 3.7. Particle temperature history is illustrated in Figure 3.6. Coarser particles take a longer time to reach the environmental temperature. This delay is mainly due to the longer dehydration period, during which the heat penetrating from outside the particle is consumed to drive the dehydration reaction. Regarding the internal vapour pressure, the maximum value will occur at the end of dehydration, as seen in Figure 3.7. The maximum pressure value depends strongly on particle size. The larger the particle, the higher the vapour pressure build up inside the particle, increasing the potential for the parallel dehydration reaction that produces boehmite, as well as for physical damage to the particle structure, such as crack formation and particle breakage.

3.4.5 Effect of external water vapour pressure

Recently, gibbsite calcination under high pressure conditions, and hence high external water vapour pressures, was investigated at the pilot-scale (Williams and Misra, 2011). The driver for their work was a low effective fuel consumption of 1.55 GJ/t Al_2O_3. This is lower than the best current practice at atmospheric pressure, which has a fuel consumption of around 2.79 GJ/t Al_2O_3 (Klett et al., 2011). In a high-pressure calciner, the water vapour pressure around particles can be thirty times higher than in atmospheric calciners. As mentioned earlier, particle breakage at high temperature, including anecdotal evidence on explosive breakage (Perlander, 2010), has been observed in industrial operations, but there is a lack of quantitative analysis of the potential causes and also of appropriate methods to prevent it. This study provides insight on the influence of the external water vapour pressure on dehydration behaviour and some quantification of this industrially-important phenomenon.

As can be seen in Figure 3.8(a), the model predicts only a small effect of the external water vapour pressure on the gibbsite conversion rate. At an external water vapour pressure of 0 atm, the dehydration time is around 150 s, while at 15 atm it increases to around 160 s, a change of less than 10%. However, Figure 3.8(b) shows in these two cases that the evolution of the maximum vapour pressure inside the particle is

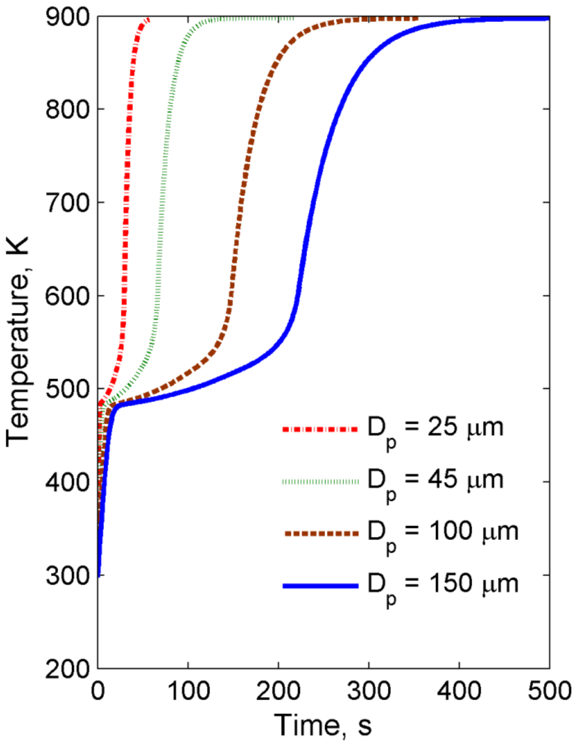

Figure 3.6 – Evolution of particle temperature for different particle sizes; T_b=898 K.

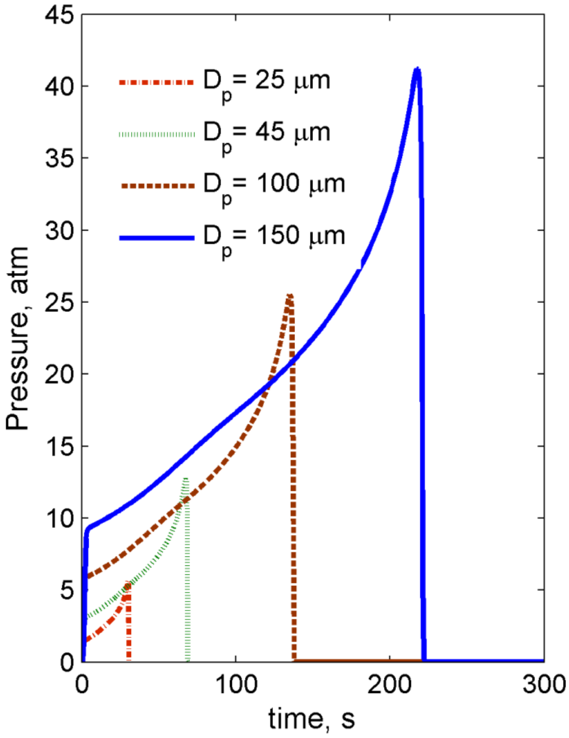

Figure 3.7 – Evolution of maximum internal vapour pressure for different particle sizes; T_b=898 K.

different. For external pressures between 0 and 15 atm, the maximum internal pressure is approximately constant at around 28 atm, while above 15 atm external pressure, the maximal internal pressure increases. It is proposed that particle breakage would be more affected by the *difference* between the peak internal pressure and the external pressure, than by the absolute value of the internal pressure. At higher external pressures, the pressure difference between inside and outside the particle is lower, suggesting a reduced possibility of breakage.

The calciner operating pressure could be optimized with respect to capital and operating costs in the context of other process demands. However, a qualitative examination of the results in Figure 3.8 suggests the following reasons why an external water vapour pressure of 15 atm may be preferred for industrial operation in comparison to the higher or lower pressures considered in this study. First, the *difference* between internal and external pressure is less for 15 atm than for the lower pressures, 1 atm for instance, which should decrease the potential for breakage. Second, 15 atm is lower than 30 atm, which would result in lower costs for equipment, maintenance and operation. Third, little delay in the completion of dehydration is caused by increasing the external pressure from 0 to 15 atm at the temperatures of interest (823 K and higher). Fourth, it is possible that a more homogenous and stronger, more attrition-resistant alumina product (Sucech and Misra, 1986) may be produced at 15 atm external vapour pressure, as the vapour profile inside the particle is flatter in contrast to that at lower pressures.

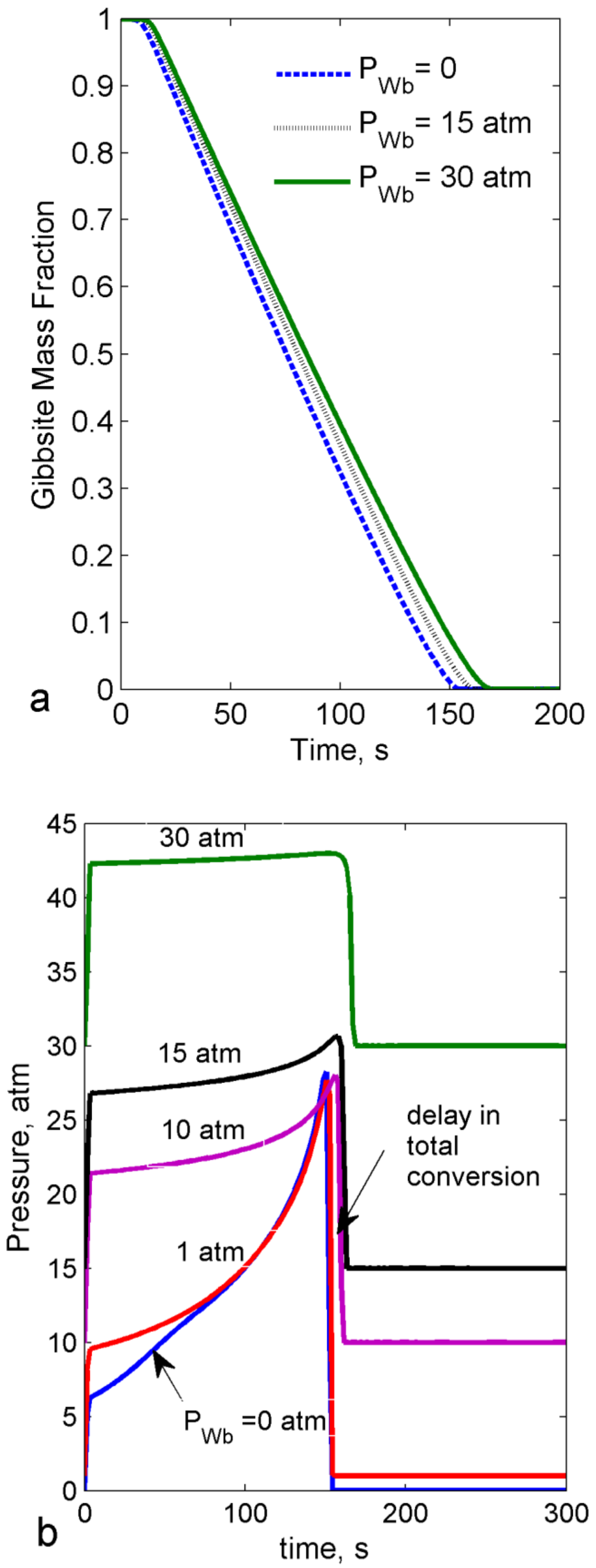

Figure 3.8 – The effect of external water vapour pressure (P_{Wb}) at T_b=898 K on the evolution of (a) gibbsite mass fraction, and (b) maximum internal water vapour pressure.

3.4.6 Effect of heat transfer coefficient

To test the sensitivity of the model to external heat transfer, the dehydration rate of gibbsite is studied for three different values of the heat transfer coefficient, h. Note that all other parameters, including k and E_a, are fixed at the values reported, which were deduced from model fitting using h = 1.5 W/m^2 K. As can be seen in Figure 3.9(a), conversion time is strongly affected by the heat transfer coefficient, emphasising the difference in reaction rate for a stagnant system, such as autoclave, in contrast to a fluidized system with a higher h, such as a circulating fluidized bed reactor. Further, the process intensification achieved in industrial practice through replacement of rotary kilns with fluidized bed reactors, can be partly explained by the enhanced gas-particle heat transfer rate.

Figure 3.9(b) illustrates that, for the original best-fit dehydration kinetics reported in Table 3.1, the gibbsite particles in an environment with a low heat transfer coefficient experience a moderate temperature gradient in time with a long delay in the completion of dehydration. On the other hand, for particles that experience a high heat transfer coefficient, as would occur in a fluidized bed for instance, the conversion of gibbsite to alumina is quickly completed and they undergo very rapid heating. An important conclusion of this analysis is that estimation of the rate of single gibbsite particle calcination needs model parameters corresponding to the correct operating environment. The model becomes less sensitive to the heat transfer coefficient as h is increased, for example by increasing the local gas velocity.

3.4.7 Effect of mass transfer coefficient

The effect of mass transfer rate in the surrounding gas layer on the overall dehydration rate was investigated by running the model for different mass transfer coefficients K, which represent various hydrodynamic environments. A low external mass transfer coefficient could potentially influence the rate of gibbsite conversion and the particle temperature history. Estimation of the minimum K value, corresponding to diffusion from an isolated sphere ($Sh=KD_p/D_b=2$), which could approximate an autoclave, yields $K \sim 0.1$ m/s. No significant change was observed in any of the model outputs for this K value or higher.

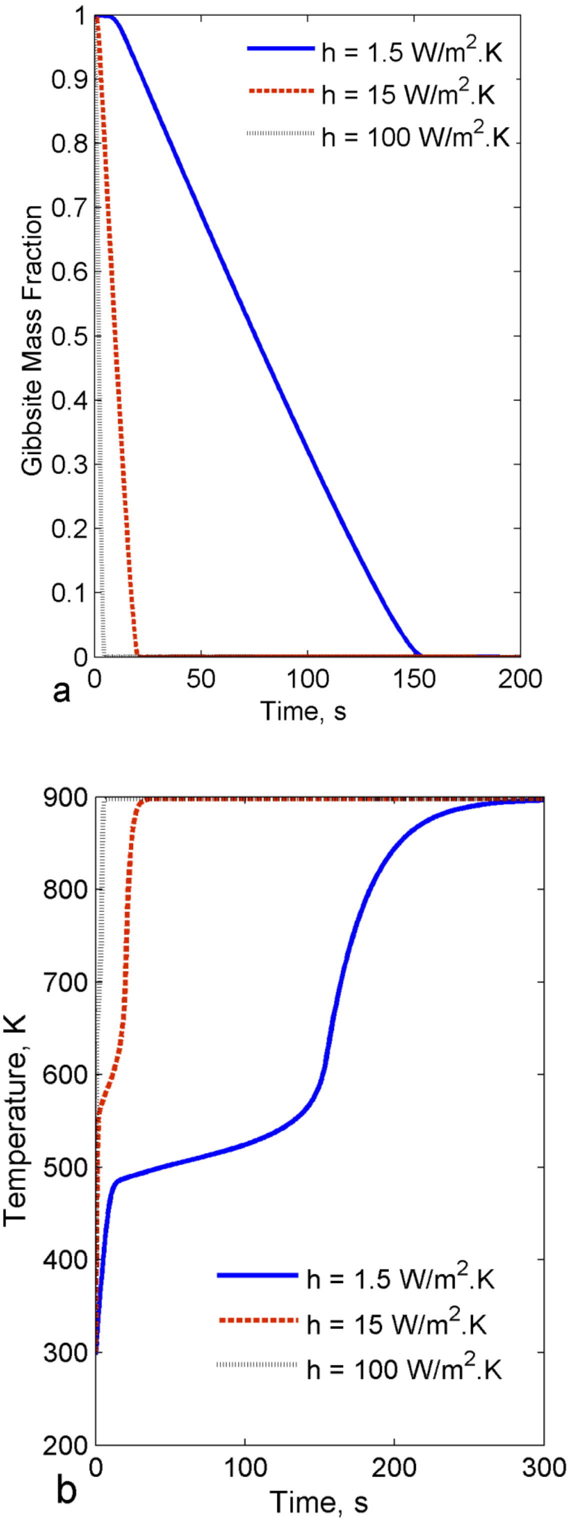

Figure 3.9 – The effect of heat transfer coefficient at T_b=898 K on (a) the change in gibbsite mass fraction over the reaction period, and (b) the evolution of the particle temperature.

Even for *K* values conservatively lower than 0.1 m/s, for example 0.01 and 0.001 m/s, no significant effect on model performance was detected. Mass transfer coefficients would certainly be higher than 0.1 m/s in a fluidized bed. This indicates that the mass transfer resistance in the surrounding gas layer can be ignored safely for practical gibbsite calcination, and that internal diffusion and dehydration control the rate of mass transfer.

The finding of the insensitivity of the results to K suggests that the model could be simplified by replacing Eq. (3.6), the Robin boundary condition for external mass transfer, by a simpler fixed concentration Dirichlet boundary condition:

$$C_W\big|_{r=R_p} = C_{Wb} \tag{3.18}$$

3.4.8 Effect of effective diffusivity

The model is very sensitive to the value of the effective diffusivity, D_e. Figure 3.10 illustrates how the maximum internal water vapour pressure changes if the effective diffusion coefficient is varied. Reliable values for the effective diffusivity for this system are not available in the open literature. However, if consideration is restricted to a meaningful range for the internal water vapour pressure, realistic values for the applicable effective diffusivity can be proposed. Very high and low internal pressures are not acceptable physically. Tentatively, it is proposed that the reasonable range of the effective diffusivity is narrow and between 2×10^{-10} and 2×10^{-9} m^2/s, which is consistent with the D_e value for alumina reported in Fowler et al. (1977). The model currently uses a constant D_e since that is the simplest assumption that is supported by any experimental data, but further investigations could consider the influence of temperature and structural changes brought about by the dehydration on the diffusivity.

3.5. Summary

One of the main purposes of this study was to quantify the role of internal and external water vapour pressure on calcination of a single gibbsite particle, which has before been dealt with only qualitatively. A model that couples dynamic, spatially-distributed mass and energy balances with appropriate thermal transformation

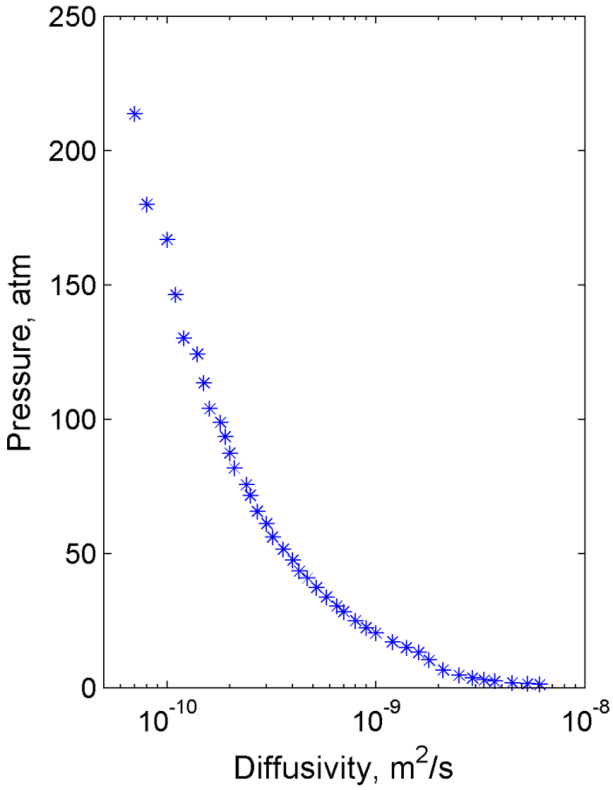

Figure 3.10 – Influence of the effective diffusivity value on the maximum water vapour pressure inside the particle at T_b=873 K.

kinetics has been developed. The model, which predicts distributed gibbsite and water concentrations, and the temperature profile inside the particle, was validated against laboratory gibbsite calcination data in a temperature range from 873 to 923 K. Based on the literature experimental data, assuming an order of 1 with respect to gibbsite concentration and order of –1 with respect to water vapour pressure, the thermal transformation rate parameters were estimated as $k_0=2.5\times10^{13}$ mol/m^3 s and E_a =131 kJ/mol.

For the first time, the evolution of temperature and internal pressure in a gibbsite particle undergoing thermal dehydration was predicted by a mathematical model. The water vapour pressure at the centre of a dehydrating gibbsite particle can reach values in the order of 100 atm, which can help explain the occurrence of particle fracture and the possibility of forming a boehmite phase. The assumed effective diffusion coefficient has a strong influence on the model prediction; the lower the effective diffusivity, the higher the value of the maximum particle internal pressure.

The model prediction was shown to be very sensitive to the heat transfer coefficient, effective diffusivity, particle size and external pressure, but relatively less sensitive to the external mass transfer coefficient and particle thermal conductivity.

The model results suggest that gibbsite particles undergoing calcination are spatially uniform in terms of temperature, and are insensitive to the external mass transfer environment. This means that the proposed model can potentially be simplified by replacing the distributed energy balance by a lumped capacity energy balance, and by replacing the external mass transfer Robin boundary condition by a given concentration Dirichlet boundary condition.

The distributed model developed in this chapter is compared to a shrinking core model proposed in Chapter 4. Further this model is the one that will be utilized in the integrated, multi-scale model in Chapter 6.

Nomenclature

Bi	Biot number, [–]
C_p	Particle molar heat capacity, [J/mol K]
C_G	Gibbsite molar concentration, [mol/m^3]
C_{G0}	Initial gibbsite molar concentration, [mol/m^3]
C_W	Water vapour molar concentration, [mol/m^3]
C_{Wb}	External water vapour molar concentration, [mol/m^3]
D_b	Water diffusivity in environment, [m^2/s]
D_e	Effective water diffusivity in particle, [m^2/s]
D_p	Particle diameter, [μm]
E_a	Activation energy, [kJ/mol]
h	Heat transfer coefficient, [W/m^2 K]
ΔH	Enthalpy of gibbsite dehydration, [kJ/mol]
k	Dehydration rate constant, [mol/m^3]
k_0	Pre-exponential coefficient, [mol/m^3]
K	Mass transfer coefficient, [m/s]

M_A	Alumina molecular weight, [g/mol]
M_G	Gibbsite molecular weight, [g/mol]
n_1	Reaction order with respect to water vapour concentration, [–]
n_2	Reaction order with respect to gibbsite concentration, [–]
N_{Tb}	Number of experimental data points at temperature T_b, [–]
P_{Wb}	External water vapour pressure, [kPa]
r	Radial position, [μm]
r_G	Gibbsite dehydration rate, [mol/m^3]
R	Universal gas constant, [J/mol K]
R_p	Particle radius, [μm]
Sh	Sherwood number, [–]
t	Time, [s]
t_{end}	End time of simulation, [s]
T	Temperature, [K]
T_b	External temperature, [K]
T_0	Initial particle temperature, [K]
W_G	Gibbsite mass fraction, [–]
X	Gibbsite conversion, [–]

Greek symbols

α	Ratio of water to gibbsite stoichiometric coefficients, [–]
β	Ratio of alumina to gibbsite stoichiometric coefficients, [–]
ε	Particle porosity, [–]
λ_e	Effective particle thermal conductivity, [W/m K]
ρ	Particle molar density, [mol/m^3]

References

Altundoğan, H.S., & Tümen, F. 2003. Removal of phosphates from aqueous solutions by using bauxite II: The activation study. *Journal of Chemical Technology & Biotechnology*. 78, 824–833.

Beyer, H.K., Borbély, G., Miasnikov, & P. Rózsa, P. 1989. A new potential large-scale application of zeolites as fire-retardant material, in: Karge, H.G., Weitkamp, J. (Eds.), *Zeolites as Catalysts, Sorbents, and Detergent Builders: Applications and Innovations*, Elsevier, Amsterdam, pp. 635–644.

Bird, R.B., Stewart, W.E., & Lightfoot, E.N. 2002. *Transport phenomena*, second ed. John Wiley, New York, p. 565.

Candela, L., & Perlmutter, D.D. 1986. Pore structure and kinetics of the thermal decomposition of $Al(OH)_3$. *AIChE Journal*. 32, 1532–1545.

Candela, L., & Perlmutter, D.D. 1992. Kinetics of boehmite formation by thermal decomposition of gibbsite, *Industrial & Engineering Chemistry*. 31, 694–700.

Chang, Y.I., & Kuo, J.A. 1999. Application of the three-stage shrinking core model in the transport of reactive gas in the porous media. *Journal of Petroleum Science and Engineering*. 22, 205–216.

Chern, J.S., & Hayhurst, A.N. 2010. A simple theoretical analysis of the pyrolysis of an isothermal particle of coal. *Combustion and Flame*. 157, 925–933.

Doremus, R.H. 2006. Diffusion in alumina. *Journal of Applied Physics*. 100, 101301.

Fowler, J.D., Chandra, D., Elleman, T.S., Payne, A.W., & Verghese, K. 1977. Tritium diffusion in Al_2O_3 and BeO. *Journal of the American Ceramic Society*. 60, 155–161.

Gan, B.K., Madsen, I.C., & Hockridge, J.G. 2009. *In situ* X-ray diffraction of the transformation of gibbsite to α-alumina through calcination: Effect of particle size and heating rate, *Journal of Applied Crystallography*. 42, 697–705.

Homma, S., Ogata, S., Koga, J., & Matsumoto, S. 2005. Gas-solid reaction model for a shrinking spherical particle with unreacted shrinking core. *Chemical Engineering Science*. 60, 4971–4980.

Incropera, F.P., DeWitt, D.P., Bergman, T.L., & Lavine, A.S. 2007. *Fundamentals of Heat and Mass Transfer*, sixth ed. John Wiley, Hoboken.

Jovanović, N., Novaković, T., Janaćković, J., & Terlecki-Baričević, A. 1992. Properties of activated alumina obtained by flash calcination of gibbsite. *Journal of Colloid and Interface Science*. 150, 36–41.

Kasaoka, S., Sakata, Y., & Tong, C. 1985. Kinetic evaluation of the reactivity of various coal chars for gasification with carbon dioxide in comparison with steam. *International Journal of Chemical Engineering*. 25, 160–175.

Klett, C., Reeb, B., Missalla, M., & Schmidt, H.-W. 2011. Methods to reduce operating costs in circulating fluidized bed calcination. In: Lindsay, S.J. (Ed.), *Light Metals 2011*. John Wiley & Sons, New York, pp. 125–130.

Kunii, D., & Levenspiel, O. 1991. *Fluidization Engineering,* second ed. Butterworth-Heinemann, Boston, pp. 268–271.

Levenspiel, O., 1999. *Chemical Reaction Engineering,* third ed. John Wiley & Sons, New York, pp. 568–570.

Lopushan, V.I., Kuznetsov, G.F., Pletnev, R.N., & Kleshev, D.G. 2007. Kinetics of phase transitions of gibbsite during heat treatment in air and in water vapour. *Refractories and Industrial Ceramics*. 48, 378–382.

Marsh, C., 2009. CFD Modelling of alumina calciner furnaces. In: *Seventh International Conference on CFD in the Minerals and Process Industries,* Melbourne, Australia, 9–11 December 2009.

Molina, A., & Mondragón, F. 1998. Reactivity of coal gasification with steam and CO_2. *Fuel*. 77, 1831–1839.

Perlander, L.M., 2010. *Evolution of Nano- and Microstructure during the Calcination of Bayer Gibbsite to Produce Alumina.* PhD thesis, University of Auckland, pp. 49, 88, 143.

Rožić, L., Novaković, T., Jovanović, N., Terlecki-Baričević, A., & Grbavčić, Ž., 2001. The kinetics of the partial dehydration of gibbsite to activated alumina in a reactor for pneumatic transport. *Journal of the Serbian Chemical Society*. 66, 273–280.

Shackelford, J.F., & Alexander, W. 2001. *CRC Materials Science and Engineering Handbook,* third ed. CRC Press LLC, Boca Raton.

Silcox, G.D., Kramlich, J.C., & Pershing, D.W., 1989. A mathematical model for the flash calcination of dispersed calcium carbonate and calcium hydroxide particles. *Industrial & Engineering Chemistry Research*. 28, 155–160.

Skeel, R.D., & Berzins, M. 1990. A method for the spatial discretization of parabolic equations in one space variable. *SIAM Journal on Scientific Computing*. 11, 1–32.

Stacey, M.H. 1987. Kinetics of decomposition of gibbsite and boehmite and the characterization of the porous products, *Langmuir*. 3, 681–686.

Stendardo, S., & Foscolo, P.U. 2009. Carbon dioxide capture with dolomite: A model for gas–solid reaction within the grains of a particulate sorbent. *Chemical Engineering Science*. 64, 2343–2352.

Sucech, S.W., & Misra, C. 1986. Alcoa pressure calcination process for alumina, in: Miller, R.E., Peterson, W.S. (Eds), *Light Metals 1986*, TMS, Warrendale, PA, pp. 119–124.

Wang, H., Xu, B., Smith, P., Davies, M., DeSilva, L., & Wingate, C. 2006. Kinetic modelling of gibbsite dehydration/amorphization in the temperature range 823–923 K. *Journal of Physics and Chemistry of Solids*. 67, 2567–2582.

Wefers, K., & Misra, C. 1987. *Oxides and hydroxides of aluminium.* Technical Paper No. 19, Alcoa Laboratories, Pittsburgh, PA.

Williams, F.S., & Misra, C. 2011. Pressure calcination revisited. In: Lindsay, S.J. (Ed.), *Light Metals 2011*. John Wiley & Sons, New York, pp. 131–136.

Wind, S., Wu, M., Jensen, T.V., & Raahauge, B.E. 2011. Dynamic simulation of gas suspension calciner (GSC) for alumina. In: Lindsay, S.J. (Ed.), *Light Metals 2011*. John Wiley & Sons, New York, pp. 137–143.

Whittington, B., & Ilievski, D. 2004. Determination of the gibbsite dehydration reaction pathway at conditions relevant to Bayer refineries. *Chemical Engineering Journal*. 98, 89–97.

Every reasonable effort has been made to acknowledge the owners of copyright material. I would be pleased to hear from any copyright owner who has been omitted or incorrectly acknowledged.

4

An unreacted shrinking core model for calcination and similar solid-to-gas reactions

In this chapter, a variation on the unreacted shrinking core model has been developed for calcination and similar non-catalytic thermal solid-to-gas decomposition reactions in which there is no gaseous reactant involved and the reaction rate decreases with increasing product gas concentration. The numerical solution of the developed model has been validated against an analytical solution for the isothermal case. The model parameters have been tuned using literature data for the thermal dehydration (calcination) of gibbsite to alumina over a wide range of temperatures, from 490 K to 923 K. The model results for gibbsite conversion are found to agree well with the published experimental data. A reaction order with respect to water vapour concentration of n = –1 was found to give a good fit to the data and yield activation energies consistent with literature values. Predictions of the non-isothermal unreacted shrinking core model compare well with the more complex distributed model developed in Chapter 3. The shrinking core model is extended in Chapter 5 to cover more complex aspects of self-inhibiting gas-to-solid reactions by accounting for parallel and series reactions with a diversity of reaction orders.

4.1Introduction

Gas-solid reaction has wide application in the metallurgical and chemical industries. Due to its importance, the modelling of these heterogeneous reactions has been of strong interest to investigators for decades, resulting in a variety of modelling approaches. These include the homogeneous, unreacted core, grain, random pore and modified volumetric models, in addition to a variety of customised models developed for specific cases (Chang and Kuo, 1999; Homma et al., 2005; Kasaoka et al., 1985; Molina and Mondragón, 1998; Silcox et al., 1989). Volumetric reaction models find application where the intrinsic reaction rate is relatively low compared to internal mass transfer. In contrast, unreacted shrinking core models are commonly used for nonporous, and in some cases for low-porosity, solid reactants, where the intrinsic reaction rate is higher than the diffusion rate. In some cases, it may not be possible to decide which of these two simple but opposing models is the more applicable —

complicating factors include the change of particle properties, for example, porosity, effective diffusion coefficient and effective thermal conductivity, with reaction conversion. This diversity in particle scale modelling is exemplified by lime calcination, which is a solid-to-gas thermal decomposition reaction. Although the shrinking core modelling approach has been widely used in this case (Bluhm-Drenhaus et al., 2010; Garcìa-Labiano et al., 2002; Moffat and Walmsley, 2005), the application of volumetric modelling has also been demonstrated and justified (Hu and Scaroni, 1996; Stanmore and Gilot, 2005; Ying et al., 2000). As numerous particle scale experimental and modelling studies have been reported for lime calcination, it is accepted that shrinking core and volumetric models, and a combination of these two, the grain model (Garcìa-Labiano et al., 2002; Mahuli et al., 2004; Stanmore and Gilot, 2005), can describe the process. Char combustion is another example for which different modelling strategies have been proposed (Canò et al., 2007; Sadhukhan et al., 2010).

Shrinking core models have been used for reactions involving a change in the overall particle size due to gasification, drying or mass burn-off. In these cases, the unreacted core is continuously exposed to the reacting environment and the particle shrinks as the reaction occurring at the particle surface proceeds. The unreacted core model can also be used for cases in which a reaction product forms a porous “ash” layer around the unreacted solid. The so-called ash layer is considered to be an inert material through which gas diffusion is possible so that reaction can still take place on the unreacted core surface. The size of the unreacted core decreases as conversion proceeds, with the overall particle size remaining essentially constant. Although the unreacted shrinking core model does not account for all possible mechanisms in a gas-solid reaction, it is widely considered to be an acceptable, simple model for the majority of reacting gas-solid systems (Ishida and Wen, 1971).

In the case of calcination, thermal dehydration and similar reactions, the role of gaseous species is different compared to other common gas-solid heterogeneous reactions. In many gas-solid reactions, gas-phase species are both reactants and products, while in the calcination reactions of interest in this paper, the gaseous species is a reaction product only. Further, the presence of the product gas species may actually impede the rate of the reaction. Thus, while a solid-to-gas reaction may reasonably be expected to occur uniformly inside a particle of uniform porosity and temperature, when the reaction rate is dependent on the product gas concentration, spatial gradients in reaction rate may develop inside the particle. This would be especially the case for solid reactants of low porosity. There is a shortage of particle scale conversion models for calcination and similar reactions in which there is no gas-phase reactant, but in which a gaseous product forms whose presence reduces the rate of reaction. The development of a model suitable for these reactions is a key contribution of the current chapter.

As discussed already in Chapter 3, gibbsite calcination is an important stage in alumina production using the Bayer process and has been studied for many years. The majority of publications on gibbsite calcination have focused on reaction kinetics and phase transitions (Gan et al., 2009; Wang et al., 2006; Whittington and Ilievski, 2004) while only a few have looked at coupling reaction kinetics and hydrodynamics (Marsh, 2009). Of particular relevance to the current chapter is a recent study using electron microscopy by Perlander (2010) who comments that gibbsite particles appear to undergo calcination in a way that “bears some resemblance to a shrinking core model.” Gibbsite is a relatively non-porous material, while the porosity of the main solid product, alumina, is relatively high. Further, the formation of boehmite, which is a potential intermediate solid species, is also relatively non-porous according to Stacey (1987). These points, along with the previously-mentioned success for lime calcination, argue that shrinking core models are potentially applicable for gibbsite calcination. As a part of an effort to develop a multi-scale model for the thermal dehydration of gibbsite in a fluidized bed reactor (FBR), calcination of a single gibbsite particle is studied to establish a predictive model for thermal decomposition at the particle scale. In this chapter, an unreacted shrinking core model is developed to describe calcination of a gibbsite particle at different temperatures.

In Chapter 3, a distributed model for a gibbsite particle undergoing thermal dehydration was developed, in which the gaseous product (water vapour) impedes the reaction. The simpler shrinking core modelling approach has not been used before to model this kind of reaction. This chapter presents, for the first time to the author’s knowledge, a shrinking core model for gibbsite particle calcination that includes the effect of water vapour pressure inside and outside the particle. This model consists of ordinary differential and algebraic equations that are easier to solve than the partial differential-algebraic equations of the distributed model. In addition, the proposed shrinking core model has an analytical solution for the isothermal case. The computing power needed to simulate small-scale, particle-level behaviour is an important consideration when it is intended to use the small-scale model in multi-scale modelling. This is because in some forms of multi-scale modelling, for example the “simultaneous” and “embedded” frameworks (Cameron et al., 2006), the small-scale model is called very many times. The model is tested against literature data over a wide temperature range, covering conditions that are favoured in laboratory studies and at industrial scales. Despite gibbsite calcination being the focus of this chapter, the model developed is a general one, which may be applied to other reactions in which a gaseous species is a reaction product only. Examples include the pyrolysis of carbonaceous materials, thermal decomposition of some organic or inorganic compounds, and the reduction of metal oxides. The potentially retarding effect of the product gas concentration on the reaction rate is included in the model. Previous versions of the unreacted shrinking core model cannot be directly applied for this type of calcination process.

The chapter is organised as follows. First, the reaction stoichiometry and kinetics of interest are summarised. After presenting the model assumptions, the unreacted shrinking core model is derived. The model is written in dimensionless form and an analytical solution is presented for a particular isothermal case. Then application of the model is demonstrated by focusing on a case study – the calcination of gibbsite to alumina. Parameter estimation and model validation for this variant of the unreacted shrinking core model are conducted using experimental data on gibbsite calcination available in the literature over a wide range of temperatures. Finally, the current model is compared to the distributed model of Chapter 3 and other gas-solid reaction models that assume a first order reaction with respect to the gas concentration. Sensitivity studies into the effect of the surrounding water vapour pressure, particle size and reaction order are also presented.

4.2 Mathematical model

4.2.1 Reaction kinetics

Unreacted core models for gas-solid reactions, in which the reaction rate is based on the reactant gas concentration, have been used in a wide range of applications in the literature. The majority of previous works have considered gas-solid reactions that were often represented by a reaction of the form:

$$aA_{(g)} + bB_{(s)} \rightarrow cC_{(g)} + dD_{(s)} \tag{4.1}$$

The reaction was usually assumed to follow first order kinetics based on the reacting gas (A) concentration, and the modelling proceeded on that basis.

However, in several applications, such as thermal dehydration, a gas-phase species is not needed for reaction, but occurs as a reaction product, only appearing on the right hand side of the reaction equation:

$$bB_{(s)} \rightarrow cC_{(g)} + dD_{(s)} \tag{4.2}$$

Corresponding surface reaction rate expressions have been developed that involve the concentration of the gaseous product species (C), which impedes the reaction rate as indicated in Eq. (4.3):

$$(-r_B) = kC_C^n C_{B0} \tag{4.3}$$

where n has a negative value. Generally, the reaction rate coefficient is supposed to obey the Arrhenius relation:

$$k = k_0 e^{(-E/RT)} \tag{4.4}$$

4.2.2 Model assumptions

The assumptions of the model are as follows:

- The particle is initially pure species B and has low, but non-zero, permeability.
- A reaction of the form of Eq. (4.2) takes place on the surface of an unreacted core of B to produce a gas C and a permeable layer of product D, which adheres to the solid core. The rate of reaction is given by Eq. (4.3), and the presence of the gaseous product C may reduce the rate of reaction.

- The gas species formed diffuses through the permeable product layer, and a pseudo-steady state condition applies for modelling the gas-phase concentration profile in the product layer. The pseudo-steady state assumption is reasonably acceptable for gas-solid reactions, as in the majority of cases the criterion $C_C/C_B < 10^{-3}$ holds (Gómez-Barea and Ollero, 2006).
- The particle is spherical with constant shape and constant outer diameter during the reaction.
- The particle temperature is assumed to be spatially uniform, but may vary with time.
- The mass transfer rate through the gas film surrounding the particle is assumed to be very high, so that the gas concentration at the outer surface of the particle surface and in the bulk gas is the same.

The physical picture corresponding to the modelling assumptions is as follows. A small particle of species *B* with low, but non-zero, permeability enters the reaction environment. Reaction (4.2) takes place throughout the particle and a high concentration of gas species *C* inside the particle is quickly established. The production of vapour *C* does not cause the particle to fragment because the gas is able to diffuse to the particle surface. The high internal concentration of *C* retards the reaction, except near the outer surface of the particle where the gas can escape to the environment. The solid product species *D* is more permeable than the reactant *B*, and gas can diffuse easily through the product layer. In this way, the geometry of a shrinking core model is approximated, but the boundary of the core is not sharp. It is a result of the high internal concentration of gas inside the particle suppressing further reaction, and also the ease of diffusion of the gas through the product layer.

4.2.3 The unreacted shrinking core model

A schematic diagram of the reacting particle is shown in Figure 4.1. As mentioned in Section 4.2.2, reaction and diffusion in an isothermal particle having a high mass transfer coefficient is considered in this study. Based on those assumptions, and inspired by Ishida and Wen (1971) and Homma et al. (2005), an expression for the rate of each process and hence an equation for the rate of core shrinking is developed, which is finally related to particle conversion. Note that we cannot directly use the results of Ishida and Wen (1971), Homma et al. (2005) and similar studies because their reaction stoichiometry (Eq. 4.1) and corresponding rate equation contain a reacting gas species *A* whose presence promotes the reaction, while we have only a product gas species *C* that may impede the reaction. Thus, while the use of reaction (4.2) and rate equation (4.3) are relatively small changes from a theoretical viewpoint, they mean that the analytical and numerical solutions developed by those previous authors cannot be used, and that the resulting model predictions are different.

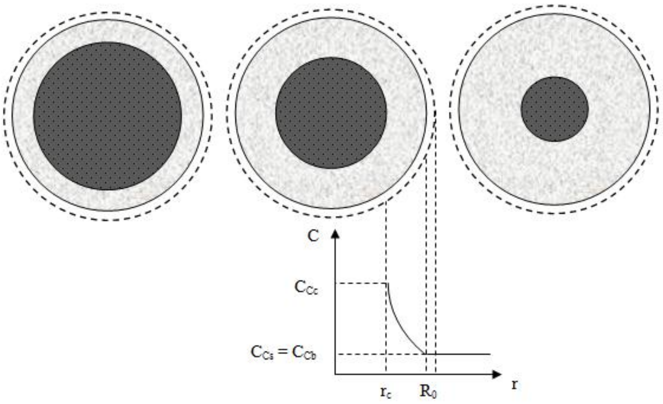

Figure 4.1 – Schematic diagram of a single particle undergoing thermal dehydration according to the unreacted shrinking core model. Shown are the core (dark grey), porous product layer (light grey) and the gas concentration profile.

On the unreacted core surface, the molar rate of gas (*C*) production can be expressed through the surface reaction rate Eq. (4.3) and the core surface area:

$$W_1 = 4\pi r_c^2 \vartheta k C_{B0} C_{Cc}^n \tag{4.5}$$

where C_{B0} and C_{Cc} are the concentration of solid reactant *B* and gas product *C* at the core surface respectively, ϑ is the ratio of stoichiometric coefficients (*c*/*b*) and r_c is the current core radius. The rate of diffusion of gas in the product layer can be represented as

$$W_2 = -4\pi r^2 D_e \frac{dC_C}{dr} \tag{4.6}$$

where D_e is the effective diffusion coefficient of *C* in the product layer. For constant W_2 (pseudo-steady state conditions), Eq. (4.6) can be solved analytically for the following boundary conditions:

$$C_C = C_{Cs} \text{ at } r = R_0 \tag{4.7}$$

$$C_C = C_{Cc} \text{ at } r = r_c \tag{4.8}$$

The solution is

$$W_2 = 4\pi D_e \frac{C_{Cc} - C_{Cs}}{\frac{1}{r_c} - \frac{1}{R_0}} \tag{4.9}$$

Further, under pseudo-steady state conditions, the diffusion rate of gas in the product layer is equal to the rate of gas production on the surface of the unreacted core:

$$W_1 = W_2 \tag{4.10}$$

By combining Eqs. (4.5), (4.9) and (4.10), the vapour concentration on the core surface C_{Cc} can be determined from

$$C_{Cc} - C_{Cs} - \frac{\vartheta k C_{Cc}^n C_{B0}}{D_e} r_c^2 \left(\frac{1}{r_c} - \frac{1}{R_0} \right) = 0 \tag{4.11}$$

Now, the solid B consumption rate and size of the unreacted core are related by

$$\dot{N}_B = -\frac{d}{dt} \left(\frac{(4/3)\pi r_c^3 \rho_B}{Mw_B} \right) \tag{4.12}$$

On the other hand, the reaction rate of solid species B is also related to the gas production rate:

$$\dot{N}_B = \frac{1}{\vartheta} W_1 \tag{4.13}$$

Subsequently from Eqs. (4.5), (4.12) and (4.13), an expression for rate of change of the core radius can be obtained:

$$-\frac{dr_c}{dt} = \frac{Mw_B}{\rho_B} k C_{B0} C_{Cc}^n \tag{4.14}$$

with the initial condition

$$r_c = R_0 \text{ at } t = 0 \tag{4.15}$$

The assumption of spatially uniform temperature allows the energy balance over the particle to be written as

$$\frac{R_0^3 \rho_B C_p}{3Mw_B}\frac{dT}{dt} = R_0^2 h(T_b - T) - r_c^2 k C_{B0} C_{Cc}^n \Delta H \tag{4.16}$$

where C_p is the particle molar heat capacity, h is the heat transfer coefficient, T_b is the external temperature and ΔH is the enthalpy of reaction. The initial condition is

$$T = T_0 \text{ at } t = 0 \tag{4.17}$$

The new version of the unreacted shrinking core model is thus given by the system of equations (4.11), (4.14) and (4.16). The governing equations may be represented in dimensionless form by using following dimensionless groups:

$$\xi = \frac{r_c}{R_0} \tag{4.18}$$

$$\gamma_C = \frac{C_{Cc}}{C_{Cb}} \tag{4.19}$$

$$\phi = \sqrt{\vartheta R_0 k_0 C_{B0} / (D_e C_{Cb}^{1-n})} \tag{4.20}$$

$$\tau = \frac{k_0 Mw_B C_{B0}}{\rho_B R_0 C_{Cb}^{-n}} t \tag{4.21}$$

$$\theta = \frac{T}{T_b} \tag{4.22}$$

$$\eta = \frac{3\Delta H}{T_b C_p} \tag{4.23}$$

$$\omega = \frac{3hC_{Cb}^{-n}}{C_p k_0 C_{B0}} \tag{4.24}$$

$$\beta = E / RT_b \tag{4.25}$$

where ξ, γ_C, θ, and τ are the dimensionless size of the shrinking core, vapour concentration at the core, temperature and time, respectively; ϕ is the average Thiele modulus, which represents the ratio of intrinsic chemical reaction rate in the absence of mass transfer limitations to the rate of diffusion through the particle. The physical interpretation of ϕ^2 is analogous to the Damkohler number. The parameter, η is termed the cooling potential as it is proportional to the adiabatic cooling temperature which is the ratio of the reaction enthalpy to the heat capacity of the particle and inversely proportional to the environmental temperature. Further, ω measures the heat absorption capacity which characterises the ratio of heat transferred into the particle from the environment to the thermal capacity of the particle. Finally, the parameter β is the dimensionless activation energy.

Consequently, the unreacted shrinking core model given by Eqs. (4.11), (4.14) and (4.16) can be represented in dimensionless form for general *n* as:

$$\gamma_C - 1 - \phi^2 \gamma_C^n \xi (1-\xi) e^{-\frac{\beta}{\theta}} = 0 \tag{4.26}$$

$$-\frac{d\xi}{d\tau} = \gamma_C^n e^{-\frac{\beta}{\theta}} \tag{4.27}$$

$$\xi = 1 \text{ at } \tau = 0 \tag{4.28}$$

$$\frac{d\theta}{d\tau} = \omega(1-\theta) - \eta \xi^2 \gamma_C^n e^{-\frac{\beta}{\theta}} \tag{4.29}$$

$$\theta = \theta_0 \text{ at } \tau = 0 \tag{4.30}$$

The ordinary differential-algebraic system of Eqs. (4.26)–(4.30) needs to be solved simultaneously for given values of the model parameters ϕ, *n*, η, β and ω. In general, a numerical solution is needed to predict how the core radius changes with time. This in turn can be used to determine the solid conversion. The simple mathematical form and consequent fast numerical solution of the model are significant because of its intended use for multi-scale reactor modelling. In a two-scale model that combines a particle scale model with a reactor scale model, for example, the particle scale model may be evaluated many times in a single simulation of the reactor.

For the special case of $n = -1$ and the particle temperature being constant at the environmental temperature, which has significance in the later calcination case study, an explicit expression for γ_C can be found from Eq. (4.26):

$$\gamma_C = \left[\phi^2 \xi (1-\xi) e^{-\beta} + \frac{1}{4}\right]^{1/2} + \frac{1}{2} \tag{4.31}$$

so that Eq. (4.27) becomes

$$-\frac{d\xi}{d\tau} = \frac{e^{-\beta}}{\left[\phi^2 \xi (1-\xi) e^{-\beta} + \frac{1}{4}\right]^{1/2} + \frac{1}{2}} \tag{4.32}$$

The analytical solution of Eq. (4.32) is

$$\tau = \left[\frac{1}{4} + \frac{1}{2\sqrt{4S^2-1}}\left[\frac{1}{2}\sqrt{S^2-\frac{1}{4}} + S^2 \tan^{-1}\left(\frac{1}{2\sqrt{S^2-\frac{1}{4}}}\right)\right] - \frac{1}{2\sqrt{4S^2-1}}\left[\left(\xi-\frac{1}{2}\right)\sqrt{S^2-\left(\xi-\frac{1}{2}\right)^2} + S^2 \tan^{-1}\left(\frac{\xi-\frac{1}{2}}{\sqrt{S^2-\left(\xi-\frac{1}{2}\right)^2}}\right)\right] - \frac{1}{2}\left(\xi-\frac{1}{2}\right)\right] e^{-\beta} \tag{4.33}$$

where

$$S^2 = \frac{1}{4}\left(\frac{1}{\phi^2 e^{-\beta}} + 1\right) \tag{4.34}$$

and the time needed for complete reaction of the particle is

$$\tau_\infty = \left[\frac{3}{4} + \frac{S^2}{\sqrt{4S^2-1}} \tan^{-1}\left(\frac{1}{\sqrt{4S^2-1}}\right)\right] e^{-\beta} \tag{4.35}$$

Note that Eqs. (4.31)–(4.35) apply only for $n = -1$ and the particle temperature being constant at the environment temperature.

Finally, for any value of n, the conversion X of solid reactant B may be related to the volume of the unreacted core:

$$1 - X(t) = \frac{\text{Volume of unreacted core at time } t}{\text{Volume of particle}} \tag{4.36}$$

and therefore

$$X(t) = 1 - \xi^3(t) \tag{4.37}$$

Further, the mass fraction of the solid reactant B in the particle at any time can be calculated from the dimensionless core radius also:

$$m_B(t) = \frac{(1-X)Mw_B}{(1-X)Mw_B + (d/b)XMw_D} \tag{4.38}$$

Figure 4.2(a) shows typical conversion versus time profiles for different values of the Thiele modulus. Further, the typical evolution of the product gas (C) concentration profile inside the particle is shown in Figure 4.2(b). Over the total reaction time, the gas concentration at the shrinking particle surface increases up to a maximum value before declining, but for any given time the maximum concentration of gas C occurs at the surface of the shrinking core. Note that the gas concentration profile is only defined in the porous product layer, $\xi \leq (r/R_0) \leq 1$. Higher values of the Thiele modulus lead to a higher gas pressure build up at the unreacted core surface at a given time. This is because high a Thiele modulus corresponds to a high reaction rate and a low diffusion rate of the product gas species.

4.3 Case study: gibbsite calcination

4.3.1 Reaction kinetics

A mentioned in the previous chapter, Section 3.2.1, the gibbsite calcination reaction displays complex behaviour in terms of its reaction kinetics and controlling mechanisms. In this chapter, a lumped (overall) reaction is considered for application with the proposed shrinking core model, as follows:

$$\underset{\textit{Gibbsite}}{2Al(OH)_3} \rightarrow 3H_2O + \underset{\textit{Alumina}}{Al_2O_3} \tag{4.39}$$

Subsequently the role of water vapour concentration on reaction rate is considered by using Eq. (4.40):

$$(-r_G) = k_0 e^{-E/(RT)} C_C^n C_{G0} \tag{4.40}$$

In Chapter 3 it was discussed that the activation energy of gibbsite calcination appears to vary with the operating conditions. More detail is given in Chapter 3.

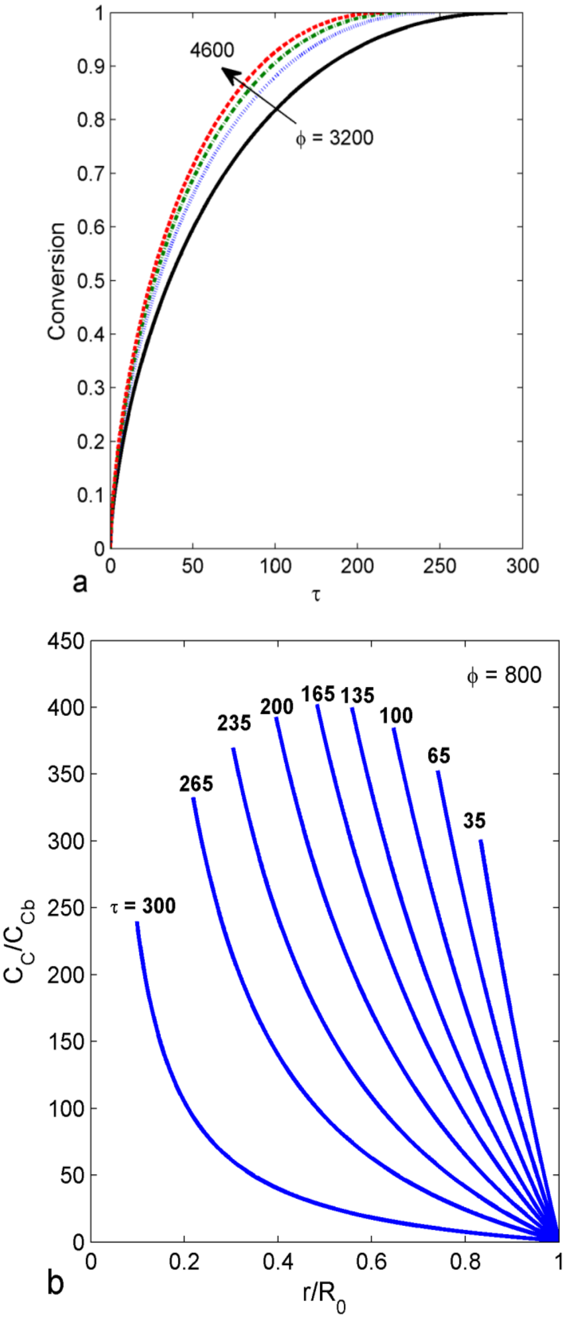

Figure 4.2 – Representative dimensionless model predictions for *n* = –1 and *θ* = *1*: (a) Conversion-time plots for different values of the Thiele modulus, ϕ ; (b) Concentration-radial position profile for product gas (*C*) inside the porous product layer as a function of time for ϕ = 800.

In this study, average E and k_0 values for low temperatures are estimated via data fitting by minimising Eq. (4.41). For high temperatures, however, the E value estimated in Chapter 3, Table 3.2 is used, but the k_0 must be re-fitted as the reaction rate in this study is based on the surface area of the unreacted core, while Chapter 3 used a reaction rate expressed on a volumetric basis. Thus, in the high temperature range, the Eq. (4.42) is used as the objective function for error minimization purposes.

$$f(k_0, E) = \sum_{T_b=\{490,510,530\mathrm{K}\}} \sum_{i=1}^{N_{Tb}} (X_i - X_{exp,i})^2 \tag{4.41}$$

$$f(k_0) = \sum_{T_b=\{873,898,923\mathrm{K}\}} \sum_{i=1}^{N_{Tb}} (m_i - m_{exp,i})^2 \tag{4.42}$$

Note also in Eq. (4.41) the objective is to minimise the difference between the model and experimental conversions, while in Eq. (4.42) the difference in gibbsite mass fraction is minimised. These reflect the different ways in which the experimental data were reported in the literature. The estimated values of k_0 and E are shown in Table 4.1 along with the other parameter values used in the model.

4.3.2 Model validation

The model developed in Section 4.2 is restricted to a spatially uniform temperature inside the particle. This assumption needs to be checked for gibbsite particles undergoing calcination. The Biot number criterion, Bi = $hD_p/k_p < 0.1$, has been used to confirm isothermality, even in the presence of a solid phase reaction, such as pyrolysis (Chern and Hayhurst, 2010). In the most conservative case for gibbsite calcination considered in the current chapter, with a particle diameter of 1 mm fluidized by air at 400 K with a superficial velocity of three times the estimated minimum fluidization velocity, the heat transfer coefficient between the gas and the particle would be around 420 W/m^{2}K according to Kunii and Levenspiel (1991). A conservative particle thermal conductivity of 16 W/m.K for alumina at 400K (Shackelford and Alexander, 2001), yields Bi = 0.03, which confirms that assuming isothermal conditions inside the particle is reasonable in our case study. Smaller particles, lower heat transfer coefficients and higher particle thermal conductivities would satisfy the isothermality criterion even more easily. While the particle is spatially uniform in temperature, the temperature does change with time.

Table 4.1 – Literature and fitted parameters used in the model for gibbsite calcination.

Parameter	Value	Reference / comment
$C_{G0}(mol/m^3)$	3.03×10^4	Wefers and Misra (1987)
$C_p(J/mol.K)$	80	Wefers and Misra (1987)
$D_e(m^2/s)$	7×10^{-10}	Value for alumina; Fowler et al. (1977)
$D_p(\mu m)$	100 30	High T_b range; Wang et al. (2006) Low T_b range; Lopushan et al. (2007)
$E(kJ/mol)$		
High T_b range	131	Amiri et al. (2012)
Low T_b range	150±3	Found by parameter estimation via Eq. (4.41).
$h(W/m^2.K)$	1.5	Combines radiation and convection; Incropera et al. (2007)
$\Delta H(kJ/mol)$	147	Beyer at al. (1989)
$k_0(mol/m^2.s)$		
High T_b range	5×10^7	Found by parameter estimation via Eq. (4.42).
Low T_b range	4×10^6	Found by parameter estimation via Eq. (4.41).
$k_e(W/m.K)$	16	Shackelford and Alexander (2001)
$Mw_A(g/mol)$	102	Alumina molecular weight
$Mw_G(g/mol)$	80	Gibbsite molecular weight
$P_{Cb}(kPa)$	3	Typical environmental water vapour pressure
n	–1	As discussed in Sections 4.3.1 and 4.3.3.6
$T_b(K)$		
High range	873–923	Experimental conditions of Wang et al. (2006)
Low range	490–530	Experimental conditions of Lopushan et al. (2007)
$T_0(K)$	298	Particle initially at ambient temperature
$\rho_G(kg/m^3)$	2420	Wefers and Misra (1987)

Eqs. (4.4), (4.11), (4.14) and (4.16) with their corresponding initial conditions, which comprise the unreacted shrinking core model, were solved simultaneously using numerical methods for the parameters given in Table 4.1.

The performance of the proposed model was examined against experimental gibbsite conversion versus time data reported by Lopushan et al. (2007) and Wang et al. (2006) over a wide range of temperatures. Since there is uncertainty over the dependency of the reaction rate on water vapour pressure and temperature as outlined in Sections 3.2.1 and 4.3.1, a parameter estimation approach is adopted and explored in two cases. In the first case, it was assumed that $n = 0$, which represents a considerably simplified model. At each experimental temperature, different reaction rate parameters were fitted to the experimental data. In the second case, after initial scoping studies, a constant value of $n = –1$ was used, and again kinetic parameters were fitted to the experimental data at each temperature. The estimated kinetic parameters for the second case are shown in Table 4.1. The comparison between the model and the data is divided into two temperature ranges, low and high, and is presented in Sections 4.3.2.1 and 4.3.2.2. Note that the low temperature range data are for fine (30 µm) particles, while the high temperature data are for much coarser particles (100 µm).

4.3.2.1 Low temperature range

Figures 4.3(a)–(c) show the model predictions at relatively low temperatures (490, 510 and 530 K) for two reaction orders, *n*, as well as the experimental data published by Lopushan et al. (2007). This temperature range is primarily of interest in experimental studies into kinetics as the reaction times are relatively long, simplifying measurement; industrial-scale alumina production is always operated at higher temperatures. The agreement between the practical data and the model prediction with *n* = –1 is considerably better than for *n* = 0, which helps confirm the importance of including the water vapour concentration in the reaction rate expression.

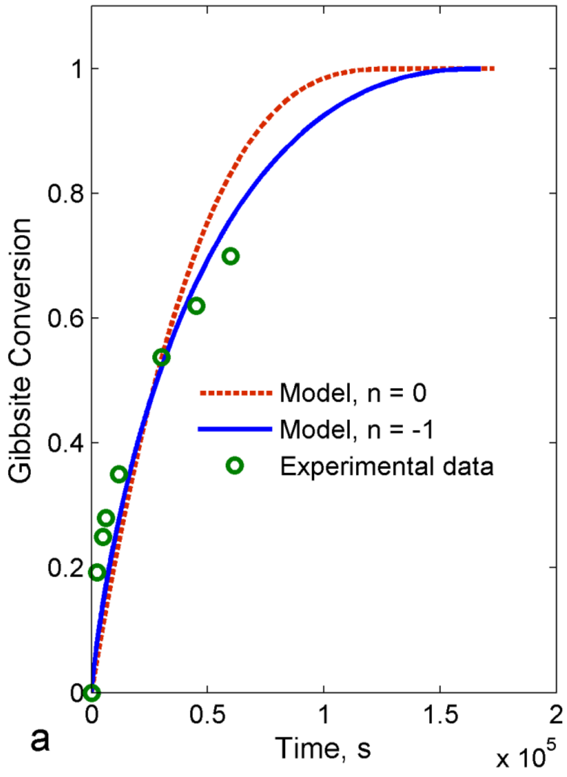

Figure 4.3(a) – Comparison between model predictions for *n* = 0 and *n* = –1 and experimental conversion data (Lopushan et al., 2007) at 490 K.

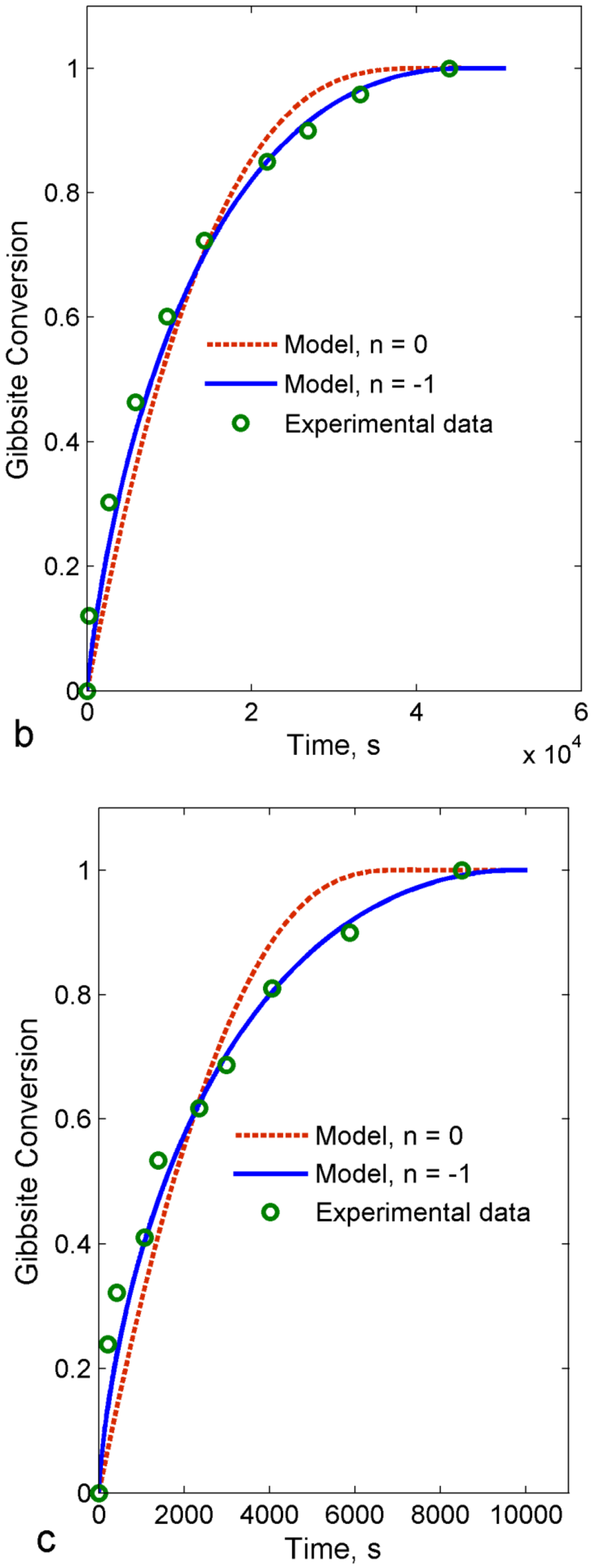

Figure 4.3(b, c) – Comparison between model predictions for *n* = 0 and *n* = –1 and experimental conversion data (Lopushan et al., 2007) at (b) 510 K and (c) 530 K.

4.3.2.2. High temperature range

To test the model at high temperatures, the experimental calcination data published by Wang et al. (2006) were used as shown in Figures 4.4(a)–(c). In their work, the kinetics of gibbsite dehydration were investigated at Bayer process conditions (823–923 K). Those authors reported data on the mass fraction of gibbsite in a single particle as a function of time, rather than conversion, and the model results have been presented in the same way by using Eq. (4.38). The model results are in good agreement with the experimental data, and $n = -1$ performs slightly better than $n = 0$.

Since a relatively coarse particle size (100 µm) was used in their experiments, some intermediate boehmite formation, in addition to direct formation of alumina, is a strong possibility (Candela and Perlmutter, 1986; Whittington and Ilievski, 2004). While the reaction order of the water vapour concentration for the conversion of gibbsite to boehmite is unknown, Stacey (1987) reported a reaction order of –0.4 for the conversion of boehmite to alumina. In the current unreacted shrinking core model, it is assumed that all the reactions and phase transformations are lumped together and can be approximated by Eqs. (4.39) and (4.40) and an overall n value. The results of Stacey (1987) suggest that the formation of boehmite might favour an overall n value between 0 and –1, but it is not possible to say definitively which value of n is better in the high temperature range. Currently, there are data only for fine particles in the low temperature range, and only for coarse particles at high temperatures. Extra experimental data for both fine and coarse particles over the entire temperature range considered (490–923 K) would assist in finding the most appropriate value of n.

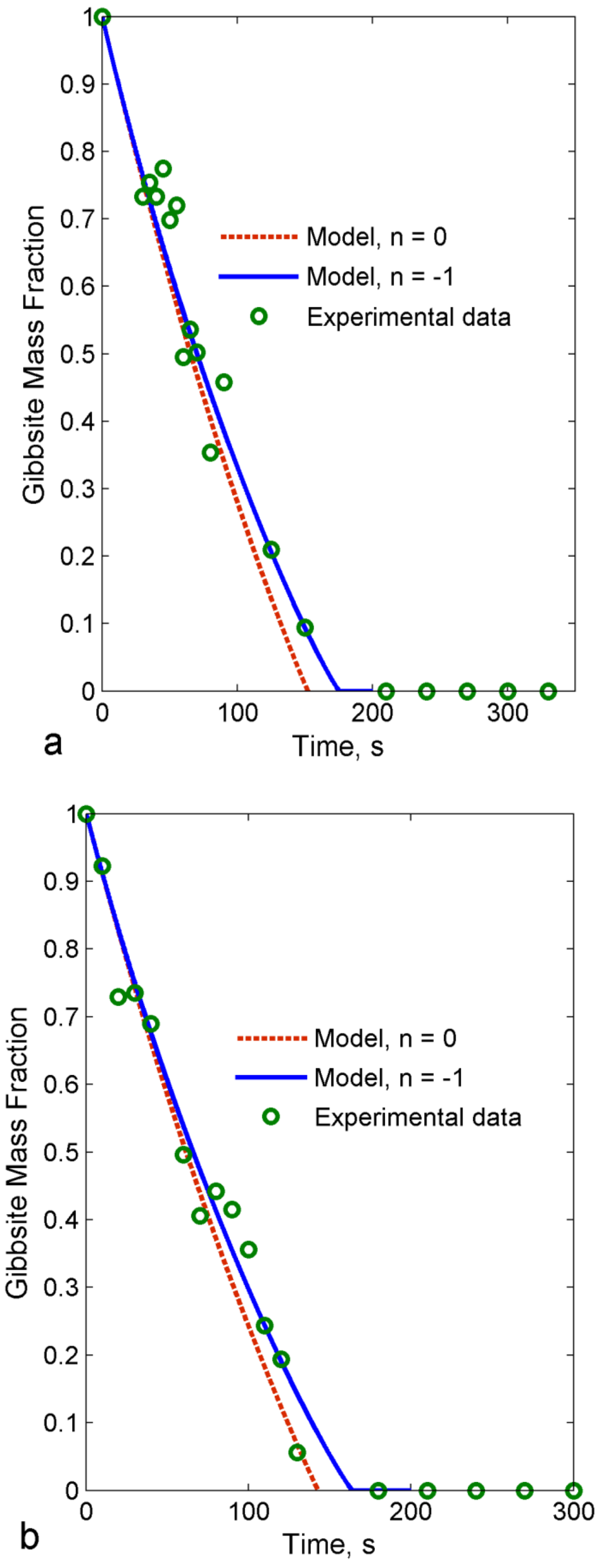

Figure 4.4(a, b) – Comparison between model predictions for *n* = 0 and *n* = –1 and experimental data (Wang et al., 2006) at (a) 873 K and (b) 898 K.

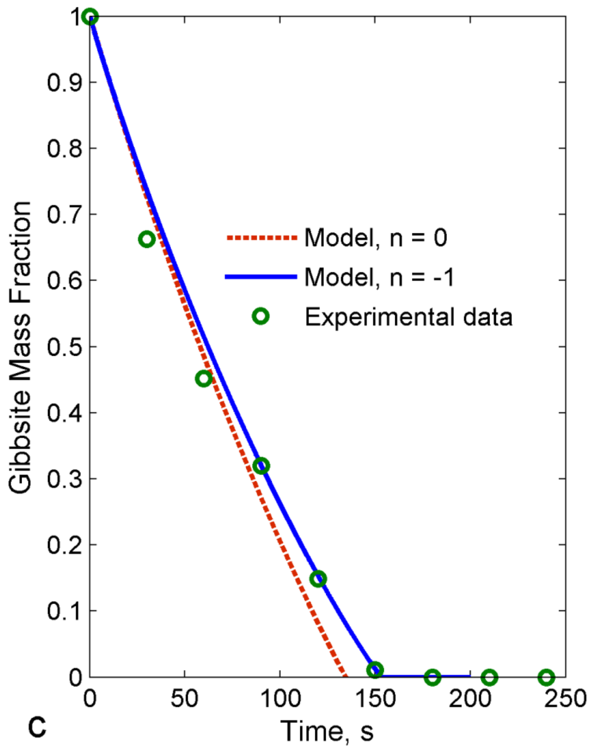

Figure 4.4(c) – Comparison between model predictions for *n* = 0 and *n* = –1 and experimental data (Wang et al., 2006) at 923 K.

4.3.3 Analysis of the model

4.3.3.1 Interpretation of temperature profile

Temperature history plays an important role in model performance. Ignoring temperature variations during the reaction may result in incorrect conclusions about the reaction rate and kinetic parameters. As can be seen in Figures 4.5(a) and (b), the particle temperature is not steady, particularly in the high operating temperature range, even under high heat transfer rate conditions. This can be attributed to the high rate of the endothermic calcination reaction, which moderates the particle's temperature rise. The unsteady behaviour is less significant in the low temperature range (Figure 4.5b) as it lasts a very short time in comparison to the total conversion time. At 530 K, the particle reaches the external temperature T_b in less than 50 s, while total reaction time is around 8000 s. An increase in the heat transfer coefficient reduces the length of the unsteady period. It can be concluded that the particle's temperature dynamics are unimportant when T_b is low – the model can be used without the energy balance, since the particle very rapidly reaches the external

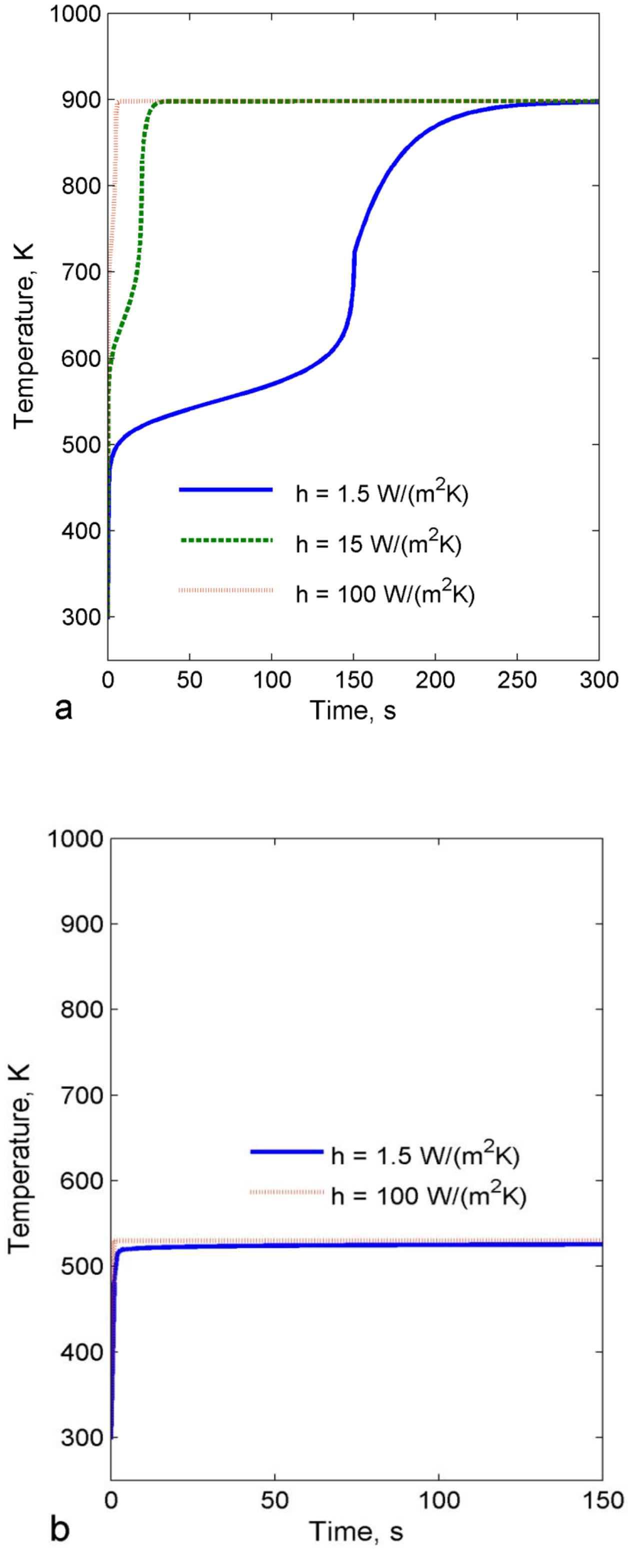

Figure 4.5 – Particle temperature profile for different heat transfer environments for (a) a high external temperature (898 K), and (b) a low external temperature (530 K).

temperature T_b. In that situation, the analytical solution, Eq. (4.33), will be applicable. Figure 4.6 compares two sets of model predictions – the full model with the dynamic energy balance solved numerically and the analytical solution of Eq. (4.33), which assumes that $T = T_b$.

From Figure 4.6 it is clear that there is negligible difference between model with and without the energy balance at low temperatures. The results also help validate the numerical approach that was used in this chapter. However, at elevated T_b, ignoring the particle's temperature dynamics would cause a considerable error in the model predictions, which emphasises the need to be cautious about making simplifying assumptions.

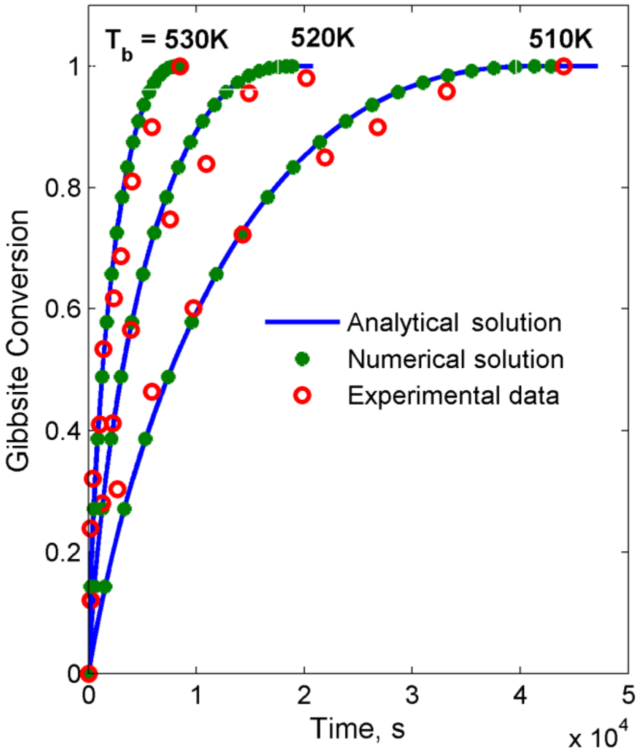

Figure 4.6 – Experimental data (Lopushan et al., 2007) compared with model predictions in the low temperature range for the full model with the dynamic energy balance (numerical solution) and the model without the energy balance in which temperature is constant at T_b (analytical solution).

4.3.3.2 Comparison of shrinking core and distributed models

Figure 4.7 compares the results of the proposed new variation of the shrinking core model to those of the distributed model developed in Chapter 3. As can be seen in

Figure 4.7(a), both models predict similar reductions in the gibbsite mass fraction with time. The temperature profiles also show satisfactory agreement (Figure 4.7b). It should be noted that except for k_0, all other parameters are kept the same in the two models. Actually, k_0 should not be equal in the two models as the reaction rate in the current model is expressed on a surface area basis, while it is a volumetric rate in the distributed model.

The main advantage of the shrinking core model over the distributed model is the simplicity and speed of solution, as the latter requires more complicated numerical methods. However, the distributed model can give more insight into the temperature and species distributions inside the particle. For instance, the internal water vapour pressure profile can be better explained by the distributed model, while the shrinking core model may be preferred for use in multi-scale modelling due to its computational efficiency. Thus, the choice of model depends on the modelling goal.

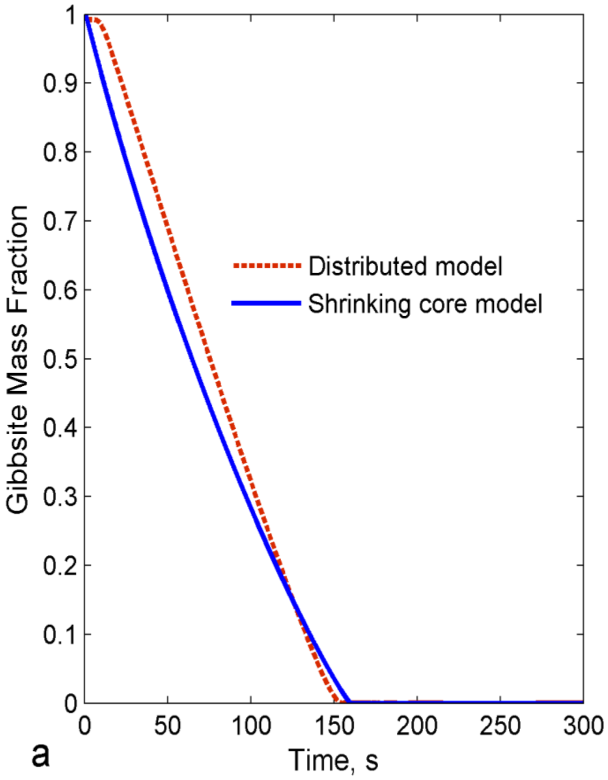

Figure 4.7(a) – Comparison of shrinking core and distributed models at 898 K: predicted evolution of the gibbsite mass fraction.

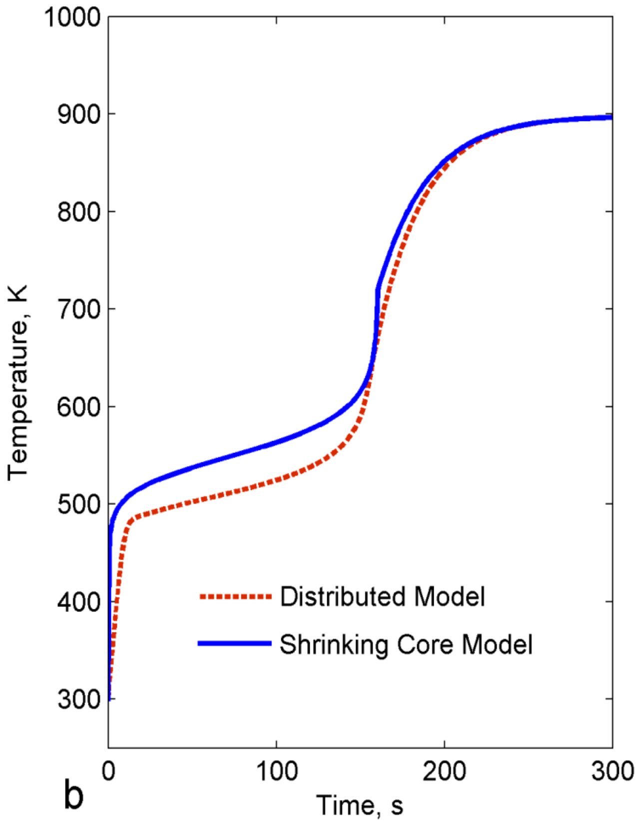

Figure 4.7(b) – Comparison of shrinking core and distributed models at 898 K: predicted evolution of the particle temperature.

4.3.3.3 Role of the water vapour

Ishida and Wen (1971) reported an analytical solution, Eq. (4.43), for a kinetically-controlled shrinking unreacted core model in which the gas-solid reaction was considered to be of the form of Eq. (4.1). In their work, the reaction rate equation was first order in the concentration of a reactant gas species *A*. Figure 4.8 shows how mis-consideration of the role of water vapour in calcination reactions results in an incorrect conversion profile. Also shown is a comparison of the current model with an ideal diffusion-controlled shrinking core model, Eq. (4.44).

$$\frac{t}{t_\infty} = 1 - (1 - X)^{1/3} \tag{4.43}$$

$$\frac{t}{t_\infty} = 1 - 3(1 - X)^{2/3} + 2(1 - X) \tag{4.44}$$

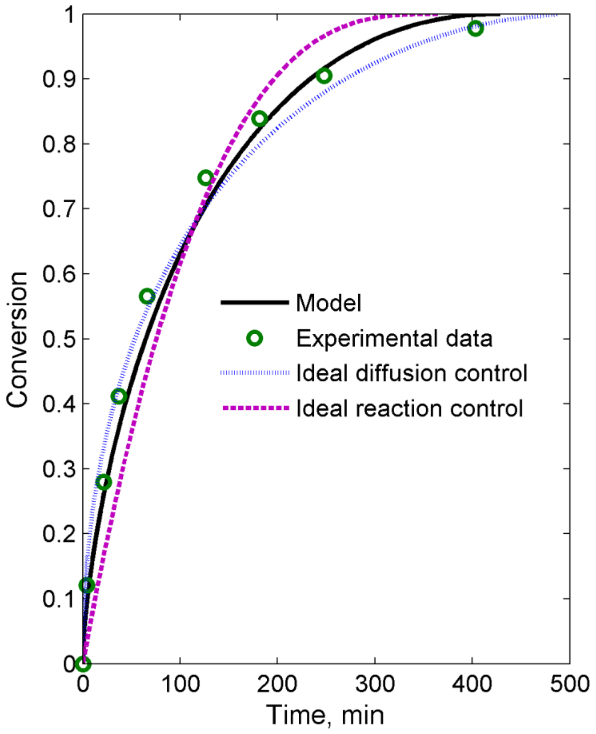

Figure 4.8 – Comparison between results of the current model, the ideal reaction-controlled and diffusion-controlled models of Eqs. (4.43) and (4.44), respectively, and the experimental data of Lopushan et al. (2007) at 520 K.

In both equations, t_∞ is the reaction completion time. This comparison indicates that, in spite of the dominant role that diffusion plays, the shrinking core model proposed in this work can offer a better prediction of gibbsite conversion by accounting for reaction as well as diffusion.

4.3.3.4 Effect of surrounding vapour pressure

Water vapour diffuses from the surface of the unreacted core where it is formed towards the particle surface, with the vapour pressure gradient acting as the driving force for mass transfer. As the surrounding vapour pressure is raised, the rate of gas diffusion is decreased due to a lower vapour pressure gradient. In addition, the reaction rate is negatively affected by a higher vapour pressure. It should be noted that pressure has no effect on Knudsen diffusivity and has a slight influence on the effective diffusivity of vapour in the alumina layer. The rate of conversion decreases considerably with increasing external vapour pressure at low temperature, while no significant effect is seen at higher temperatures (Figure 4.9). At high temperatures, the water vapour pressure inside the particle is significantly higher than outside; this high difference damps out the effect of relatively small changes in the external vapour pressure.

As mentioned previously in Section 3.1, Williams and Misra (2011) determined that the effective fuel consumption may be as low as 1.55 GJ/t alumina in an exploratory high-pressure alumina calciner. This compares favourably to the best current atmospheric pressure calciners that have fuel consumptions of around 2.79 GJ/t alumina (Klett et al., 2011). In the high-pressure calciner, the water vapour pressure surrounding a gibbsite particle can be 30 times above that in atmospheric calciners, and it can change by a factor of more than two as the particle travels through the vessel. However, as mentioned previously, at least based on the current modelling results, the conversion of a single particle will not be significantly influenced by the surrounding vapour pressure at the elevated temperatures used in industrial-scale operations. Therefore, high-pressure calcination offers the potential for a reduction in energy consumption without a significant negative effect on the rate of gibbsite conversion. If the unreacted shrinking core model is to be applied to high-pressure calcination, it should be verified by further experimental data obtained at elevated pressures.

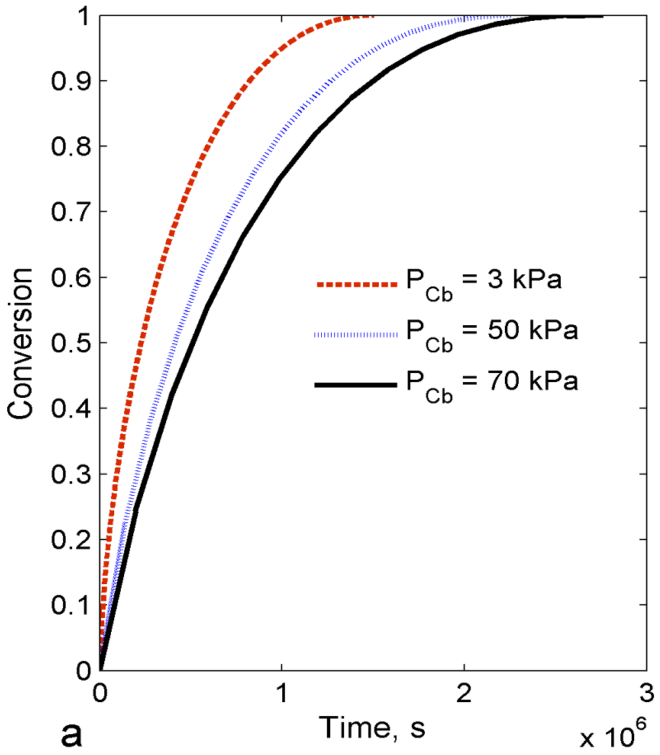

Figure 4.9(a) – The effect of surrounding water vapour pressure on the conversion-time relationships at 450 K.

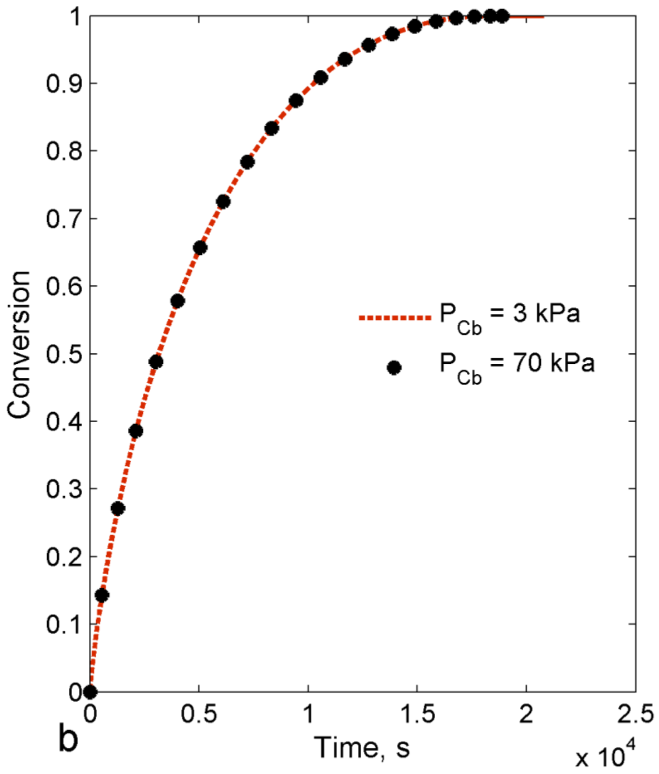

Figure 4.9(b) – The effect of surrounding water vapour pressure on the conversion-time relationships at 510 K.

4.3.3.5 Effect of particle size

The effect of particle size on conversion rate and complete calcination time is presented in Figure 4.10. Investigations into the effect of particle size on calcination behaviour in FBRs involve both hydrodynamic and chemical reaction aspects. From the reaction kinetics point of view, fine particles will be thermally decomposed quickly, resulting in a more homogenous (or sharply distributed) product. For instance, a fine particle will be calcined in a short time with alumina being the main product. A coarser particle would take more time to complete the calcination process, producing alumina and possibly boehmite. Therefore, smaller particle sizes are favoured in terms of reaction time and selectivity. From the hydrodynamic viewpoint, however, a very fine particle will have a shorter residence time at a given fluidization velocity, which could lead to incomplete calcination. Consequently, a moderate particle size may be best to meet process requirements in terms of calcination degree, product selectivity, process productivity and control. Particle size is a variable that has importance at both the individual particle scale and at the vessel scale, and is a key consideration in multi-scale modelling work.

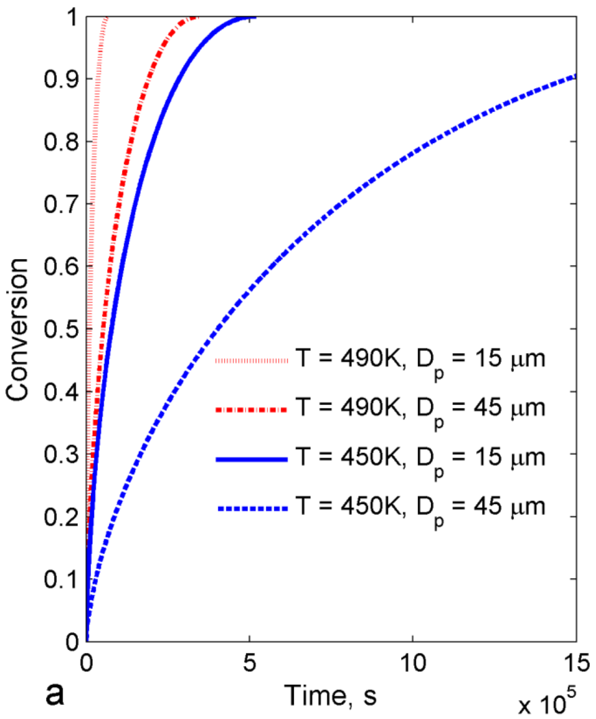

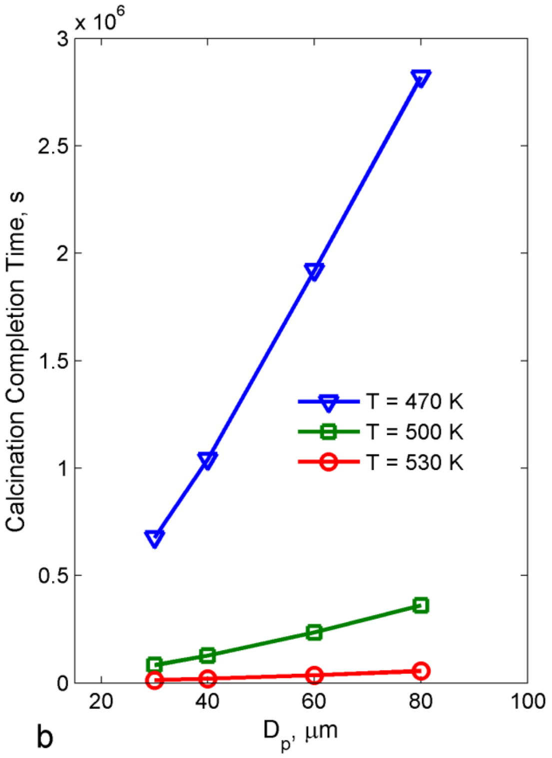

Figure 4.10 – The importance of particle size: (a) The effect of particle size on gibbsite conversion as a function of time at 450 K and 490 K for a surrounding water vapour pressure of 350 Pa, and (b) the effect of particle size on calcination completion time.

4.3.3.6 Reaction order

Even though a negative order reaction produces clearly better results, it should be noted that conversion-time results of Figures 4.3 and 4.4 alone are not sufficient to identify the correct value of n, the reaction order with respect to water vapour, particularly at high temperatures, making it necessary to employ complementary information. An interpretation of the temperature profiles corresponding to each reaction order leads to a more informed judgment about n. However, since uncertainty also exists for the other kinetic parameters, E and k_0, a sensitivity analysis approach has been adopted in an attempt to arrive at a robust conclusion about n in the high temperature range. In the first case, different n values (1, 0, –1, –2) have been selected and best-fit values of k_0 for each n have been determined for a common best-fit value of E (131 kJ/mol). These results are reported in Table 4.2, and a corresponding predicted evolution of the particle temperature is shown in Figure 4.11.

Table 4.2 – Fitted pre-exponential coefficients for different reaction orders for a fixed activation energy of *E* = 131 kJ/mol in the high temperature range (823–923 K).

n	k_0 (mol^{-n}m^{3n+1}/s)
1	4.9×10^3
0	5.1×10^5
–1	5×10^7
–2	4.3×10^8

In the second case, the same n values as above were selected and best-fit values of E for each n were determined for a common best-fit value of k_0 (5×10^7 mol^{-n}m^{3n+1}/s). These results are reported in Table 4.3, and a corresponding predicted evolution of the particle temperature is shown in Figure 4.12.

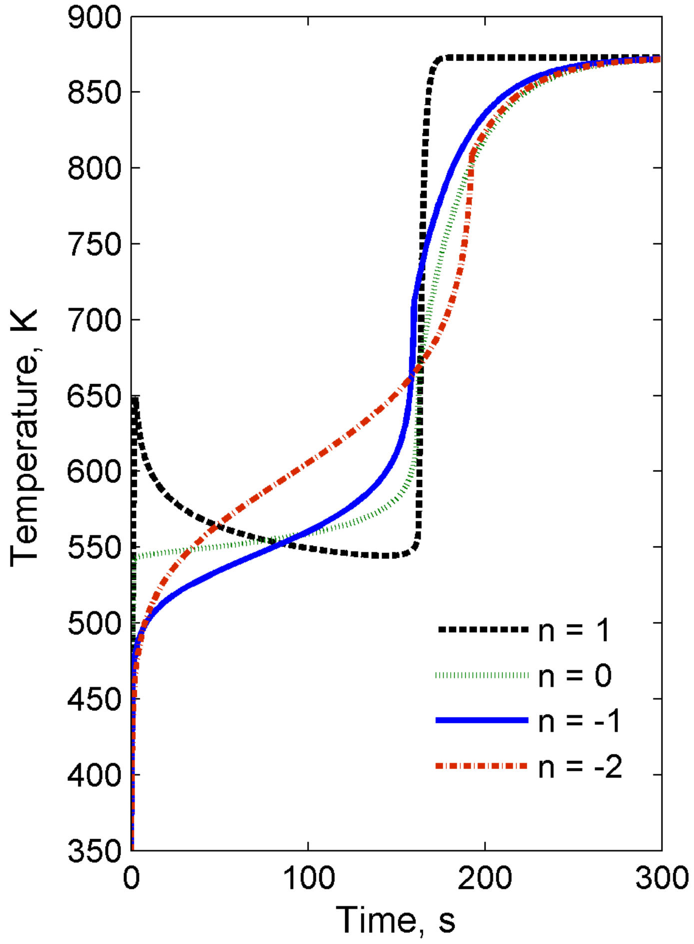

Figure 4.11 – Predicted evolution of particle temperature for different reaction orders, but for fixed activation energy *E* = 131 kJ/mol, at T_b = 898 K.

Table 4.3 – Fitted activation energy coefficients for different reaction orders for a fixed pre-exponential coefficient of $k_0 = 5\times10^7$ $\text{mol}^{-n}\text{m}^{3n+1}$/s in the high temperature range (823–923 K).

n	*E* (kJ/mol)
1	200
0	160
–1	131
–2	115

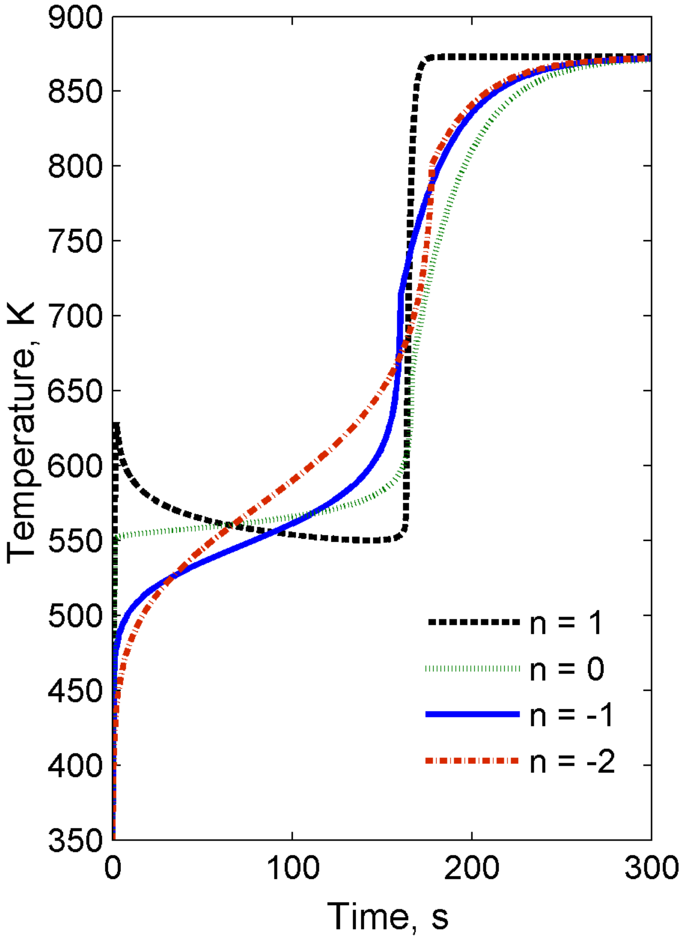

Figure 4.12 – Predicted evolution of particle temperature for different reaction orders, but for fixed pre-exponential coefficient of k_0 = 5×10^7 (mol^{-n}m^{3n+1}/s), at T_b = 898 K.

It can be seen that, for a particular reaction order n, the corresponding particle temperature evolutions in Figure 4.11 and Figure 4.12 are very similar. However, for different reaction orders, the temperature profiles reported in both Figures 4.11 and 4.12 are considerably different. These two observations suggest that it is possible to draw conclusions about the value of n, despite uncertainties in k_0 and E. Stacey (1987) reported an experimental temperature history for a gibbsite particle undergoing thermal decomposition that shows the particle first warming up and then reaching a plateau temperature of about 500 K as the endothermic calcination reaction begins. This plateau endures until conversion is complete and is then followed by a rapid increase in temperature, since the reaction is no longer consuming the energy received from the environment. It is clear from Figures 4.11

and 4.12 that for a reaction order of $n = 1$, the predicted temperature profile is unreasonable, since there is an initial temperature peak followed by a decline and this is not consistent with the observed data. Further, despite the existence of a plateau in the temperature profile for $n = 0$, the plateau temperature is not consistent with the data of Stacey (1987), being about 80 K too high. Both $n = -1$ and $n = -2$ are more compatible with the experimental data, confirming that n should be negative. While $n = -1$ does appear to show better agreement with the experimental data, it is not conclusive and more data are needed. The best reaction order, however, is expected to lie in the range –1 to –2, which agrees with the experimental results of Stacey (1987) and Candela and Perlmutter (1986).

4.4 Summary

Based on the unreacted shrinking core approach, a new predictive model has been developed for solid-to-gas thermal decomposition, in which the gas product species exhibits a negative effect on the reaction rate. Shrinking core models developed previously by other authors cannot be directly applied to such cases as they include gas-phase reactants in their stoichiometry and reaction rate equations. The model predicts particle conversion and temperature as functions of time. For the isothermal case, the numerical solution of the unreacted shrinking core model has been validated against a newly-developed analytical model solution. For non-isothermal conditions, the unreacted shrinking core model results closely match those from a distributed model. The non-isothermal unreacted shrinking core model is simpler and easier to solve than the partial differential-algebraic distributed model developed in the previous chapter. Computational efficiency is relevant in multi-scale modelling since the small-scale model may be run many times during a multi-scale simulation, and this can be a significant advantage if the model is used within an overarching multi-scale model.

A gas-solid reaction, the thermal dehydration of gibbsite to alumina, was used as a case study to verify the model, as well as to investigate its behaviour through a sensitivity study. Using experimental data available in the literature, gibbsite dehydration rate parameters were estimated over a wide temperature range, from 490 K to 923 K. The order of the reaction rate with respect to water vapour concentration was found to be $n = -1$. The inhibiting effect of the water vapour concentration (negative n) leads to improved agreement of the model with experimental data, and yields an activation energy that is in good agreement with values found in the literature. Estimated values of the activation energy and Arrhenius pre-exponential coefficients are reported separately for low and high temperature ranges. Model results show that smaller gibbsite particles achieve complete decomposition in a shorter time.

Nomenclature

a, b, c, d	Stoichiometric coefficients, [–]
Bi	Biot number, [–]
C_{B0}	Initial solid reactant concentration, [mol/m^3]
C_{Cc}	Product gas concentration on core surface, [mol/m^3]
C_{Cb}	Product gas concentration in surrounding environment, [mol/m^3]
C_{Cs}	Product gas concentration on outer particle surface, [mol/m^3]
C_{G0}	Initial gibbsite concentration, [mol/m^3]
C_p	Average molar heat capacity, [J/mol K]
D_e	Effective diffusion coefficient, [m^2/s]
D_p	Particle diameter, [m], $R_p = D_p/2$
E	Activation energy, [J/mol]
ΔH	Reaction enthalpy, [J/mol]
h	Particle heat transfer coefficient, [W/m^2 K]
k	Surface reaction rate constant, [mol^{-n}m^{3n+1}/s]
k_0	Arrhenius pre-exponential coefficient, [mol^{-n}m^{3n+1}/s]
k_p	Particle thermal conductivity, [W/m K]
Mw_B	Molecular weight of solid reactant, [g/mol]
Mw_G	Gibbsite molecular weight, [g/mol]
m	Mass fraction, [–]
$\dot{N}_B$	Solid reactant consumption rate, [mol/s]
N_{Tb}	Number of experimental data points at temperature T_b, [–]
n	Reaction order with respect to water vapour concentration, [–]
P_{Cb}	Water vapour pressure around particle, [Pa]

R	Ideal gas constant, [J/mol K]
R_0	Particle radius, [m]
r	Radial position, [m]
r_c	Unreacted core radius at any time, [m]
r_B	Solid surface reaction rate, [mol/m^2 s]
r_G	Gibbsite surface reaction rate, [mol/m^2 s]
S	Term in analytical solution, [–]
T	Particle temperature, [K]
T_0	Initial particle temperature, [K]
T_b	External temperature, [K]
t	Time, [s]
W_1	Vapour production rate on unreacted core due to reaction, [mol/s]
W_2	Vapour diffusion rate in porous product layer, [mol/s]
X	Reaction conversion, [–]

Greek symbols

β	Dimensionless activation energy, [–]
γ_C	Dimensionless concentration of gas, [–]
ϑ	Ratio of stoichiometric coefficients (*c*/*b*), [–]
ξ	Dimensionless unreacted core radius, [–]
ρ_B	Solid reactant density, [kg/m^3]
ρ_D	Solid product density, [kg/m^3]
ρ_G	Gibbsite density, [kg/m^3]
τ	Dimensionless time, [–]
θ	Dimensionless temperature, [–]
η	Cooling potential defined by Eq.(4.23), [–]
ϕ	Average Thiele modulus, [–]
ω	Heat absorption capacity defined by Eq. (4.24), [–]

References

Amiri, A., Ingram, G.D., Maynard, N., Livk, I., & Bekker, A. 2010. A multiscale modelling outlook for gibbsite calcination. In: *Chemeca 2010*, Adelaide, Australia, 26–29 September 2010.

Amiri, A., Bekker A.V., Ingram, G.D., Livk, I., & Maynard N.E. 2012. A 1-D non-isothermal dynamic model for the thermal decomposition of a gibbsite particle, *Chemical Engineering Research and Design*. 91, 485–496.

Beyer, H.K., Borbély, G., Miasnikov, P. & Rózsa, P. 1989. A new potential large-scale application of zeolites as fire-retardant material, in: Karge, H.G., Weitkamp, J. (Eds.), *Zeolites as Catalysts, Sorbents, and Detergent Builders: Applications and Innovations*, Elsevier, Amsterdam, pp. 635–644.

Bluhm-Drenhaus, T., Simsek, E., Wirtz, S., & Scherer, V. 2010. A coupled fluid dynamic-discrete element simulation of heat and mass transfer in a lime shaft kiln. *Chemical Engineering Science*. 65, 2821–2834.

Cameron, I.T., Ingram, G.D., & Hangos, K.M. 2006. Multiscale process modelling, in: Puigjaner, L., Heyen, G. (Eds.), *Computer Aided Process and Product Engineering*, Vol. 1, Wiley-VCH, Weinheim, pp. 189–221.

Candela, L., & Perlmutter, D.D. 1986. Pore structure and kinetics of the thermal decomposition of $Al(OH)_3$. *AIChE Journal*. 32, 1532–1545.

Candela, L., & Perlmutter, D.D. 1992. Kinetics of boehmite formation by thermal decomposition of gibbsite, *Industrial & Engineering Chemistry Research*. 31, 694–700.

Canò, G., Salatino, P., & Scala, F. 2007. A single particle model of the fluidized bed combustion of a char particle with a coherent ash skeleton: Application to granulated sewage sludge. *Fuel Processing Technology*. 88, 577–584.

Chang, Y.I., & Kuo, J.A. 1999. Application of the three-stage shrinking core model in the transport of reactive gas in the porous media. *Journal of Petroleum Science and Engineering*. 22, 205–216.

Chern, J.S., & Hayhurst, A.N. 2010. A simple theoretical analysis of the pyrolysis of an isothermal particle of coal. *Combustion and Flame*. 157, 925–933.

Fowler, J.D., Chandra, D., Elleman, T.S., Payne, A.W., & Verghese, K. 1977. Tritium diffusion in Al2O3 and BeO. *Journal of the American Ceramic Society*. 60, 155–161.

Gan, B.K., Madsen, I.C., & Hockridge, J.G. 2009. *In situ* X-ray diffraction of the transformation of gibbsite to α-alumina through calcination: effect of particle size and heating rate, *Journal of Applied Crystallography*. 42, 697–705.

Garcìa-Labiano, F., Abad, A., de Diego, L. F., Gayán, P., & Adánez, J. 2002. Calcination of calcium-based sorbents at pressure in a broad range of CO_2 concentrations, *Chemical Engineering Science*. 57, 2381–2393.

Gómez-Barea, A., & Ollero, P. 2006. An approximate method for solving gas-solid non-catalytic reactions, *Chemical Engineering Science*. 61, 3725–3735.

Homma, S., Ogata, S., Koga, J., & Matsumoto, S. 2005. Gas-solid reaction model for a shrinking spherical particle with unreacted shrinking core. *Chemical Engineering Science*. 60, 4971–4980.

Hu, N., & Scaroni, A.W. 1996. Calcination of pulverized limestone particles under furnace injection conditions. *Fuel*. 75, 177–186.

Incropera, F.P., DeWitt, D.P., Bergman, T.L., & Lavine, A.S. 2007. *Fundamentals of Heat and Mass Transfer*, sixth ed. John Wiley, Hoboken.

Ishida, M., & Wen, C.Y. 1971. Comparison of zone-reaction model and unreacted-core shrinking model in solid-gas reactions – I Isothermal analysis. *Chemical Engineering Science*. 26, 1031–1041.

Jovanović, N., Novaković, T., Janaćković, J., & Terlecki-Baričević, A. 1992. Properties of activated alumina obtained by flash calcination of gibbsite. *Journal of Colloid and Interface Science*. 150, 36–41.

Kasaoka, S., Sakata, Y., & Tong, C. 1985. Kinetic evaluation of the reactivity of various coal chars for gasification with carbon dioxide in comparison with steam. *International Journal of Chemical Engineering*. 25, 160–175.

Klett, C., Reeb, B., Missalla, M., & Schmidt, H.-W., 2011. Methods to reduce operating costs in circulating fluidized bed calcination. In: Lindsay, S.J. (Ed.), *Light Metals 2011*. John Wiley & Sons, New York, pp. 125–130.

Kunii, D., & Levenspiel, O. 1991. *Fluidization Engineering*, second ed. Butterworth-Heinemann, Boston, pp. 268–271.

Lopushan, V.I., Kuznetsov, G.F., Pletnev, R.N., & Kleshev, D.G. 2007. Kinetics of phase transitions of gibbsite during heat treatment in air and in water vapour. *Refractories and Industrial Ceramics*. 48, 378–382.

Mahuli, S.K., Agnihotr, R., Jadhav, R., Chauk, S., & Fan, L.-S. 1999. Combined calcination, sintering and sulfation model for $CaCO_3$-SO_2 reaction. *AIChE Journal*. 45, 367–382.

Marsh, C. 2009. CFD Modelling of alumina calciner furnaces. In: *Seventh International Conference on CFD in the Minerals and Process Industries*, Melbourne, Australia, 9–11 December 2009.

Moffat, W., & Walmsley, M.R.W. 2005. Understanding lime calcination kinetics for energy cost reduction. In: *59th Appita Annual Conference and Exhibition*, Auckland, New Zealand, 16–19 May 2005.

Molina, A., & Mondragón, F. 1998. Reactivity of coal gasification with steam and CO_2. *Fuel*. 77, 1831–1839.

Perlander, L.M., 2010. *Evolution of Nano- and Microstructure during the Calcination of Bayer Gibbsite to Produce Alumina.* PhD thesis, University of Auckland, pp. 49, 88.

Sadhukhan, A.K., Gupta, P., & Saha, R.K. 2010. Modelling of combustion characteristics of high ash coal char particles at high pressure: Shrinking reactive core model. *Fuel*. 89, 162–169.

Shackelford, J.F., & Alexander, W. 2001. *CRC Materials Science and Engineering Handbook*, third ed. CRC Press LLC, Boca Raton.

Silcox, G.D., Kramlich, J.C., & Pershing, D.W. 1989. A mathematical model for the flash calcination of dispersed calcium carbonate and calcium hydroxide particles. *Industrial & Engineering Chemistry Research*. 28, 155–160.

Stacey, M.H. 1987. Kinetics of decomposition of gibbsite and boehmite and the characterization of the porous products, *Langmuir*. 3, 681–686.

Stanmore, B.R., & Gilot, P., 2005. Review—calcination and carbonation of limestone during thermal cycling for CO2 sequestration. *Fuel Processing Technology*. 86, 1707–1743.

Wang, H., Xu, B., Smith, P., Davies, M., DeSilva, L., & Wingate, C. 2006. Kinetic modelling of gibbsite dehydration/amorphization in the temperature range 823–923 K. *Journal of Physics and Chemistry of Solids*. 67, 2567–2582.

Wefers, K., & Misra, C. 1987. Oxides and hydroxides of aluminium. Technical Paper No. 19, *Alcoa Laboratories*, Pittsburgh, PA.

Whittington, B., & Ilievski, D. 2004. Determination of the gibbsite dehydration reaction pathway at conditions relevant to Bayer refineries. *Chemical Engineering Journal*. 98, 89–97.

Williams, F.S., & Misra, C. 2011. Pressure calcination revisited. In: Lindsay, S.J. (Ed.), *Light Metals 2011*. John Wiley & Sons, New York, pp. 131–136.

Ying, Z., Chuguang, Z., Zhaohui, L., & Xuefeng, S. 2000. Modelling for flash calcination and surface area development of dispersed limestone particles. *Developments in Chemical Engineering and Mineral Processing*. 8, 233–243.

5

A multi-stage, multi-reaction shrinking core model for self-inhibiting gas-solid reactions

Some thermal decomposition reactions display self-inhibiting behaviour, where the produced gas negatively influences the reaction progress. Further, a build-up of internal pressure caused by the product gas may alter the reaction pathway over the reaction duration in a way that favours a particular pathway over others. Two well-known cases of this kind of reaction are the thermal decomposition of limestone and gibbsite, in which carbon dioxide and water vapour are the produced gases, respectively. In this chapter, a multi-stage, multi-reaction, shrinking core model is proposed for this type of process. The model emphasises the role of the produced gas, not only in mass transfer, but also in the reaction kinetics. It extends the single-reaction models of Chapters 3 and 4 by including parallel and series reaction pathways, allowing for the formation of an intermediate species. The model has been applied to the conversion of gibbsite to alumina, including the formation intermediate boehmite. The model results are in good agreement with experimental data from the literature for gibbsite conversion, boehmite formation and subsequent consumption, as well as alumina formation. Further, the corresponding kinetic parameters are estimated for all reactions. Significantly, the experimentally-observed plateaux in the particle's temperature history are predicted by the model. In addition, the role of heating rate and particle size on boehmite formation is evaluated using the model, and is in agreement with practical observations.

5.1. Introduction

Many modelling techniques have been reported on both catalytic and non-catalytic gas-solid particle reactions using a variety of approaches depending upon the physical and chemical properties of the solid and the type of reaction considered. Comprehensive reviews of the major modelling categories and their features are given by Ramachandran and Doraiswamy (1982) and Molina and Mondragón (1998). The importance of developments in gas-solid reaction modelling is still high since a wide variety of reactions encountered in the process industries belong to this class. Combustion, gasification, roasting, calcination, reduction of metal ores, and catalyst regeneration are typical industrial gas-solid processes demanding new modelling tools for process intensification and product design. Modelling becomes crucial when prediction and control of transients during reaction at high conversion rates and at high temperature is the subject of investigation. In such cases deeper insight will be achieved by carefully establishing the relationships between dominant mechanisms, including reaction kinetics and transport processes, as well as structural changes taking place over the reaction period. Further, the combination of different sub-models at different time and length scales in a multi-scale modelling framework makes it possible to deal with product quality issues (small scale) via control of the process (large scale).

To date, particle reaction models have been mainly based on reactions with a positive order, particularly first order reactions. The variation of the reaction mechanism over the reaction period due to a change of internal conditions, like the build-up of gas pressure inside the particle, has not been extensively studied.

Mantri et al. (1976) proposed a three-zone model comprised of a core, an outer product layer and a reacting zone in between them. The model is based on a single reaction and it is assumed that the reaction is first order with respect to gas concentration and zero order with respect to the solid. This model was applied by Chang and Kuo (1999) to predict the transport of reactive gas in a packed bed of porous media. A variation of the shrinking core model with an intermediate layer was also proposed by Homma et al. (2005). In their work, fresh reactant is converted to an intermediate followed by conversion of the intermediate to a gas product without leaving any ash (solid) layer. This model was also based on a first order reaction with respect to the gaseous reactant. The intermediate component formed immediately and the final product was formed only via consumption of the intermediate. Suresh and Ghoroi (2009) developed a model for solid-solid reactions in series for a single particle. In their work, multiple reactions were considered and reaction rates were first order with respect to the solid concentrations.

The objective of this chapter is to extend the shrinking core model developed in Chapter 4, which considered a particular class of gas-solid reactions in which the released gas reduces the reaction rate, so that changes in the reaction mechanism and the formation of an intermediate solid species are accounted for. Calcination and thermal dehydration / decomposition of solid particles belong to this category of gas-solid reactions. The prediction of the formation and consumption of an intermediate species is a leading feature of the model developed in this chapter. This kind of information is needed for maximization or minimization of the amount of the intermediate in the product via process control. The involvement of multiple reactions with different orders, and determination of reaction-switching times are other notable features of this new version of the shrinking core model.

As in Chapters 3 and 4, the calcination of gibbsite to alumina is used as a case study, but unlike those previous chapters, allowing for the production of intermediate boehmite is the focus of this chapter. The importance of this system and the extent of previous modelling work have already been noted in Sections 3.1 and 4.1. A single gibbsite particle undergoing calcination is studied in this chapter to establish a predictive three-stage model for particle conversion at the high temperatures relevant to industrial operations. This study explores the effect of water vapour pressure inside the particle on competing reactions and it includes the reaction orders with respect to vapour concentration for the various gibbsite calcination reactions.

Parameter estimation is performed by using two sets of experimental data from Wang et al. (2006), then the model is validated against another data set at a different temperature. While gibbsite calcination is the focus of this paper, the model developed is general enough to be applied to other reactions in which a gaseous species is a reaction product only, for example pyrolysis of carbon-based materials, thermal decomposition of some organic and inorganic compounds, and the reduction of metal oxides.

In Section 5.2, the nature of the reaction system is presented and discussed along with model assumptions. The model’s geometry, temporal stages, equations and numerical solution methodology are presented in Section 5.3, with two supporting appendices containing the model derivation details. Section 5.4 applies the model to a case study, the dehydration of gibbsite to alumina, which involves parameter estimation, model validation and sensitivity analyses. The study’s conclusions are presented in Section 5.5.

5.2. Reaction kinetics and modelling assumptions

As noted previously, unreacted core models for gas-solid reactions, in which the reaction rate is based on the reactant gas concentration, have been widely applied in the literature. Most previous investigations have focused on gas-solid reactions that were generally represented by a reaction such as: *gas* + *solid* → *solid* + *gas*. First order kinetics with respect to the reacting gas concentration were usually assumed. However, in several industrially-important reactions, gas-phase species are reaction products only. In this chapter, three reactions are considered and there is no gaseous reactant. The following stoichiometric equations are used to represent parallel and series gas-solid reactions in a single particle:

$$aA_{(s)} \xrightarrow{k_1} dD_{(s)} + cC_{(g)} \tag{5.1}$$

$$a'A_{(s)} \xrightarrow{k_2} b'B_{(s)} + c'C_{(g)} \tag{5.2}$$

$$b''B_{(s)} \xrightarrow{k_3} d''D_{(s)} + c''C_{(g)} \tag{5.3}$$

Species *A* is the solid reactant; *B* is the solid intermediate; *D* is the final solid product, which may be formed directly from *A* through reaction (5.1) or via *B* in reactions (5.2) and (5.3); and *C* is the gaseous product.

The assumptions on which the mathematical model stands are

- The particle is initially pure, non-porous species *A*.
- A reaction of the form of Eq. (5.1) initially takes place on the surface of the unreacted core to produce a gas and a porous product layer, which adheres to the solid core. After a particular point, the reactions of Eqs. (5.2) and (5.3) begin, forming and consuming the layer of intermediate solid *B*. Details of the reaction transition criteria are given later.
- The gas species formed diffuses through the porous product and intermediate layers, and a pseudo-steady state gas-phase concentration profile exists in the two layers. The effective diffusion coefficient is assumed to be the same in both layers. The pseudo-steady state assumption is reasonably acceptable for gas-solid reactions as in the majority of cases the criterion $C_{(g)} / C_{(s)} \leq 10^{-3}$ holds (Gómez-Barea and Ollero, 2006).
- The particle is spherical with constant outer diameter during the reaction.

- The mass transfer rate through the surrounding gas layer outside the particle is assumed to be very high, so that the gas concentration at the particle surface and in the bulk gas is the same.
- The particle temperature is spatially uniform (Chapter 3), but may vary with time. The particle exchanges energy with its surroundings by a combined convection and radiation heat transfer coefficient.

These assumptions are very similar to those of the unreacted shrinking core model developed in Chapter 4, with the exception of the more complicated set of reactions involved.

Although competition between different reaction pathways can be assessed by comparing intrinsic reaction rate constants at the same conditions, more factors, however, need to be considered to evaluate the reaction pathway selectivity. For instance, heating rate, gas pressure inside the particle and particle size may alter the reaction mechanism to favour one pathway over others (Candela and Perlmutter, 1986). This issue will be discussed later. This study couples the reaction pathways given by Eqs. (5.1)–(5.3) in a reacting particle model to investigate the effect of dominant parameters including reaction and diffusion rates.

Solid conversion is considered to be negatively affected by the presence of the gas product *C*. The reaction rate has been modelled as being proportional to the difference between the partial pressure of the gaseous reactant and the equilibrium partial pressure; however, the following expression with a flexible order for the surface reaction rate has been used (Candela and Perlmutter, 1992):

$$(-r_s) = kC_{S0}C_C^n \tag{5.4}$$

where $S = A$ or B, n is negative, and the rate coefficient obeys the Arrhenius equation:

$$k = k_0 e^{(-E/RT)} \tag{5.5}$$

5.3. Mathematical model description and development

In the model, the particle is converted over several stages as presented in Figure 5.1. During the first stage ($0 \leq t \leq t_{12}$), the reaction of A starts at the outer surface of the particle, forming porous solid D and gas C according to reaction (5.1). As the thickness of the D layer increases with the reaction progress, escape of the produced gas becomes more difficult due to internal diffusion resistance, causing higher gas pressure at the reaction front. At a certain level of C gas pressure, the reaction mechanism changes and intermediate species B begins to form via reaction (5.2), and this point marks the end of stage 1. In the first stage, therefore, the particle consists of an unreacted core of A surrounded by a layer of D.

At time t_{12}, which marks the beginning of stage 2, the intermediate species B starts to form. The B then reacts to D via reaction (5.3). Thus, during stage 2, the particle has three zones – an inner unreacted core of A, a middle zone of the intermediate B, and an outer zone of product D. During stage 2, reactions (5.2) and (5.3) occur simultaneously at the A-B and B-D interfaces, respectively. Diffusive mass transfer of C also occurs in the intermediate and product layers.

The beginning of stage 3 occurs at time t_{23}, which happens when the A core disappears completely and the particle again has two zones – a B core and an outer product D layer. During this stage only reaction (5.3) is taking place at the B core surface. This stage ends with a completely converted particle that consists of D only.

5.3.1 Model derivation

The derivations of the governing ordinary differential and algebraic equations for stage 1 and 2 (Figure 5.1) are presented in Appendices A and B of this chapter, respectively. The governing equations for stage 3 are similar to those of stage 1 if species A is replaced by B. The model equations for all stages are summarised in Table 5.1.

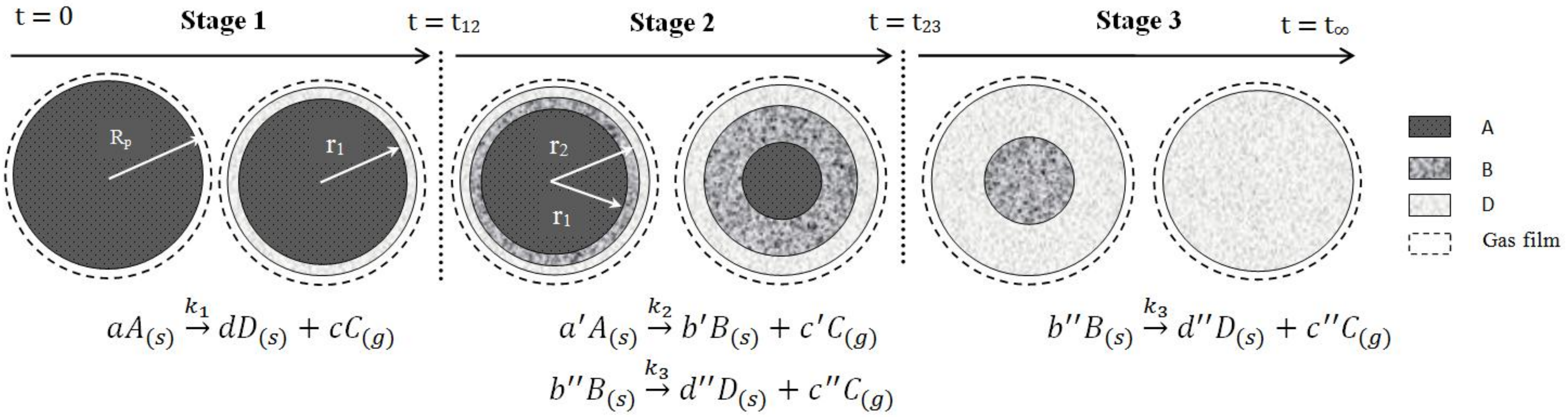

Figure 5.1 – Schematic of solid particle reaction including intermediate formation.

Table 5.1 – Governing equations of the multi-stage model.

Stage 1		
$C_{C1}-C_{Cs}-\frac{\vartheta_1 k_1 C_{C1}^{n_1} C_{A0}}{D_e} r_1^2\left(\frac{1}{r_1}-\frac{1}{R_p}\right)=0$	with $k_1=k_{01}e^{(-E_1/RT)}$	(5.6)
$-\frac{dr_1}{dt}=\frac{Mw_A}{\rho_A}k_1 C_{A0} C_{C1}^{n_1}$	$r_1 = R_p$ at $t = 0$	(5.7)
$\frac{R_p^3 \rho_e C_{pe}}{3Mw_e}\frac{dT}{dt}=R_p^2 h(T_b-T)-r_1^2 k_1 C_{A0} C_{C1}^{n_1}\Delta H_1$	$T = T_0$ at $t = 0$	(5.8)
Stage 2		
$C_{C1}-C_{C2}-\frac{\vartheta_2 k_2 C_{C1}^{n_2} C_{A0}}{D_e} r_1^2\left(\frac{1}{r_1}-\frac{1}{r_2}\right)=0$	with $k_2=k_{02}e^{(-E_2/RT)}$	(5.9)
$C_{C2}-C_{Cs}-\frac{\vartheta_2 k_2 C_{C1}^{n_2} C_{A0} r_1^2+\vartheta_3 k_3 C_{C2}^{n_3} C_{B0} r_2^2}{D_e}\left(\frac{1}{r_1}-\frac{1}{R_p}\right)=0$	and $k_3=k_{03}e^{(-E_3/RT)}$	(5.10)
$-\frac{dr_1}{dt}=\frac{Mw_A}{\rho_A}k_2 C_{A0} C_{C1}^{n_2}$	$r_1 = r_{12}$ at $t = t_{12}$	(5.11)
$-\frac{dr_2}{dt}=\frac{Mw_B}{\rho_B}k_3 C_{B0} C_{C2}^{n_3}$	$r_2 = r_{12}$ at $t = t_{12}$	(5.12)
$\frac{R_p^3 \rho_e C_{pe}}{3Mw_e}\frac{dT}{dt}=R_p^2 h(T_b-T)-r_1^2 k_2 C_{A0} C_{C1}^{n_2}\Delta H_2-r_2^2 k_3 C_{B0} C_{C2}^{n_3}\Delta H_3$	$T = T_{12}$ at $t = t_{12}$	(5.13)
Stage 3		
$C_{C2}-C_{Cs}-\frac{\vartheta_3 k_3 C_{C2}^{n_3} C_{B0}}{D_e} r_2^2\left(\frac{1}{r_2}-\frac{1}{R_p}\right)=0$		(5.14)
$-\frac{dr_2}{dt}=\frac{Mw_B}{\rho_B}k_3 C_{B0} C_{C2}^{n_3}$	$r_2 = r_{23}$ at $t = t_{23}$	(5.15)
$\frac{R_p^3 \rho_e C_{pe}}{3Mw_e}\frac{dT}{dt}=R_p^2 h(T_b-T)-r_2^2 k_3 C_{B0} C_{C2}^{n_3}\Delta H_3$	$T = T_{23}$ at $t = t_{23}$	(5.16)
Calculation of r_{12} and C_{12}		
$C_{12}-C_{Cs}-\frac{\vartheta_1 k_1 C_{12}^{n_1} C_{A0}}{D_e} r_{12}^2\left(\frac{1}{r_{12}}-\frac{1}{R_p}\right)=0$		(5.17)
$C_{12}-C_{Cs}-\frac{\vartheta_2 k_2 C_{12}^{n_2} C_{A0} r_{12}^2+\vartheta_3 k_3 C_{12}^{n_2} C_{B0} r_{12}^2}{D_e}\left(\frac{1}{r_{12}}-\frac{1}{R_p}\right)=0$		(5.18)

Calculation of t_{12} and t_{23} is based on requiring continuity of the model predictions during the transition from stages 1 to 2, and stages 2 to 3, respectively. During the numerical integration of Eqs. (5.6)–(5.13), the transition between stages 1 and 2 takes place at t_{12}, which is the time when the product gas C reaches a critical concentration, C_{12}, at the reacting core surface. The critical concentration, which is temperature-dependent, is found by requiring that the governing equations of stage 1 and stage 2 predict the same gas concentration at the core at the point of transition. In particular, at time t_{12}, the gas-species mass balances Eqs. (5.6) and (5.10) should both apply and yield $C_{C1} = C_{C2} = C_{12}$ for $r_1 = r_2 = r_{12}$. The nonlinear system of algebraic equations (5.17) and (5.18), which are derived from Eqs. (5.6) and (5.10), therefore needs to be solved simultaneously at each integration step to find r_{12} and C_{12}. Consequently, t_{12} is the time taken for r_1 to decrease from R_p to r_{12}. On the other hand, t_{23} is the integration time when the last A at the centre of the particle finally disappears; that is, when r_1 reaches zero according to Eq. (5.11). The particle temperatures at t_{12} and t_{23} are denoted by T_{12} and T_{23}, respectively.

5.3.2 Model solution

The model was solved numerically in Matlab® R2010b. During each model stage, the relevant ordinary differential-algebraic equations (DAEs) were integrated using the Matlab DAE solver *ode23t*. The transitions between stages needed some consideration and the entire simulation proceeded as follows:

(i) Initial estimates of r_{12} and C_{12} were produced by solving Eqs. (5.17) and (5.18) using the Matlab zero-finding routine *fzero* for k_1–k_3 evaluated at $T = T_b$. The time and particle temperature for which $r_1 = r_{12}$ were denoted as t_{12} and T_{12}, respectively.

(ii) The stage 1 equations (5.6)–(5.8) were integrated from $t = 0$ to large t.

(iii) Eqs. (5.17) and (5.18) were again solved using *fzero* to find new values of r'_{12} and C'_{12} for k_1–k_3 evaluated at $T = T_{12}$. New values for the time and particle temperature for which $r_1 = r'_{12}$ were denoted as t'_{12} and T'_{12}, respectively.

(iv) If the difference between T_{12} and T'_{12} was greater than a given tolerance, then $t_{12} = t'_{12}$, $T_{12} = T'_{12}$ was set and steps (ii) and (iii) were repeated.

(v) The stage 2 equations (5.9)–(5.13) were integrated from $t = t_{12}$ to large t.

(vi) The stage 2 / stage 3 transition time t_{23} was identified as the time for which $r_1 = 0$.

(vii) The stage 3 equations (5.14)–(5.16) were integrated from $t = t_{23}$ to large t.

(viii) The reaction completion time t_∞ was identified as the time at which $r_2 = 0$. Numerical results generated in step (vii) for $t > t_\infty$ were discarded.

5.3.3 Conversion and mass fractions

At any stage over the reaction period, the conversion of A and the mass fraction of each species in the particle can be calculated from the radius of the reaction front and the particle radius. The conversion of A is given by

$$1 - X(t) = \left(\frac{r_1}{R_p} \right)^3 \tag{5.19}$$

The mass fraction of a solid component in the particle can be calculated by

$$m_i(t) = \frac{n_i Mw_i}{\sum_j n_j Mw_j} \tag{5.20}$$

where Mw_i and n_i are the molecular weight and number of moles of species $i \in \{A, B, D\}$. The conversion of A and mass fractions are evaluated in post-processing.

5.4. Case study

The calcination of gibbsite ($Al(OH)_3$) to alumina (Al_2O_3) takes place mainly via two well-known reaction and phase transition pathways, one of which involves boehmite (AlOOH). Heating rate, particle size distribution and water vapour pressure inside and around the particles are the main parameters that affect the reaction pathway. Regardless of any additional intermediate phases, the gibbsite calcination pathways may be summarized as:

$$2Al(OH)_3 \xrightarrow{k_1} Al_2O_3 + 3H_2O \tag{5.21}$$

$$Al(OH)_3 \xrightarrow{k_2} AlOOH + H_2O \tag{5.22}$$

$$2AlOOH \xrightarrow{k_3} Al_2O_3 + H_2O \tag{5.23}$$

A comparison of the gibbsite calcination reactions of Eqs. (5.21)–(5.23) with the reactions of the general model, Eqs. (5.1)–(5.3), indicates the following correspondence: A = Al(OH)$_3$, D = Al$_2$O$_3$, B = AlOOH, C = H$_2$O, $a = b'' = 2$, $c = 3$, and $a' = b' = c' = c'' = d = d'' = 1$.

According to Whittington and Ilievski (2004) and Candela and Perlmutter (1992), boehmite formation occurs more readily in the presence of high water vapour pressure and in large particles. However, even at high vapour pressures and for large particles (above 50 µm), the maximum boehmite mass fraction in a reacting gibbsite particle is reported as 30% by Whittington and Ilievski (2004).

In the above reactions, water vapour is a product and causes a barrier to reaction progress. The reaction rate equations include the influence of the water vapour concentration, and may include or exclude the solid concentration; for example, for the reaction of gibbsite, either of the following equations could apply:

$$-r_G = k_0 C_{G0} e^{(-E/RT)} C_A^n \tag{5.24}$$

$$-r_G = k_0^{'} e^{(-E/RT)} C_G C_A^n \tag{5.25}$$

where n denotes the order of reaction and C_G and C_A represent the gibbsite concentration and water vapour concentration, respectively. In this study, the reaction rate was considered to be independent of the solid concentration, so Eq. (5.24) was used. Similar rate expressions were used for boehmite dehydration.

5.4.1. Parameter estimation and model validation

Wang et al. (2006) performed gibbsite calcination experiments at elevated temperature (823 to 923 K) with a particle size range from 20 nm to 2000 µm. Two of their data sets were used for parameter estimation and one for model validation. Most of the model's parameter values were taken from the literature as noted in Table 5.2; however, k_{01}, k_{02} and k_{03} were determined via least squares parameter estimation using the experimental data of Wang et al. (2006) at 898 and 923 K according to

$$\min_{\substack{k_{01},k_{02},\\ k_{03}}} \sum_{S=A,B,D} \sum_{i=1}^{N} [m_{S,model}(i) - m_{S,expt}(i)]^2 \tag{5.26}$$

Table 5.2 – Model parameters.

Parameter	Value	Reference / comment
$C_{pe}(J/mol.K)$	80	Wefers and Misra (1987)
$D_e(m^2/s)$	7×10^{-10}	Value for alumina; Fowler et al. (1977)
$R_p\,(\mu m)$	50	Wang et al. (2006)
$E_1(kJ/mol)$	131	Determined in Chapter 3
$E_2(kJ/mol)$	142	Ruff et al. (2008)
$E_3(kJ/mol)$	145	Estimated in Appendix C of this chapter
$h(W/m^2.K)$	1.5	Incropera et al. (2007)
$k_{01}(mol^{-n}m^{3n+1}/s)$	6.18×10^7	Found by parameter estimation via Eq. (5.26)
$k_{02}(mol^{-n}m^{3n+1}/s)$	1.3×10^6	Found by parameter estimation via Eq. (5.26)
$k_{03}(mol^{-n}m^{3n+1}/s)$	3.5×10^5	Found by parameter estimation via Eq. (5.26)
$P_{Cb}(kPa)$	3	Typical environmental water vapour pressure
n_1	–1	Determined in Chapter 3
n_2	–0.5	Approximate value established in scoping studies
n_3	–0.4	Stacey (1987)
$T_b(K)$	873–923	Experimental conditions of Wang et al. (2006)

The reaction orders n_1 and n_3 were taken from previous publications while n_2 was estimated in scoping studies as reported in Table 5.2. Independent estimation of the value for E_3, the activation energy of the boehmite to alumina reaction, is provided in Appendix C. Figure 5.2 demonstrates the good fit of the model to the data at 898 and 923 K, where the coefficients of determination (R^2) were 0.87 and 0.95, respectively. Using these fitted parameters, the model was validated against the data at 873 K, which results in very good agreement ($R^2 = 0.89$) as shown in Figure 5.3.

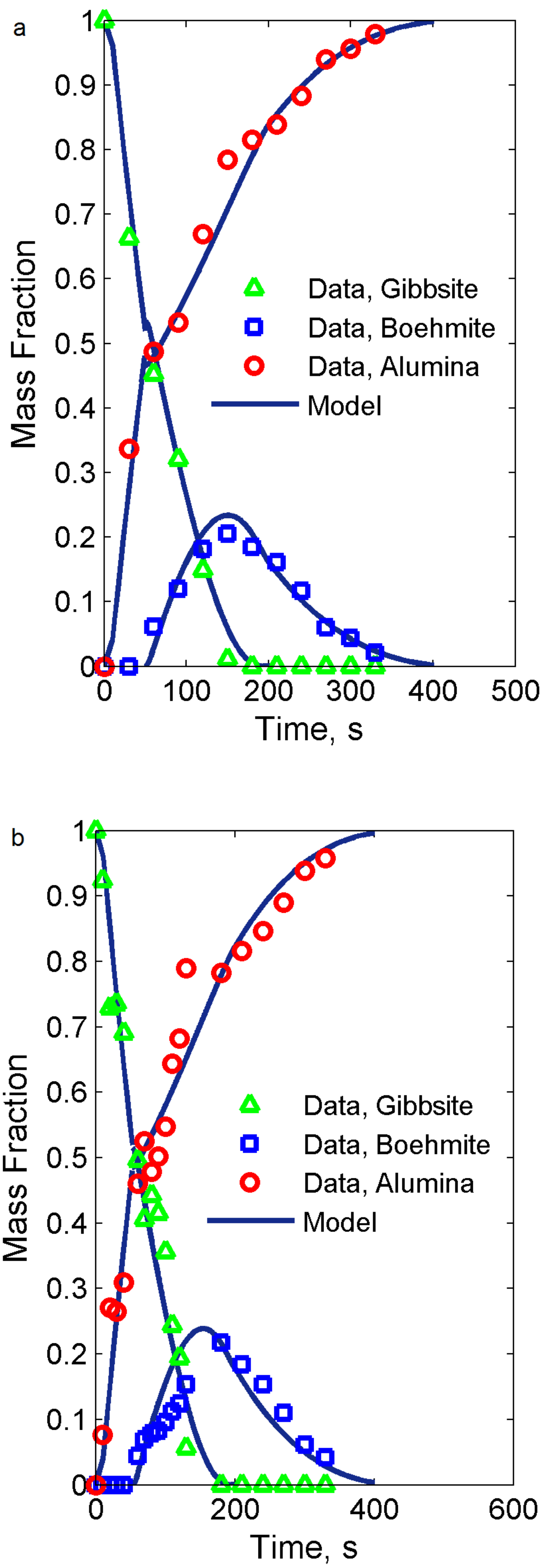

Figure 5.2 – The results of parameter estimation at different environmental temperatures: 923 K (a) and 898 K (b), using data from Wang et al. (2006).

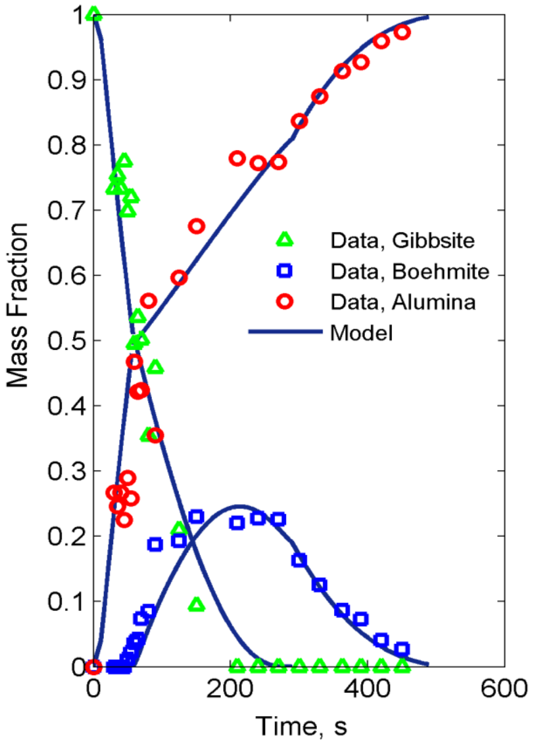

Figure 5.3 – Model validation at 873 K using data from Wang et al. (2006).

5.4.2. Comparison of single and multi-reaction scenarios

Figure 5.4 compares the current model's predictions with those of a reduced version of the model in which boehmite formation is ignored and it is assumed that gibbsite reacts entirely according to Eq. (5.1). The full model predicts the depletion of gibbsite, the production and consumption of intermediate boehmite, and the production of alumina, with $R^2 = 0.95$ as noted in the previous section. The reduced model, however, offers a moderately acceptable prediction for gibbsite consumption, but overestimates the rate of alumina production and completely ignores the presence of boehmite, resulting in $R^2 = 0.41$. It should be noted that the same kinetic parameters are used in both full and reduced models in this comparison. While the single-stage model prediction for gibbsite consumption could be improved by a separate parameter fitting, it will still display unreasonable results for alumina and boehmite formation. Figure 5.4 clearly shows the current multi-stage, multi-reaction model is superior to a single-stage, single-reaction model.

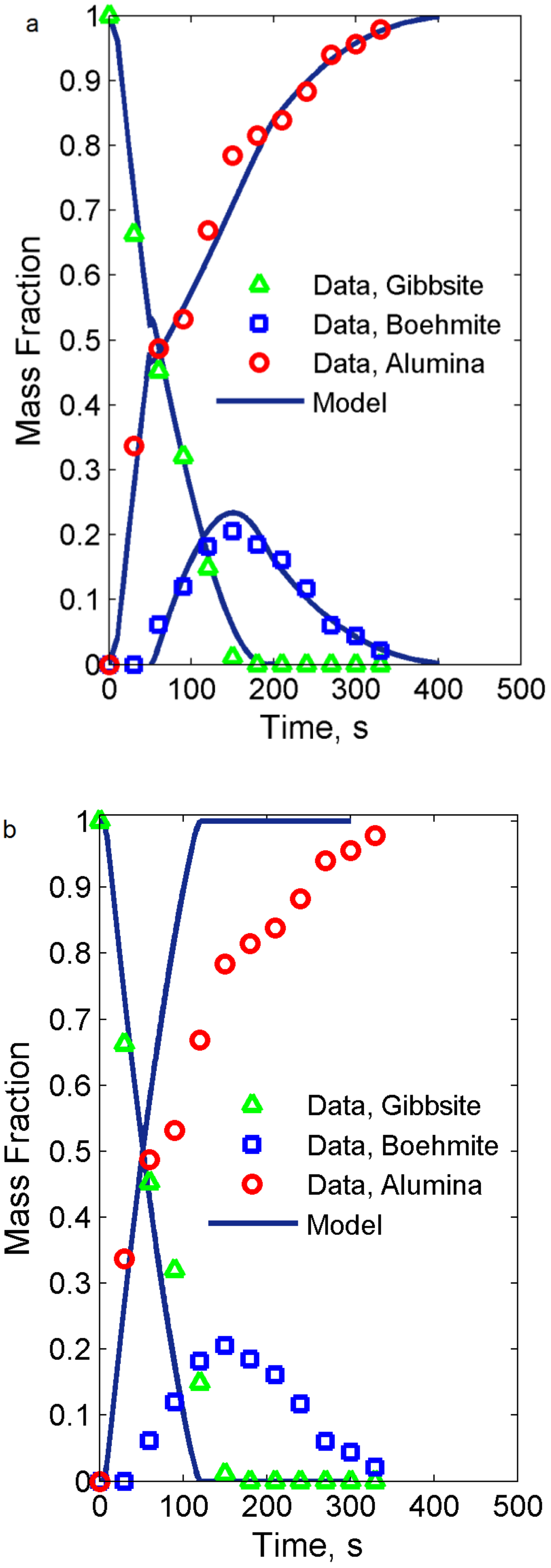

Figure 5.4 – Comparison of model predictions and experimental data from Wang et al. (2006) at 923 K: (a) the multi-stage, multi-reaction model, and (b) the reduced, single-reaction version.

5.4.3. Particle temperature history

Consideration of the temperature history of the reacting particle can give insight into the conversion progress. It is possible to interpret the change in the dominant reaction mechanism over the reaction time using the temperature history of the reacting particle. Stacey (1987) reported a range of experimental dynamic temperature profiles for the thermal decomposition of gibbsite and boehmite. The plateaux in the dynamic temperature profiles and the transitions between them result from switching of the reaction pathways, Eqs. (5.21)–(5.23), and also how long each pathway endures. In Chapter 3, it was confirmed that the distributed model with a single gibbsite to alumina reaction (Eq. 5.21) reproduces the low temperature gibbsite plateau from Stacey (1987). It is also shown in Appendix C of this chapter that the current model, modified to consider only the boehmite to alumina reaction (Eq. 5.23), can replicate the boehmite temperature plateau reported by Stacey (1987) for E_3 = 145 kJ/mol.

Figure 5.5 shows the temperature history of a gibbsite particle undergoing thermal decomposition based on the proposed model for the conditions in Table 5.2, along with an interpretation of the processes taking place. This temperature history results from the interaction of three reactions: (i) gibbsite to alumina, (ii) gibbsite to boehmite, and (iii) boehmite to alumina. The extent to which each reaction pathway is followed and the reaction durations vary with the process parameters (particle size, environmental temperature, and others), as examined in this chapter and in Chapters 3 and 4. The current model predicts boehmite formation and its consumption during the reaction, producing an additional temperature plateau, as shown in Figure 5.5, that was not reported by Stacey (1987). Boehmite formation is also reported by Stacey (1987) at the beginning of calcination, while the experiments of Wang et al. (2006) and the current model show a clear delay in boehmite formation. The differences between these experimental studies, and between the present temperature predictions and the data of Stacey, are partly due to differences in the process parameters used in the model.

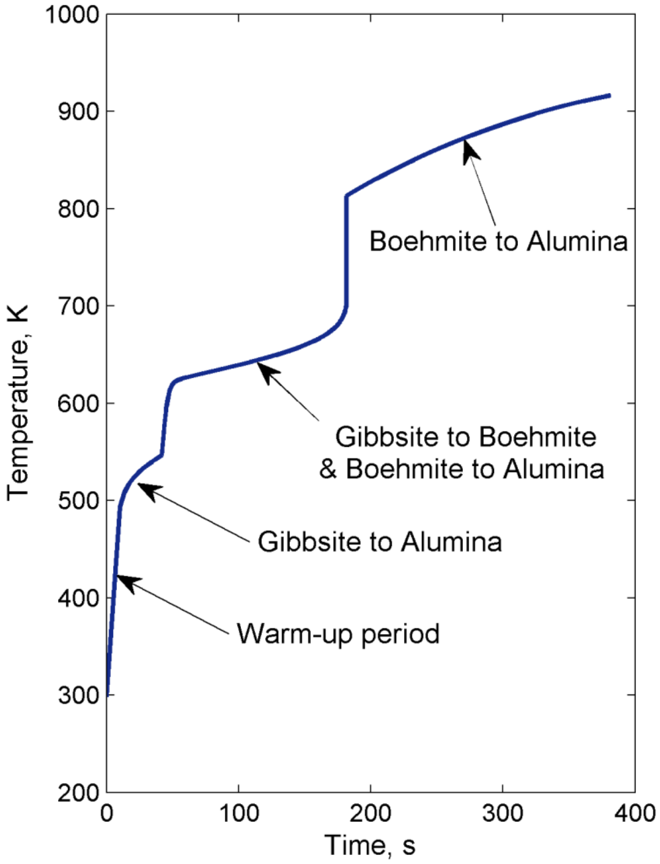

Figure 5.5 – Predicted particle temperature history for T_b = 923 K.

5.4.4. Effect of particle size on intermediate formation

As mentioned earlier, experimental investigations have shown a higher propensity for boehmite formation in coarser particles (Whittington and Ilievski, 2004; Candela and Perlmutter, 1992). The behaviour of the proposed model is consistent with this finding. As presented in Figure 5.6, boehmite formation increases significantly as the particle size increases. As expected, total conversion time also increases with particle size. The controlling parameter for boehmite formation is mainly the water vapour pressure inside the particle. As the escape of the produced vapour is more difficult in a coarser particle, higher vapour pressure builds up in those particles, and this favours boehmite production. However, the induction time for boehmite formation does not change significantly with particle size.

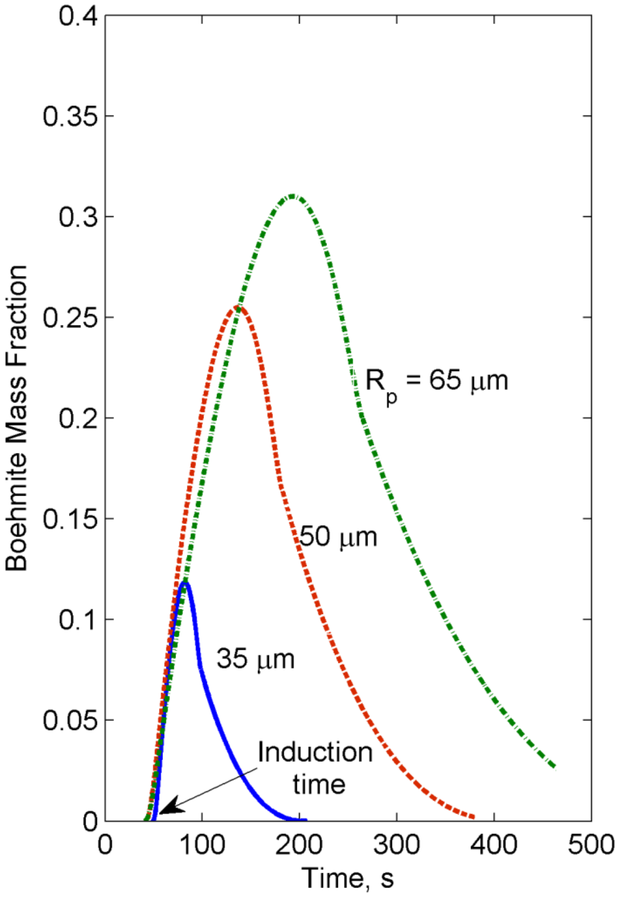

Figure 5.6 – Effect of particle size on intermediate product (boehmite) formation.

5.4.5. Effect of heating rate on intermediate formation

Heating rate is accepted as an important parameter that affects gibbsite transformation pathways and the formation of different phases (Gan et al., 2009). The proposed model may be used to explore the effect of the heating rate on boehmite formation, which is the intermediate product. To this end, the environmental temperature (T_b) was used as a forcing function, increasing it from the initial particle temperature ($T_b(0) = T_0 = 298$ K) at different linear rates (5–15 K s^{-1}) until the particle had been completely converted to alumina.

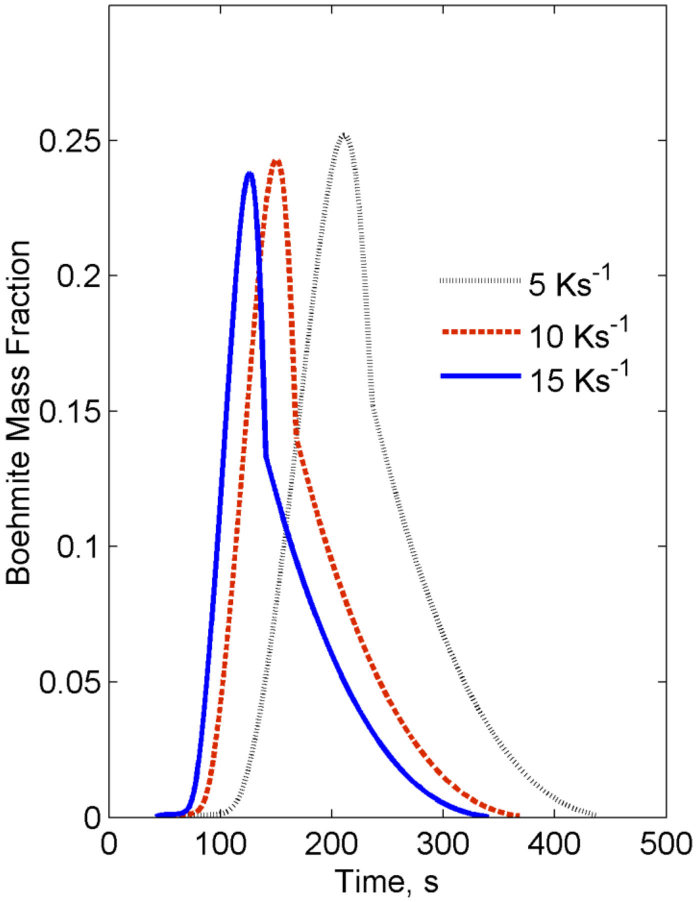

Figure 5.7 – Effect of heating rate on intermediate product (boehmite) formation for an initial environmental temperature of 298 K.

As seen in Figure 5.7, the maximum mass fraction of boehmite is not strongly affected by different heating rate conditions. This result is in good agreement with experimental data reported by Gan et al. (2009), which indicate no effect of heating rate on the maximum amount of boehmite formed. Figure 5.7 also shows a clear difference in the induction time and time of peak boehmite composition, with faster heating leading to earlier formation of boehmite. As mentioned earlier, a minimum level of water vapour pressure is needed to form boehmite. The faster the reactor or autoclave temperature rises, the faster that the build-up of vapour inside a particle occurs, which accelerates boehmite formation and reduces the induction time.

5.5. Summary

A multi-stage, multi-reaction, non-isothermal shrinking core model is proposed for gas-solid decomposition reactions in which the produced gas inhibits the reaction and in which a solid intermediate product forms. The model consists of three stages and accounts for transitions in the reaction pathways. It consists of a set of ordinary differential and algebraic equations that were solved numerically. The model results display good agreement with experimental data for the calcination of gibbsite to alumina with boehmite as an intermediate product, and show a significant improvement compared to the single-stage, single-reaction model developed in Chapter 4. The predicted temperature history is consistent with trends observed in experimental studies. Different plateaux in the temperature history can be attributed to different reaction pathways and the model may help in detecting the occurrence of various pathways in particle temperature data. The effect of particle size and heating rate on the formation of the intermediate product was investigated and the results are in agreement with practical observations.

Nomenclature

$a,c,d,a',b',c',b'',c'',d''$	Stoichiometric coefficients, [–]
C_{A0}	Initial fresh solid concentration, [mol/m^3]
C_{B0}	Initial intermediate solid concentration, [mol/m^3]
C_{C1}	Gas concentration at r_1, [mol/m^3]
C_{C2}	Gas concentration at r_2, [mol/m^3]
C_{Cb}	Gas concentration in surrounding environment, [mol/m^3]
C_{Cs}	Gas concentration on particle surface, [mol/m^3]
C_{G0}	Initial gibbsite concentration, [mol/m^3]
C_{Pe}	Effective molar heat capacity, [J/mol K]
C_{12}	Gas concentration at reactant-product interface at t_{12}, [mol/m^3]
D_e	Effective diffusivity coefficient, [m^2/s]
D_p	Particle diameter, [m]
E	Activation energy, [J/mol]
ΔH	Heat of reaction, [J/mol]
h	Heat transfer coefficient, [W/m^2 K]
k	Surface reaction rate constant, [mol^{-n} m^{3n+1}/s]
k_0	Arrhenius pre-exponential coefficient, [mol^{-n} m^{3n+1}/s]
M	Gas production/diffusion rate, [mol/s]
Mw	Molecular weight, [g/mol]

Mw_e	Average molecular weight, [g/mol]
m	Mass fraction, [–]
$\dot{N}$	Solid consumption rate, [mol/s]
n	reaction order with respect to water vapour concentration, [–]
P_{Cb}	Environmental gas (C) pressure, [kPa]
R	Gas constant, [J/mol K]
R_p	Particle radius, [m]
r_G	Gibbsite surface reaction rate, [mol/m^2 s]
r_s	Solid surface reaction rate, [mol/m^{2}s]
r_1	Unreacted fresh reactant core radius at any time, [m]
r_{12}	Reactant-product interface location at t_{12}, [m]
r_2	Intermediate-product interface location at any time, [m]
r_{23}	Intermediate-product interface location at t_{23}, [m]
T	Temperature, [K]
T_b	Environmental temperature, [K]
T_0	Initial particle temperature, [K]
T_{12}	Particle temperature at t_{12}, [K]
T_{23}	Particle temperature at t_{23}, [K]
t	Time, [s]
t_{12}	Time for transition from stage 1 to 2, [s]
t_{23}	Time for transition from stage 2 to 3, [s]
t_∞	Reaction completion time, [s]
X	Reactant conversion, [–]

Greek symbols

ϑ_1, ϑ_2, ϑ_3	Ratio of stoichiometric coefficients: (c/a), (c'/a'), (c''/b''), [–]
ρ_e	Average density, [kg/m^3]

References

Candela, L., & Perlmutter, D.D. 1986. Pore structure and kinetics of the thermal decomposition of $Al(OH)_3$. *AIChE Journal*. 32, 1532–1545.

Candela, L., & Perlmutter, D.D. 1992. Kinetics of boehmite formation by thermal decomposition of gibbsite. *Industrial & Engineering Chemistry Research*. 31, 694–700.

Chang, Y-I., & Kuo, J-A. 1999. Application of the three-stage shrinking core model in the transport of reactive gas in the porous media. *Journal of Petroleum Science and Engineering*. 22, 205–216.

Fowler, J.D., Chandra, D., Elleman, T.S., Payne, A.W., & Verghese, K. 1977. Tritium diffusion in Al_2O_3 and BeO. *Journal of the American Ceramic Society*. 60, 155–161.

Gan, B.K., Madsen, I.C., & Hockridge, J.G. 2009. In situ X-ray diffraction of the transformation of gibbsite to α-alumina through calcination: Effect of particle size and heating rate. *Journal of Applied Crystallography*. 42, 697–705.

Gómez-Barea, A., & Ollero, P. 2006. An approximate method for solving gas-solid non-catalytic reactions. *Chemical Engineering Science*. 61, 3725–3735.

Homma, S., Ogata, S., Koga, J., & Matsumoto, S. 2005. Gas–solid reaction model for a shrinking spherical particle with unreacted shrinking core. *Chemical Engineering Science*. 60, 4971–4980.

Incropera, F.P., DeWitt, D.P., Bergman, T.L., & Lavine, AS. 2007. *Fundamentals of Heat and Mass Transfer*, sixth ed., John Wiley, Hoboken.

Mantri, V.B., Gokarn, A.N., & Doraiswamy, L.K. 1976. Analysis of gas-solid reactions: Formulation of a general model. *Chemical Engineering Science*. 31, 779–785.

Marsh, C. 2009. CFD Modelling of alumina calciner furnaces. in: *Seventh International Conference on CFD in the Minerals and Process Industries*, Melbourne, Australia, 9–11 December 2009.

Molina, A., & Mondragón, F. 1998. Reactivity of coal gasification with steam and CO_2. *Fuel*. 77, 1831–1839.

Ramachandran, P.A., & Doraiswamy, L.K. 1982. Modeling of noncatalytic gas-solid reactions. *AIChE Journal*. 28, 881–900.

Ruff, T.J., Toghiani, R.K., Smith, L.T., & Lindner, J.S. 2008. Studies on the gibbsite to boehmite transition. *Separation Science and Technology*. 43, 2887–2899.

Stacey, M.H. 1987. Kinetics of decomposition of gibbsite and boehmite and the characterization of the porous products. *Langmuir*. 3, 681–686.

Suresh, A.K., & Ghoroi, C. 2009. Solid-solid reactions in series: A modeling and experimental study. *AIChE Journal*. 55, 2399–2413.

Wang, H., Xu, B., Smith, P., Davies, M., DeSilva, L., & Wingate, C. 2006. Kinetic modelling of gibbsite dehydration/amorphization in the temperature range 823–923 K. *Journal of Physics and Chemistry of Solids*. 67, 2567–2582.

Wefers, K., & Misra, C. 1987. *Oxides and hydroxides of aluminium.* Technical Paper No. 19, Alcoa Laboratories, Pittsburgh, PA.

Whittington, B., & Ilievski, D. 2004. Determination of the gibbsite dehydration reaction pathway at conditions relevant to Bayer refineries. *Chemical Engineering Journal*. 98, 89–97.

Zhu, B., Fang, B., & Li, X. 2010. Dehydration reactions and kinetic parameters of gibbsite. *Ceramics International*. 36, 2493–2498.

Appendix A: Derivation of the first stage of the model

During the first stage of the model (Figure 5.1), the only reacting solid is *A* (Eq. 5.1). Therefore, on the unreacted core surface, the rate of gas production can be written using the solid reaction rate as follows:

$$M_1 = 4\pi r_1^2 \vartheta_1 k_1 C_{A0} C_{C1}^{n_1} \tag{A.1}$$

where C_{A0} and C_{C1} are, respectively, the initial concentrations of solid (*A*) and gas (*C*) at core the surface ($r = r_1$) and ϑ_1 is the ratio of stoichiometric coefficients (c/a).

The rate of diffusion of gas *C* in the layer of porous product (*D*) layer can be expressed as

$$M_2 = -4\pi r^2 D_e \frac{dC_C}{dr} \tag{A.2}$$

where D_e is the effective diffusion coefficient, which in this study is considered to be constant, with the effect of any structural changes ignored. For constant M_2, which assumes a pseudo-steady state condition of the gas concentration profile, Eq. (A.2) can be analytically integrated using the following boundary conditions:

$$C_C = C_{Cs} \text{ at } r = R_p \tag{A.3}$$

$$C_C = C_{C1} \text{ at } r = r_1 \tag{A.4}$$

The solution is

$$M_2 = 4\pi D_e \frac{C_{C1} - C_{Cs}}{\frac{1}{r_1} - \frac{1}{R_p}} \tag{A.5}$$

Under pseudo-steady state conditions, the diffusion rate of gas in the product layer is equal to the gas production rate on the surface of the unreacted core:

$$M_1 = M_2 \tag{A.6}$$

By combining this with Eqs. (A.1) and (A.5), the gas concentration on the unreacted core surface can be determined by solving

$$C_{C1} - C_{Cs} - \frac{\vartheta_1 k_1 C_{C1}^{n_1} C_{A0}}{D_e} r_1^2 \left(\frac{1}{r_1} - \frac{1}{R_p} \right) = 0 \tag{A.7}$$

Now, the solid consumption rate and size of unreacted solid core are related by

$$\overset{\bullet}{N}_A = -\frac{d}{dt} \left(\frac{4}{3} \frac{\pi r_1^3 \rho_A}{Mw_A} \right) \tag{A.8}$$

and the gas production rate is related to the solid reaction rate:

$$\overset{\bullet}{N}_A = \frac{1}{\vartheta_1} M_1 \tag{A.9}$$

Substituting Eqs. (A.1) and (A.8) into (A.9) yields

$$-\frac{dr_1}{dt} = \frac{Mw_A}{\rho_A} k_1 C_{A0} C_{C1}^{n_1} \tag{A.10}$$

with the initial condition

$$r_1 = R_p \text{ at } t = 0 \tag{A.11}$$

The assumption of spatially uniform temperature allows the energy balance over the particle to be written as

$$\frac{R_p^3 \rho_A C_{pe}}{3 Mw_A} \frac{dT}{dt} = R_p^2 h (T_b - T) - r_1^2 k_1 C_{A0} C_{Cc}^{n_1} \Delta H_1 \tag{A.12}$$

where C_{pe} is the average particle heat capacity, h is the heat transfer coefficient, T_b is the external temperature and ΔH_1 is the enthalpy of reaction (5.1). The initial condition is

$$T = T_0 \text{ at } t = 0 \tag{A.13}$$

Appendix B: Derivation of the second stage of the model

During the second stage of the model (Figure 5.1), both the original solid reactant *A* and the intermediate solid *B* are reacting. The rate of generation of gas due to conversion of the original solid reactant to the intermediate solid at r_1 is

$$M_3 = 4\pi r_1^2 \vartheta_2 k_2 C_{A0} C_{C1}^{n_2} \tag{B.1}$$

where k_2 and n_2, respectively, denote the reaction rate constant and reaction order with respect to the gas species, C_{C1} is the gas concentration at the inner core surface and r_1 is the inner core radius.

Similar to Eq. (A.5), the rate of gas diffusion in the intermediate product layer can be formulated as

$$M_4 = 4\pi D_e \frac{C_{C1} - C_{C2}}{\frac{1}{r_1} - \frac{1}{r_2}} \tag{B.2}$$

where r_2 is the radius of the interface between the final product *D* and the intermediate *B*. In other words, the intermediate product reacts to the final product at radius r_2. The gas concentration at this interface is C_{C2}.

In addition to r_1 and r_2, which vary with time as the reaction progresses, both C_{C1} and C_{C2} are unknown. They may be calculated with the help of the pseudo steady-state assumption at radius r_2:

$$M_3 = M_4 \tag{B.3}$$

Thus, after substituting Eqs. (B.1) and (B.2) into (B.3), the following is obtained:

$$C_{C1} - C_{C2} - \frac{\vartheta_2 k_2 C_{C1}^{n_2} C_{A0}}{D_e} r_1^2 \left(\frac{1}{r_1} - \frac{1}{r_2} \right) = 0 \tag{B.4}$$

The rate of consumption of the original reactant *A* is

$$\overset{\bullet}{N}_A = -\frac{d}{dt}\left(\frac{4}{3}\frac{\pi r_1^3 \rho_A}{Mw_A}\right) \tag{B.5}$$

and this is related to the gas production rate at r_1:

$$\overset{\bullet}{N}_A = \frac{1}{\vartheta_2} M_3 \tag{B.6}$$

Hence, the shrinking rate of the radius of unreacted core can be obtained:

$$-\frac{dr_1}{dt} = \frac{Mw_A}{\rho_A} k_2 C_{A0} C_{C1}^{n_2} \tag{B.7}$$

Similarly, a material balance on the gas in the intermediate layer leads to two more equations as follows. Firstly, the rate of intermediate *B* conversion to final product *D* at r_2 can be expressed by

$$M_5 = 4\pi r_2^2 \vartheta_3 k_3 C_{B0} C_{C2}^{n_3} \tag{B.8}$$

where k_3 and n_3, respectively, denote reaction rate constant and order of this reaction.

Subsequently, assuming the same diffusivity coefficient for the intermediate and final product layers, the rate of gas diffusion in the product layer may be described by

$$M_6 = 4\pi D_e \frac{C_{C2} - C_{Cs}}{\frac{1}{r_2} - \frac{1}{R_p}} \tag{B.9}$$

Since the gas produced at both reactive interfaces must escape by diffusion through the product layer, the pseudo-steady state assumption can be invoked again to yield

$$M_6 = M_3 + M_5 \tag{B.10}$$

and therefore

$$C_{C2} - C_{Cs} - \frac{\vartheta_2 k_2 C_{C1}^{n_2} C_{A0} r_1^2 + \vartheta_3 k_3 C_{C2}^{n_3} C_{B0} r_2^2}{D_e} \left(\frac{1}{r_1} - \frac{1}{R_p} \right) = 0 \tag{B-11}$$

In addition, the rate of intermediate *B* consumption can be written as

$$\overset{\bullet}{N}_B = -\frac{d}{dt}\left(\frac{4}{3}\frac{\pi r_2^3 \rho_B}{Mw_B}\right) \tag{B.12}$$

where Mw_B and ρ_B are the molecular weight and density of the intermediate component, respectively. Subsequently, using

$$\overset{\bullet}{N}_B = \frac{1}{\vartheta_3} M_4 \tag{B.13}$$

the rate of change of the intermediate radius can be calculated by

$$\frac{dr_2}{dt} = \frac{Mw_B}{\rho_B} k_3 C_{B0} C_{C2}^{n2} \tag{B.14}$$

The assumption of spatially uniform temperature allows the energy balance over the whole particle to be written as

$$\frac{R_p^3 \rho_e C_{pe}}{3Mw_e} \frac{dT}{dt} = R_p^2 h(T_b - T) - r_1^2 k_2 C_{A0} C_{C1}^{n_2} \Delta H_2 - r_2^2 k_3 C_{B0} C_{C2}^{n_3} \Delta H_3 \tag{B.15}$$

where it should be noted that there are now two reaction enthalpy terms, in contrast to the single ΔH term in Eq. (A.12). The initial condition is

$$T = T_{12} \text{ at } t = t_{12} \tag{B.16}$$

Appendix C: Estimation of the boehmite to alumina activation energy

In order to estimate the activation energy E_3 for boehmite to alumina conversion, and minimize the number of fitted parameters in the current model, several simulations were run on the non-isothermal, 1-D reacting particle model developed in Chapter 3 that was adapted to simulate the boehmite to gibbsite reaction. The evolution of the temperature of a reacting boehmite particle predicted by the 1-D model is shown in Figure C.1 for three assumed values of the activation energy. The value E_3 = 145 kJ/mol provides a temperature plateau at 690~720 K, which most closely agrees with the experimental temperature plateaux observed for the transformation of a pure boehmite particle to alumina observed by Stacey (1987). Further, the same value of E_3 was obtained in a preliminary data fitting study that used the current multi-stage shrinking core model. Although neither of these estimations is a definitive confirmation of the value for E_3, they are consistent, reasonable and provide acceptable agreement between the model predictions and experimental data.

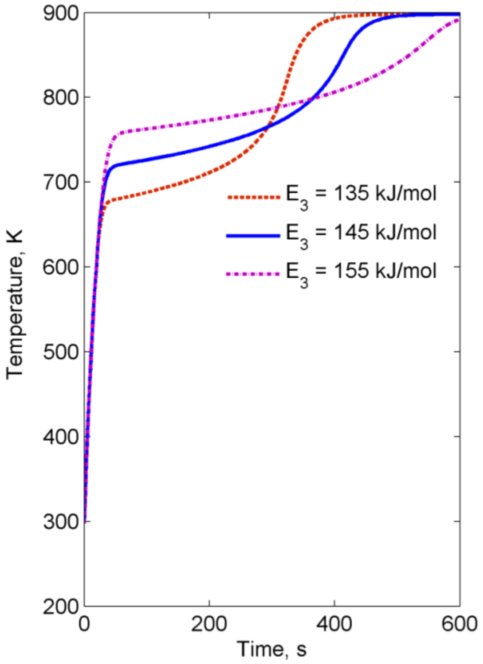

Figure C.1 – Predicted temperature history of a pure boehmite particle reacting to alumina according to the 1-D model of Chapter 3 (adapted for boehmite calcination) for different assumed values of the activation energy at T_b = 923 K.

6

Fluidized bed reactor modelling: gibbsite calcination

Particle scale models are valuable for determining kinetics from laboratory experiments into gas-solid reactions. In addition, investigation of a single reacting particle allows appropriate assumptions to be made about modelling the internal and external heat and mass transfer processes. However, engineers are always interested in equipment scale models that can predict the practical performance of units under different operating scenarios. For complex unit operations like fluidized bed reactors (FBRs), this issue is more challenging compared to reactors containing only fluids with ideal flow patterns, because for the latter, process simulation software and models are well developed. In this chapter, some of the previous work into multi-scale modelling of FBRs is outlined then a multi-scale model for a FBR is proposed that combines a particle scale model with a simplified reactor scale model. Even though a general discussion of FBRs is presented, gibbsite calcination is considered for the case study the same as in previous chapters.

6.1. Introduction

Modelling and simulation of fluidized bed reactors (FBRs) have increasingly received attention by researchers. Due to the interaction of numerous mechanisms in a FBR, prediction and explanation of the behaviour of this system is highly complicated in terms of reactions and hydrodynamics. Multi-scale modelling has been found to be a useful approach to handle these complexities, although it is currently still in its early stages.

From a multi-scale point of view, investigations into the processes in FBRs might be classified as follows:

- Qualitative (descriptive) research on the definition, application and importance of multi-scale modelling;
- Hydrodynamics of fluidized beds;
- Multi-scale modelling of mass and heat transfer and reaction;
- Quantitative research and publications on other chemical engineering processes.

This chapter is organised as follows. The remainder of Section 6.1 summarises the current state and issues in modelling for each of the four areas mentioned above. Section 6.2 discusses the various choices involved in developing a FBR model for calcination, in particular the division of the reactor phases. The assumptions and equations for a simplified reactor scale model are presented in Section 6.3. The first part of Section 6.4 explains the numerical solution of the resulting multi-scale model, while the remaining parts present sensitivity studies of various important parameters. Finally, conclusions are drawn in Section 6.5.

6.1.1. Qualitative (descriptive) research on the definition, application and importance of multi-scale modelling

This group of publications mostly focuses on new developments in multi-scale modelling and its future prospects. Although these articles do not necessarily include the technical details of modelling, they are beneficial for better understanding of systems, scales, dominating mechanisms, algorithms, and the gaps or flaws in current multi-scale modelling approaches. In addition, they help show how to develop a new model for a new process by focusing on the key points and considerations in multi-scale modelling.

Uncertainty in physico-chemical mechanisms and thermodynamic and kinetic coefficients, computational costs in solving and linking together models, a shortage of manipulated parameters, lack of straightforward evaluation of micro-scale properties and inefficient system engineering tools to meet demands for systems described by discrete and discrete-continuum models are challenges in multi-scale modelling (Braatz et al., 2004). This class of research work provides guidance on how to accomplish the following:

1. To identify the chemical engineering scales of interest.
2. To identify the main phenomena and dominant mechanism(s) on each scale.
3. To specify the governing equations (conservation and constitutive equations) for each scale and maybe analyse how these equations are interrelated between the scales.
4. To investigate modelling methods for each scale and the abilities of various models on a single scale.

5. To propose modelling goal(s) such as process control, optimization (intensification and selectivity) or design (at different scales, e.g. catalyst and reactor), and understand how they influence the construction of a multi-scale model.
6. To propose a reasonable methodology for multi-scale model validation including the Design of Experiments, as this area has considerable challenges.
7. To develop a scale-communication algorithm or flowchart.
8. To identify changeable and measurable parameters at a scale that can be useful in model validation and sensitivity analysis.

6.1.2. Hydrodynamics of fluidized beds

This category of works may provide detailed insights into the hydrodynamics of the system applicable to a multi-scale model, which involves (Schmidt, 1996; Curtis and van Wachem, 2004; van der Hoef et al., 2005; Deen et al., 2007):

1. Explanation of the system (flow regimes) at each scale, including detection of flow mechanisms and parameters (drag coefficient, …).
2. Investigation into the modelling method(s) as well as the solution techniques for each scale.
3. Computational Fluid Dynamics (CFD) modelling, involving a powerful package such as Fluent. Validation is a considerable challenge in CFD modelling as well as in other modelling methods.
4. Estimation of real-life particle drag coefficients that account for the polydispersity of particle sizes.
5. Coupling the particle size distribution (PSD) with a hydrodynamic model.
6. Providing qualitative information that can be used in higher scale models; for instance, heterogeneity caused by inelastic collisions and non-linear drag anticipated in discrete particle models.
7. Providing quantitative information that can be used in higher scales. For example, drag force relations obtained from Lattice Boltzmann Model (LBM) simulations can find direct use in both Discrete Particle Model (DPM) and Two Fluid Model (TFM) simulations.
8. Exploration of the effects of different coupling methods for models at different scales.

9. Development of improved expressions for solid pressure and viscosity, as they are used in TFM. However, it is a non-trivial task to extract direct data on solid viscosity and pressure in DPM.
10. Consideration of cluster phenomena in modelling. This scale has been focused on in recent investigations because of its lower computational load in comparison with simulating all the individual particles.
11. Modelling the flow around individual particles in a turbulent and concentrated flow, which is not resolved yet.
12. Coupling reaction with hydrodynamic models.
13. Coupling mass and heat transfer with hydrodynamic models.

6.1.3. Multi-scale modelling of mass and heat transfer and reaction

Complex, multi-phase systems like fluidized bed reactors need to be explained by three independent phenomena, including local fluid mechanics, heat and mass transfer, and reaction kinetics. The similarity of heat, mass and momentum transfer may simplify the study of these transport phenomena at various scales.

If we identify particle, bed volume element and reactor scales as micro, meso and macro-scales, respectively, as in Chapter 2, then micro-scale heat and mass transfer refer to intra-particle and inter-particle processes acting on single particles. Transfer between particle clusters as well as from cluster to fluid, represents the meso-scale processes occurring for example in circulating fluidized beds. Subsequently, macro-scale transfer phenomena include heat and mass transfer in the bulk gas-solid mixture, and between the bulk phase and the reactor walls.

Reaction kinetics could be the subject of investigation on micro or meso-scales depending on its nature (catalytic or non-catalytic, exothermic or endothermic, homogeneous or heterogeneous, …). Reaction kinetics are related to interactions between molecules in a homogeneous reaction and to particle-surface interactions for reactions involving a catalyst or solid reactant. Coupling detailed reaction kinetics with hydrodynamics for fluidized bed reactors is quite a new possibility due to recent computational advances.

Compared to packed beds, mass transfer in fluidized beds is less investigated and this can be attributed to two difficulties: conducting the mass transfer experiments, and understanding the more complex flow structure. Consequently, the mass transfer rates reported in the literature may differ considerably. Wang et al. (2005) have tried to investigate the problem from a multi-scale viewpoint. The same uncertainty also exists for heat transfer. In addition, a study of the role of reactions, including kinetics and the potential for agglomeration, in meso-scale and macro-scale models is necessary. Hence, a facet of current research is mass and heat transfer modelling for multi-scale models, which may include reaction and agglomeration processes (Breault, and Guenther, 2009; Breault, 2006; Behjat et al., 2008; Dong et al., 2008).

6.1.4. Quantitative research and publications on other chemical engineering processes

There are case studies of multi-scale modelling of other processes in chemical engineering that may be worthwhile investigating, such as bubble columns, chemical vapour deposition (CVD), nanotube production, and fluidized beds for the production of solar grade silicon and hydrogen production from ammonia. As a consequence of the difference between the natures of these processes, the relevant (time-space) scales are also different. However, conducting a survey of these various types of processes makes it possible to understand their differences as well as their similarities. For example, nanotube growth can be thought of as corresponding to agglomeration to some extent. In addition CVD is an outstanding example of a multi-scale process that includes a vast range of multi-scale phenomena. According to the authors, these processes are not fully understood, which is the same for fluidized bed systems. The concerns and flaws in those processes could be similar to those for fluidized beds also, and they may need to be addressed in any reasonable new model. Hence, doing a survey on these other chemical processes is worthwhile.

6.2. Modelling aspects of FBRs

Modelling of FBRs is highly complicated as a wide range of parameters and mechanisms are interacting simultaneously. Figure 6.1 shows some of the issues that must be considered in modelling efforts. Clear specification of the process and properly justified assumptions could simplify the complexity to some extent.

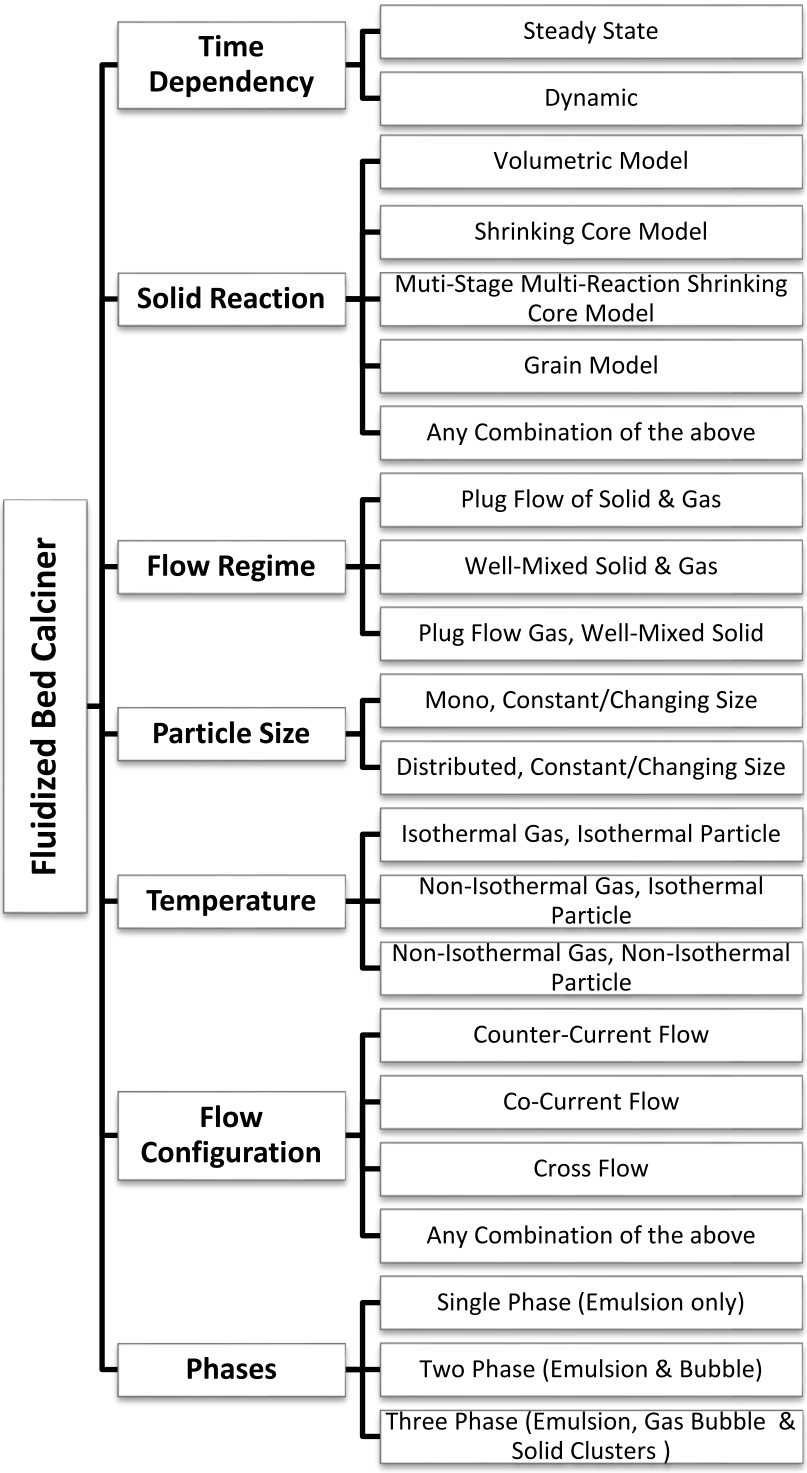

Figure 6.1 – Typical issues involved in FBR modelling for calcination processes.

In numerous publications, FBRs have been modelled as single, two and three-phase systems in which gas-solid reactions occur. However a significant gap exists in the application of these approaches to the gibbsite calcination process. Particle scale models have been studied extensively through different methodologies in this thesis, and now it is worthwhile to employ those models for reactor scale simulations. In the following sections, the possibilities for modelling FBRs for gibbsite calcination as single and two-phase systems are briefly discussed. Subsequently, a simplified single-phase model at the reactor scale is chosen and is linked with a particle scale model to form an illustrative multi-scale model.

6.2.1. Two-phase model

A large number of modelling efforts on FBRs are based on considering two phases in the fluidized bed with exchange of mass and energy between them. In this approach, the gas can be in both bubble form and well-mixed with the solids, forming an “emulsion”, with the solid particles mainly existing in the emulsion phase. In other words, the gas bubbles are almost solid-free. Having solid-free bubbles is an idealistic assumption as the existence of solids in the bubble phase has been shown experimentally and theoretically (Mostoufi et al., 2001). In spite of these simplifications, the two-phase FBR model has been of interest due to its simplicity of model development and solution. In addition, the predictions of this model are reasonably in agreement with practical data.

The two-phase model is well presented by Kunii and Levenspiel (1991). Their model is tailored here for gibbsite calcination, and hence focuses on water vapour (W) in the gas phase and gibbsite (G) in the solid phase. Figure 6.2 shows conceptually how a two-phase fluidized bed model at the reactor scale could be linked with alternative particle scale models to create a multi-scale model. Focussing on the reactor scale, Figure 6.3 presents how the two-phase FBR equations of Kunii and Levenspiel (1991) could be adapted for gibbsite calcination. However, the modelling approach embodied by Figure 6.3 will not actually be used in the simulations presented in this chapter, but it does show how communication between scales could take place in a two-phase FBR model. The multi-scale model that is actually implemented in this chapter uses a simpler, pseudo single phase, tanks-in-series model at the reactor scale.

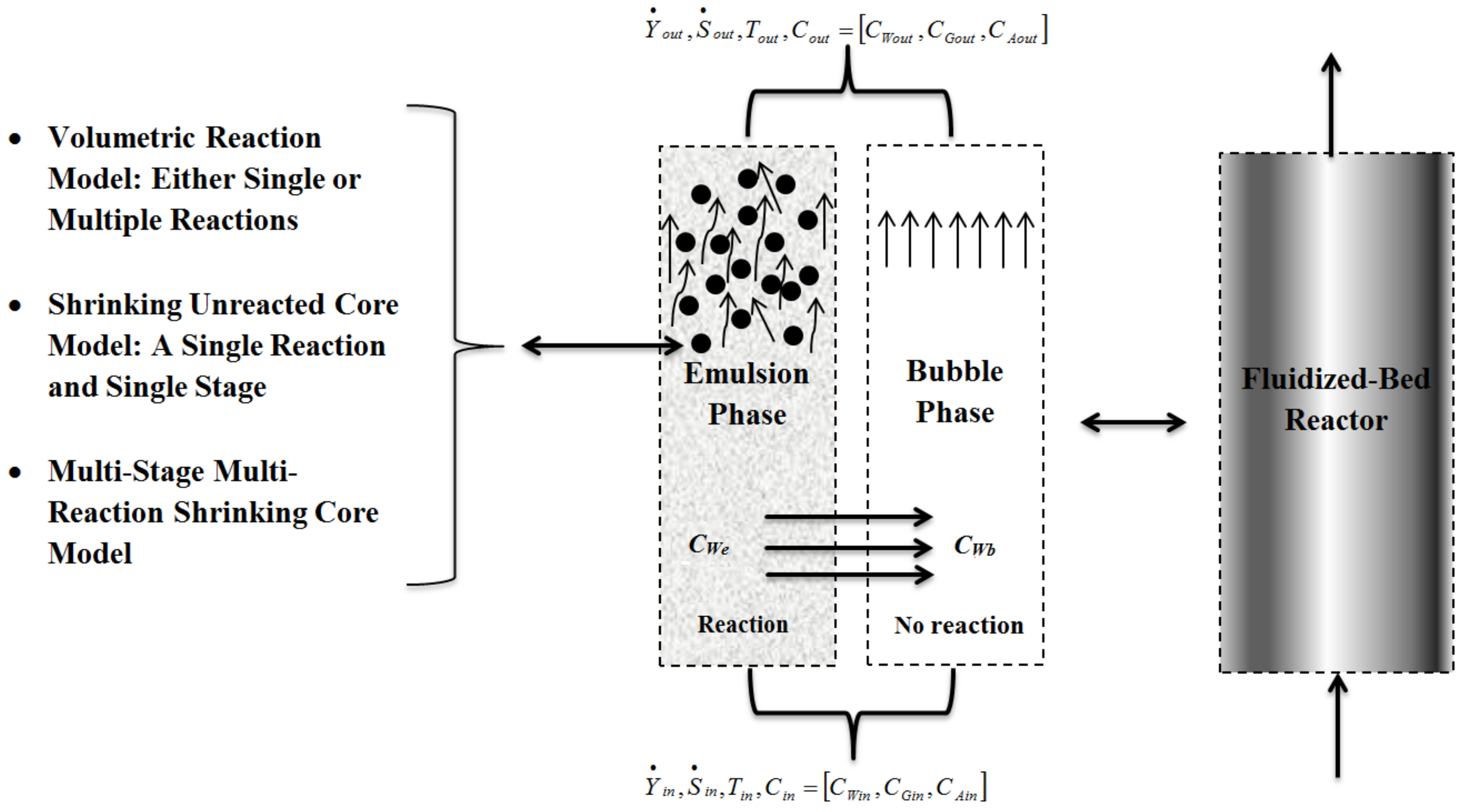

Figure 6.2 – Schematic of a conceptual two-phase model for a FBR showing communication with alternative particle scale models.

- **Mole balance of water vapour**

$$\frac{dC_{We}}{dz} = \frac{\omega R^{*}(1-\varepsilon)(1-\delta) - K_{eb}(C_{We} - C_{Wb})}{U_0(1-\delta)}$$

- **Mole balance of reactant solid**

$$\frac{dC_{Ge}}{dz} = -\frac{R^{*}(1-\varepsilon)}{U_0}$$

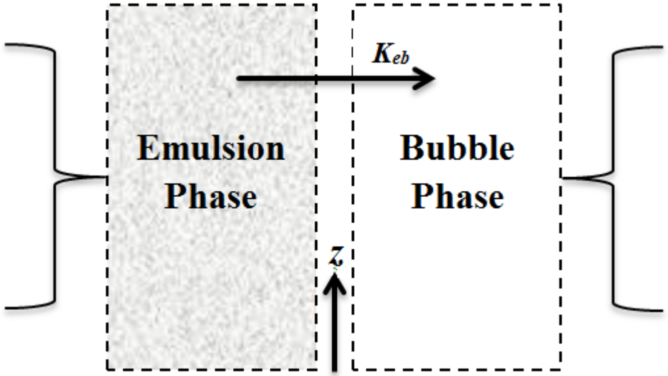

- **Mole balance of water vapour**

$$\frac{dC_{Wb}}{dz} = \frac{K_{eb}(C_{We} - C_{Wb})}{U_0(1-\delta)}$$

- **Bubble fraction**

$$\delta = \frac{U_0 - U_{mf}}{U_0 - U_{mf}}$$

- **Average concentration in water vapour**

$$\overline{C}_W = \frac{U_{mf}(1-\delta)}{U_0(1-\delta)} C_{We} + \frac{U_b \delta}{U_0} C_{Wb}$$

- **Average bed voidage**

$$\varepsilon = (1-\delta)\varepsilon_{mf} + \delta$$

- **Minimum fluidization velocity**

$$\frac{U_{mf}\rho_g d_p}{\mu_g} = \left[27.2^2 + 0.0408\, Ar\right]^{\frac{1}{2}} - 27.2$$

- **Bubble velocity**

$$U_b = U_0 - U_e + u_{br}, \quad u_{br} = 0.711\sqrt{g d_b}$$

- **Bubble diameter**

$$\frac{d_b}{D_t} = \frac{\left[-\gamma_M + \sqrt{\gamma_M{}^2 + 4D_{bm}/D_t}\right]^2}{4}$$

$$D_{bm} = 2.59 g^{-0.2}\left[(U_0 - U_e)A_t\right]^{0.4}, \quad \gamma_M = 0.02256 \frac{(D_t/g)^{0.5}}{U_{mf}}$$

- **Gas interchange coefficient**

$$\frac{1}{K_{eb}} = \frac{1}{K_{ec}} + \frac{1}{K_{cb}}, \quad K_{cb} = 4.5\left(\frac{U_e}{d_b}\right) + 5.85\left(\frac{D_e{}^{1/2} g^{1/4}}{d_b{}^{5/4}}\right), \quad K_{ec} = 6.77\left(\frac{D_e \varepsilon_e u_{br}}{d_b{}^3}\right)^{1/2}$$

Figure 6.3 – Two-phase flow element for a FBR with equations from Kunii and Levenspiel (1991) adapted for gibbsite calcination.

6.2.2. Single-phase, well-mixed model

At very high velocities, FBRs may show well-mixed properties in which it is very hard to distinguish between emulsion and gas bubbles. Under these conditions (Kunii and Levenspiel, 1991), the gas and solid flows might be considered as pseudo single-phase flow. Small bubble sizes and unrestricted interphase mass and energy transfer rates are embedded in this assumption. Therefore, temperature and concentration are approximately uniform throughout the bed (McAuley et al., 1994). This kind of model might be derived from a two-phase FBR model as a limiting case in which heat and mass transfer resistances are quite low.

6.2.3. Tanks-in-series model

A single-phase FBR might be approximated via ideal reactor models such as the Plug Flow Reactor (PFR) model or Continuous Stirred Tank Reactor (CSTR) model. However, due to complex hydrodynamics, the behaviour of a real-life reactor may fall in between the PFR and CSTR. Therefore a general model is needed to account for the non-ideal flow conditions.

The tanks-in-series model is general enough to simulate both CSTR and PFR reactors. In addition, any kind of reactor performing between these two ideals could be simulated by adjusting the number of tanks. Therefore this modelling approach is used in this chapter to illustrate how communication between particle and reactor scale models could be set up. Figure 6.4 shows the schematic of CSTRs-in-series.

6.3. Multi-scale model development

Initially, the mass and energy balances over a single CSTR element, which will form part of the general model, are developed for co-current flow of gas and solid. Subsequently a MATLAB code was developed for CSTR model solution and this interacts with codes previously developed for particle scale models. The reactor code has been designed to be flexible so that it can employ different numbers of CSTRs in series and different residence time distribution (RTD) functions. The communication between the codes at different scales was carefully established to ensure correct information transfer between the different scales.

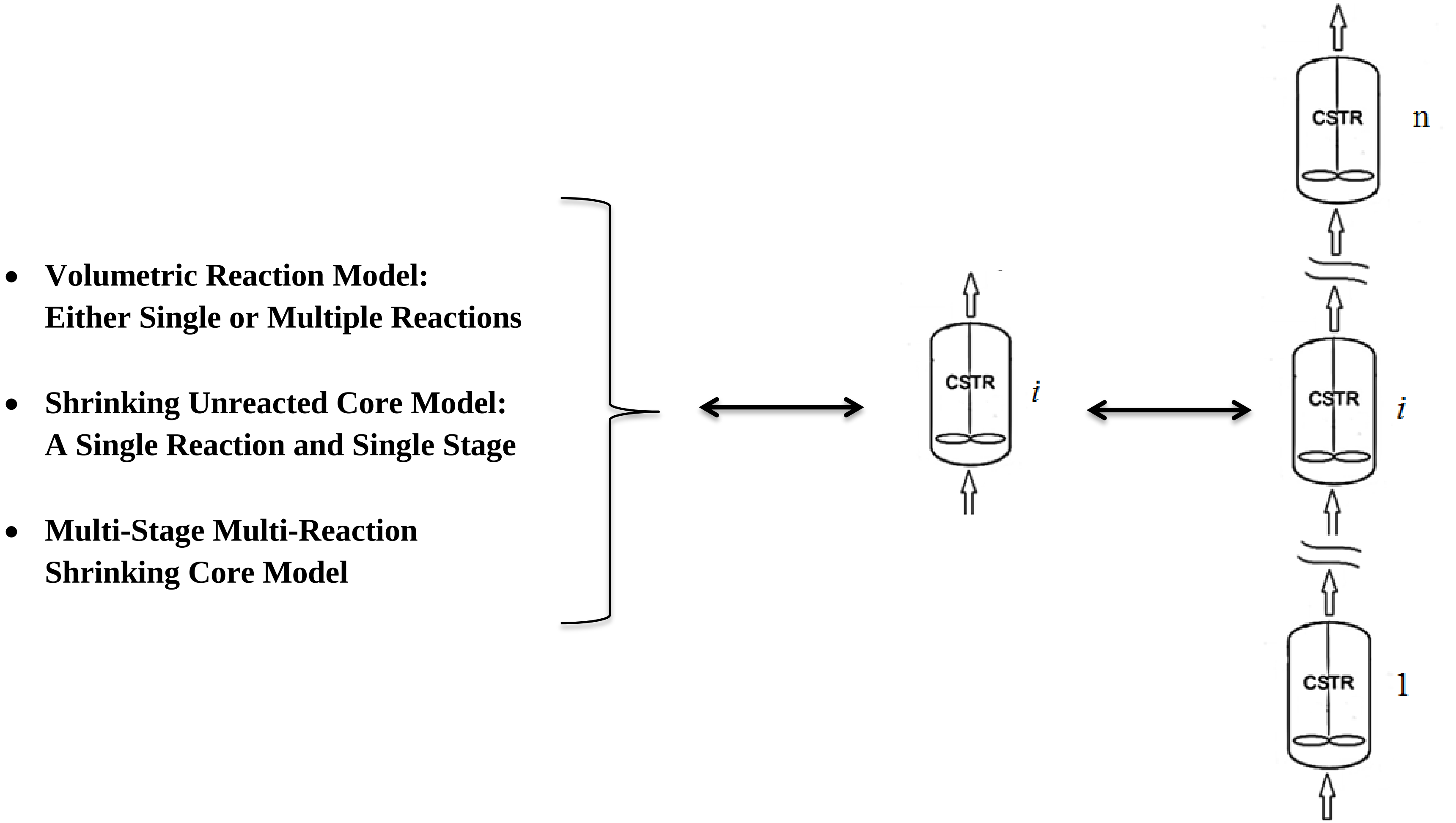

Figure 6.4 – Schematic of a multi-scale model that combines tanks-in-series at the reactor scale with alternative particle scale models.

Even though only the co-current flow regime is investigated in this chapter, the model and corresponding codes could be applied to other flow configurations, including counter-current and cross-flow of gas and solid.

6.3.1. Modelling assumptions

In the context of gibbsite calcination, the following assumptions are made:

- The model is steady state and non-isothermal.
- The reactor is oriented vertically with the gas and solid entering the base of the reactor and flowing co-currently upwards. The overall reactor is assumed to behave as a vertical collection of CSTRs connected in series.
- At each horizontal level, the gas and solid are well-mixed, showing pseudo single-phase behaviour.
- All CSTRs are considered to have equal volume and the same residence time distribution.
- The temperature and species concentrations inside the particles exiting each CSTR are obtained by averaging the temperature and concentration profiles inside a single particle with respect to radial position in the particle and over the solids residence time distribution for that CSTR.
- The voidage of the bed is constant throughout the reactor.
- Particles are assumed to have a constant size during the reaction.
- The water vapour concentration inside the reactor has no significant influence on the reaction rate at the particle scale. The validity of this assumption has already been confirmed in Chapters 3 to 5 for gibbsite calcination.
- A constant total pressure for the gas phase is assumed.
- The assumptions related to the solid physical properties are the same as those reported in Chapter 3.
- There is no reaction in the gas phase. The solid reaction is lumped, considering a pure gibbsite feed reacting to alumina. However the possibility of intermediate species inclusion through considering series and parallel reactions is discussed in Section 6.4.
- The gas phase consists of air and water vapour, and the ideal gas law applies.

Figure 6.5 depicts a single CSTR, which is one element in the reactor scale model.

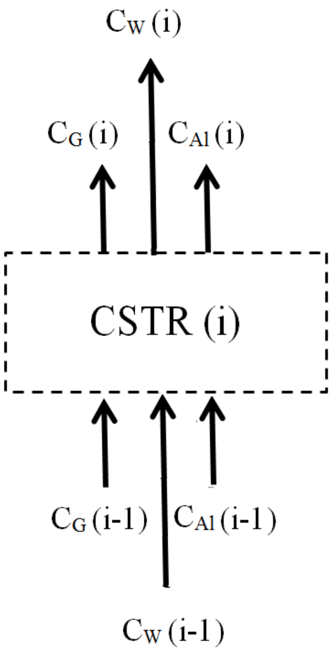

Figure 6.5 – Schematic of a single CSTR element showing the inlet and outlet concentrations of gibbsite, water vapour and alumina.

6.3.2. Conservation and constitutive equations

The mass balances of a single CSTR with respect to the individual species involved in the calcination reaction are fairly straightforward. However special attention must be paid to the energy balance since the composition of the solid and gas mixture, local temperature and reaction rate are all changing.

Table 6.1 summarises the governing conservation and constitutive equations of a single CSTR element that will be utilised in a tanks-in-series model as the i^{th} element out of n. Eq. (6.1) uses the particle scale model (via $X(t)$) and the solids residence time distribution ($E(t)$) to determine the average gibbsite conversion in the i^{th} CSTR element. Eq. (6.2) is the gibbsite material balance, estimating the outlet moles of gibbsite based on the difference between the inlet moles and the consumption due to conversion. Similarly, the material balances for the alumina and water vapour, Eqs. (6.3) and (6.4) respectively, can be determined from the inlet moles of each species, the gibbsite consumption and the appropriate stoichiometric coefficients. Even though air is inert in the calcination reaction, the local concentration of the air may change due to water vapour production and gas temperature changes. The total gas flow rate and the air concentration can be predicted by considering the water vapour production and temperature changes as shown in Eqs. (6.5) and (6.6).

Table 6.1 – Conservation and constitutive equations at the reactor scale for CSTR *i*.

$$\overline{X_i} = \int_0^\infty X(t)E(t)dt\,,\ \tau = \frac{V_R(1-\varepsilon)}{\dot{S}} = \frac{AH(1-\varepsilon)}{\dot{S}},\ \tau_i = \frac{\tau}{n} \qquad (6.1)$$

$$C_G(i) = C_G(i-1)(1-\overline{X_i}) \qquad (6.2)$$

$$C_{Al}(i) = C_{Al}(i-1) + \alpha C_G(i-1)\overline{X_i} \qquad (6.3)$$

$$C_W(i) = \left(\frac{C_W(i-1)\dot{Y}(i-1) + \omega C_G(i-1)\overline{X_i}\,\dot{S}}{\dot{Y}(i)} \right) \qquad (6.4)$$

$$\dot{Y}(i) = \left(\frac{T(i)}{T(i-1)} \right)\dot{Y}(i-1) + \omega C_G(i-1)\overline{X_i}\,\dot{S}\left(\frac{RT(i)}{P} \right) \qquad (6.5)$$

$$C_{Air}(i) = \left(\frac{\dot{Y}(i-1)}{\dot{Y}(i)} \right) C_{Air}(i-1) \qquad (6.6)$$

$$\begin{aligned} T(i) = \Big(& \dot{S}(C_G(i-1)C_{pG} + C_{Al}(i-1)C_{pAl})T_p(i-1) + \dot{Y}(i-1)(C_W(i-1)C_{pW} + C_{Air}(i-1)C_{pAir})T(i-1) \\ & - \dot{S}(C_G(i)C_{pG} + C_{Al}(i)C_{pAl})T_p(i) - \dot{S}\,C_G(i-1)\overline{X_i}\Delta H \Big) \Big/ \Big(\dot{Y}(i)(C_W(i)C_{pW} + C_{Air}(i)C_{pAir}) \Big) \end{aligned} \qquad (6.7)$$

The energy balance for i^{th} element consists of different enthalpy terms. Gas and solid enthalpies for the inlet and outlet streams of the element, as well as the reaction enthalpy, must be considered in the energy balance. Due to changes in material compositions for both solid and gas phases, local mean values of the heat capacities are employed. Eq. (6.7) shows the energy balance, rearranged for the outlet gas temperature. The first and third terms in the numerator are the enthalpy of the inlet and outlet solids. Similarly, the second and fourth terms of the numerator are the enthalpies of the inlet gas and the reaction, respectively. The denominator multiplied by $T(i)$ forms the enthalpy of the outlet gas.

At this point it is worthwhile briefly comparing the single-phase reactor model presented in Table 6.1 with the conceptual two-phase model of Figure 6.3. In Figure 6.3, a differential mole balance for gibbsite is presented, along with two other differential mole balances for the water vapour in the emulsion and bubble phases. In contrast, the material balances of the single-phase reactor are presented in discretised form. Further, hydrodynamic parameters such as minimum fluidization velocity (U_{mf}) and bubble velocity (U_b), are considered in Figure 6.3, but not in the single-phase model. In addition, unlike the single-phase model, there is no energy balance at the reactor scale in Figure 6.3, as the reactor is assumed to be isothermal with a known temperature.

In multi-scale modelling, establishing proper communication between the scales is of vital importance. This issue was explained in Chapter 2 with the help of “multi-scale frameworks”. Here, data exchange between the reactor and particle scale is briefly described to exemplify the theoretical framework presented in Chapter 2.

The reaction occurs in the solid at the particle scale. For a given particle size and surrounding gas temperature and pressure, a single particle model can be solved to obtain radially distributed and dynamic temperature, pressure, and concentration profiles inside the particle. At any given time, the conversion of gibbsite can be calculated by integration of the gibbsite concentration over the radius of the particle. In this way, a prediction of conversion as a function of time, $X(t)$, is achieved. This function is used in combination with the solid RTD function to obtain the average conversion, $\overline{X_i}$, of particle in reactor element *i*. It should be noted that the RTD is information that is passed from the reactor scale to the particle scale and $\overline{X_i}$ is information exported to the reactor scale from the particle scale. The reactor scale also receives the temperature profile, as a function of the conversion, from the particle scale. This profile is interpolated at the conversion value calculated from the inlet and outlet concentrations of gibbsite at the reactor scale for element *i* to obtain the average solid temperature leaving the *i*th reactor element. The calculation of temperature and concentration profiles at the reactor scale provides new input values at the particle scale for the surrounding gas temperature and pressure. Obviously, a new surrounding gas temperature affects all the information flows from the particle to the reactor scale. However, the water vapour pressure in the surrounding gas does not have a significant influence at the particle scale. Nevertheless, iteration is needed to ensure convergence of the exit concentrations and temperature for each CSTR element as explained in Section 6.3.4.

Due to its importance, the RTD, $E(t)$, is discussed in more detail in Section 6.3.3.

6.3.3. Residence time distribution

The residence time distribution is the tool that accounts for the different time history each reacting particle experiences inside a reactor. Obviously the time history is not the same for all particles except under ideal plug flow conditions.

Mathematical expressions for the RTDs of ideal reactors are well developed. Eqs. (6.7) and (6.8) are the RTD functions for a CSTR and PFR respectively (Fogler, 2008):

$$E(t) = \frac{1}{\tau_i}\exp(-\frac{t}{\tau_i}) \tag{6.7}$$

$$E(t) = \delta(t-\tau_i) \tag{6.8}$$

Eq. (6.8) contains the Dirac Delta function. For the purpose of numerical coding simplicity, the Delta function of the PFR can be approximated by a Gaussian function as follows:

$$E(t) = \frac{1}{\sqrt{2\pi\sigma^2}}\exp(-\frac{(t-\tau)^2}{2\sigma^2}) \tag{6.9}$$

where σ^2 is the variance. Eq. (6.9) is a reasonable approximation for the Delta function only when the variance is very small.

With regards to the CSTRs-in-series modelling approach, the RTD function for the whole reactor can be interpreted as the superposition of those of the individual reactors:

$$E(t) = \frac{t^{n-1}}{(n-1)!\tau_i^n}\exp(-\frac{t}{\tau_i}) \tag{6.10}$$

Figure 6.6 shows how the residence time distribution varies with the number of tanks, *n*. When $n = 1$, the residence time profile is the same as an ideal CSTR, while increasing *n* makes the profile tend towards an ideal PFR. Note that the dimensionless form of the RTD functions is based on $\theta = t/\tau$ and $E(\theta) = \tau E(t)$.

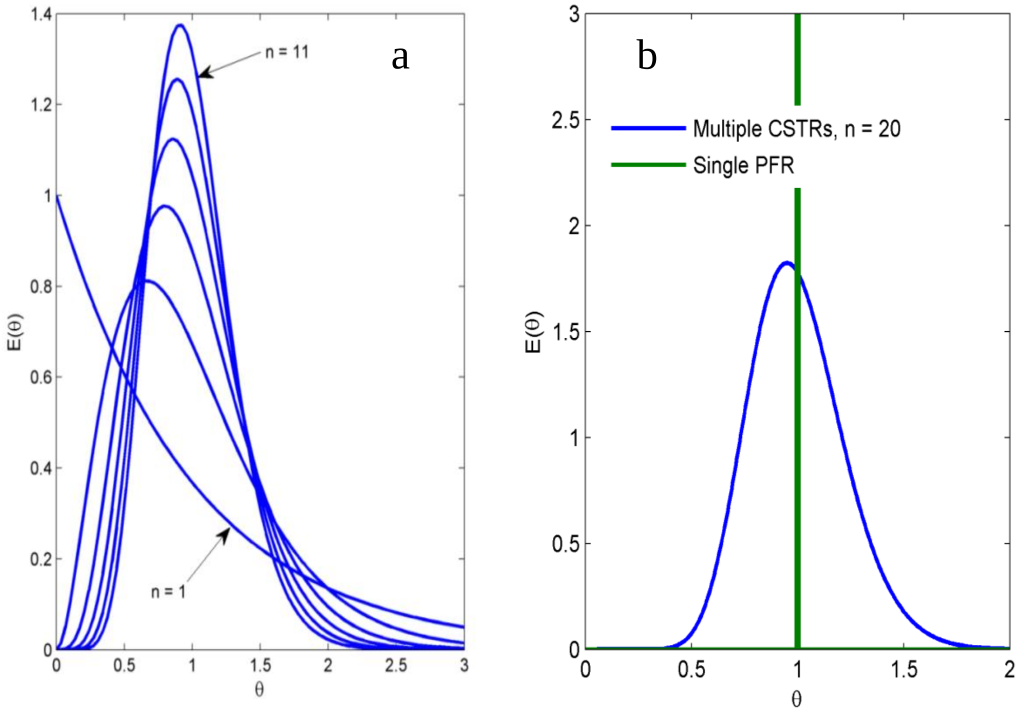

Figure 6.6 – Dimensionless RTD for different numbers of CSTRs in series (a) and comparison of PFR and CSTRs in series for *n* = 20 (b).

6.4. Model solution and analysis

The reactor scale and particle scale models must be solved simultaneously to predict the overall performance of the reactor and also update the parameters that the particle scale is receiving from the reactor scale. To address this, the spatially distributed particle scale model, developed in Chapter 3, is combined with the simplified CSTRs-in-series model developed in Section 6.3. The distributed model is used here in preference to the shrinking core models developed in Chapters 4 and 5 for two main reasons. It has more flexibility for adding all the species involved in the gibbsite calcination process in the future, including boehmite and different alumina phases. In addition, water vapour pressure, which plays such a dominant role in phase formation, can be explained in more detail by using the distributed model.

However, use of the shrinking core models in this multi-scale modelling formulation is also feasible and can proceed in a similar way to the distributed model. Further, the multi-stage, multi-reaction shrinking core model, proposed in Chapter 5, would permit the prediction of boehmite formation and consumption at the reactor scale, which is not the case in the current version of the distributed model. With regards to the shrinking core model developed in Chapter 4, the availability of an analytical solution at low temperatures could offer some advantages by shortening the model solution time.

The main model outputs are the gibbsite, alumina and water vapour concentrations in addition to the gas and solid temperatures, all as functions of height in the reactor. A numerical solution has been created by developing a MATLAB code where the governing equations of the model were solved simultaneously along with the inlet boundary conditions.

The inputs of the first CSTR are given: $C_G(0)$, $C_{Al}(0)$, $C_W(0)$, $C_{Air}(0)$, $\dot{Y}(0)$, and $T(0)$. The surrounding gas temperature inside each CSTR must be calculated, and it is a function of reaction rate at the particle scale. On the other hand, the particle reaction rate is a strong function of surrounding gas temperature, which appears as a boundary condition in the particle scale model. Therefore an iterative procedure has been employed starting with an initial guess value for the surrounding gas temperature $T(i)$. The initial guess for the temperature of element i was taken as the converged temperature of element $(i–1)$. The stopping point for these iterative calculations was set to be $|T^k(i) - T^{k-1}(i)| < 1$ K, where k is the iteration number. For each iteration, the particle scale model must be called to provide an updated conversion value based on estimated surrounding gas temperature in that particular iteration. In addition, the particle temperature has been averaged by using the (T_p, X) data exported from the particle scale to the reactor scale during each iteration. The outputs from each element i provide the inputs and also the initial guesses for the next element $(i+1)$.

In Sections 6.4.1 to 6.4.4 typical results and their interpretation are given for the multi-scale model predictions based on the reactor scale parameters given in Table 6.2. The parameters of the particle scale model are the same as those in Table 3.2, unless noted otherwise.

Validation of the reactor scale model was not possible due to a shortage of suitable experimental data in the literature. The developed model assumes that the reactor consists of well-mixed volumes in series, but industrial calciners may have complex flow patterns (Marsh, 2009). Experimental data specific to the flow pattern, for example approximating plug flow of gas and solids, would be needed for validation. Time and resources did not permit such experiments to be performed. Further, as discussed earlier in Section 2.3.3, DOE for multi-scale model validation is still an open research area.

Table 6.2 – Reactor scale model parameters.

Parameter	Value	Reference / comment
D_t (m)	0.5	Typical value.
H (m)	1	Typical value.
ΔH (kJ/mol)	147	Beyer et al. (1989).
h (W/m^2 K)	50	As discussed in Section 4.3.2.
n (–)	20	See Section 6.4.1.
P (atm)	3	–
R (J/mol K)	8.314	Ideal gas constant.
Solid inlet mass flux (kg/m^{2}s)	7.7	$\dot{S}\rho/A$
$\dot{S}$ (m^3/s)	0.0004	–
T_0 (K)	2000	In the range of Marsh (2009).
T_{p0} (K)	298	Particles at ambient temperature.
$\dot{Y}_0$ (m^3/s)	4	Typical value.
ε (–)	0.8	–

6.4.1. Comparison of modelling results of a single PFR and multiple CSTRs in series

The performance of the model with different numbers of CSTRs in series is tested against a single PFR. The results show a considerable deviation for $n < 20$ while for $n = 20$ and higher, the conversion profile is nearly the same for both reactor configurations (Figure 6.7). Accordingly, a single ideal CSTR, an ideal PFR and an arbitrary flow regime between these two ideal patterns can be simulated by using CSTRs in series with different *n*. Comparison of practical operating data with simulation results can help to estimate the appropriate *n*. For the remainder of the case studies, *n* = 20 will be used.

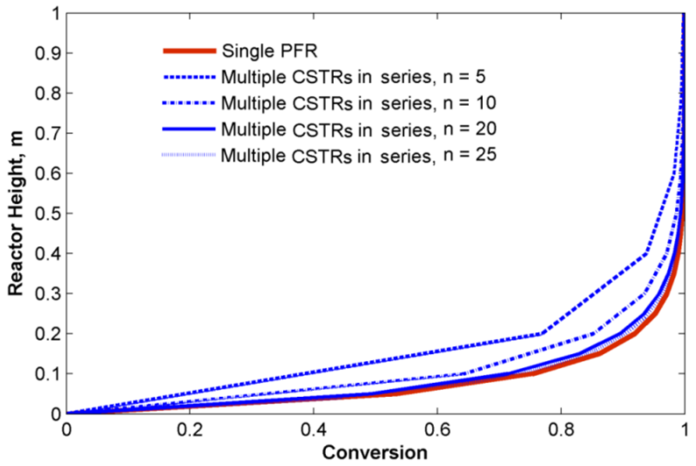

Figure 6.7 – Conversion of gibbsite in a single PFR and multiple CSTRs in series.

6.4.2. Gas temperature, particle temperature, and species profiles

The temperature profiles of the gas and reacting particles in a gibbsite calciner are of great interest for process control and the minimisation of energy consumption. The unsteady temperature profile inside a particle has already been discussed extensively in Chapters 3 to 5. The temperature profile inside a particle is strongly affected by the surrounding gas temperature, and this gas temperature changes through the reactor. One of the most important pieces of information that must be transferred from the particle scale to the reactor scale is the particle temperature. Similarly, the surrounding gas temperature has to be transferred from the reactor scale to the particle scale. This interaction is essential, because assuming independent gas and particle temperature histories will certainly result in significant errors.

As can be seen from the particle scale modelling work presented earlier in Figures 3.3 and 4.5(a), the temperature profile of a reacting particle consists of three stages (assuming only gibbsite to alumina conversion occurs). First is the initial warming stage during which the particle receives energy from the surrounding gas until its temperature is high enough to initiate the calcination reaction. After this stage the obvious temperature plateau of the reaction period can be seen, in which the environmental energy input is balanced by the endothermic reaction. Finally, another warm-up period will take place during which the particle can approach the surrounding gas temperature.

Figure 6.8 shows the average particle and gas temperature profiles, and overall conversion of the reactor at different heights, attained from the multi-scale model based on parameters reported in Table 6.2. Similar temperature behaviour can be observed in Figure 6.8 at the reactor scale as was observed at the particle scale (Chapters 3–5). In addition the temperature drop of the hot gas at inlet of the reactor suggests that more investigation on preheating the solids may have advantages.

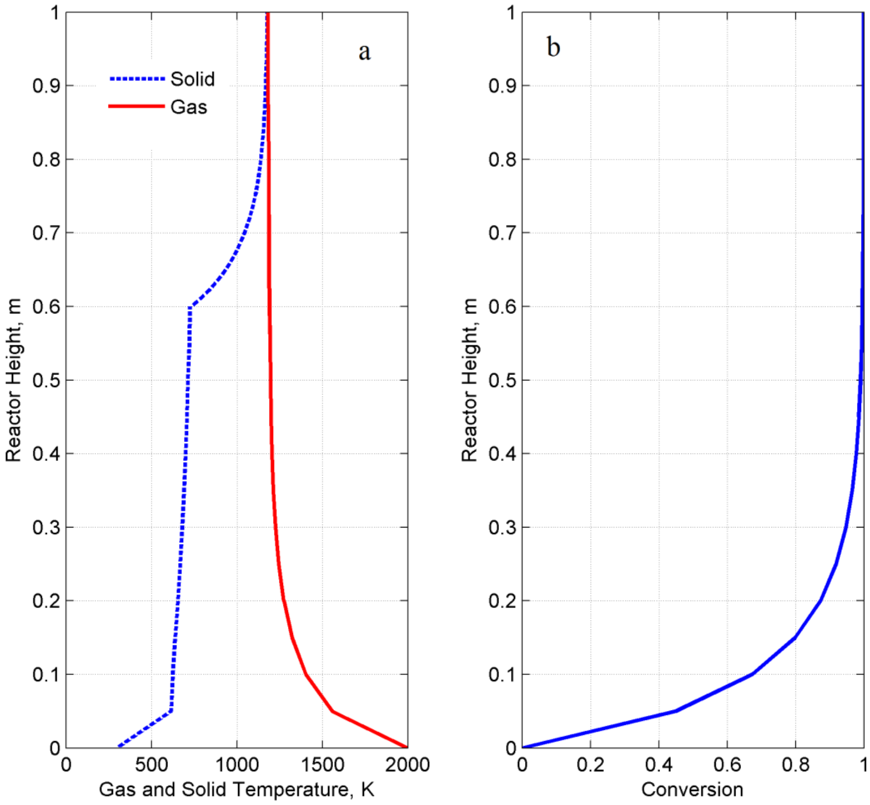

Figure 6.8 – Average particle and gas temperature profiles (a), and overall conversion of the reactor (b), at different heights in the reactor.

It should be noted that particle temperature increases sharply when the conversion reaches close to 100% (Figure 6.8). It was also observed when investigating the behaviour of a single reacting particle (Section 3.4.1). Special attention needs to be paid to the numerical discretisation approach to be able to efficiently capture this sharp change.

The temperature histories for both gas and solid phases are strongly influenced by material flow rates, reaction rates and the heat transfer rate. These effects are examined in the next sections.

Similarly the gibbsite and alumina concentrations may be estimated at different heights in the reactor as shown in Figure 6.9. This graph is consistent with the start of the post-reaction warm-up period in Figure 6.8(a) at H = 0.6 m, as it shows the gibbsite concentration is almost zero at this point, causing the reaction to stop. Information of the type shown in Figures 6.8 and 6.9 is potentially of assistance in the design of alumina calciners. For the idealised reactor configuration and the conditions considered in this study, it can be clearly seen that conversion is essentially complete at H = 0.6 m, meaning that 40% of the reactor volume is not being used for reaction.

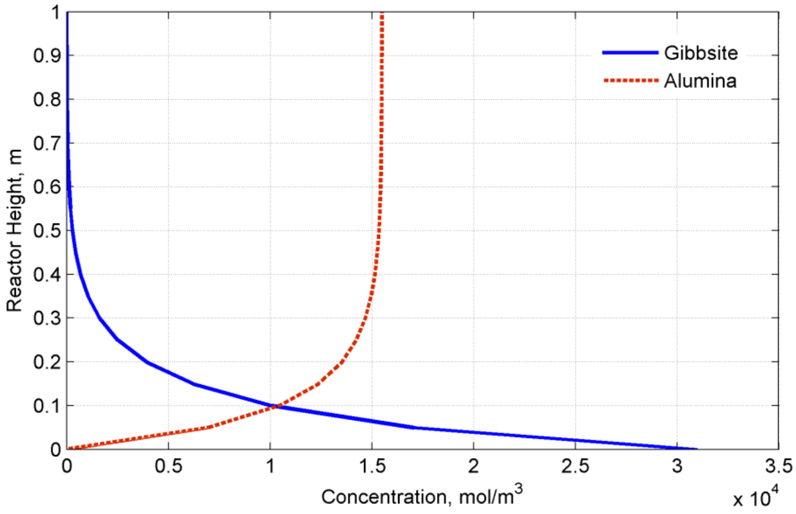

Figure 6.9 – Gibbsite and alumina concentration profiles in the particle phase inside the reactor.

6.4.3. Effect of solid input rate on overall reactor conversion

Solid throughput considerably influences the residence time of the reacting particles. Consequently, different conversion profiles can be observed for different solid mass fluxes as displayed in Figure 6.10. As expected, a greater reactor volume is needed to fully convert a higher gibbsite feed rate.

Information about the conversion profile as a function of reactor height (or volume) and the solid mass flux are valuable in optimization of the reactor height and operating conditions.

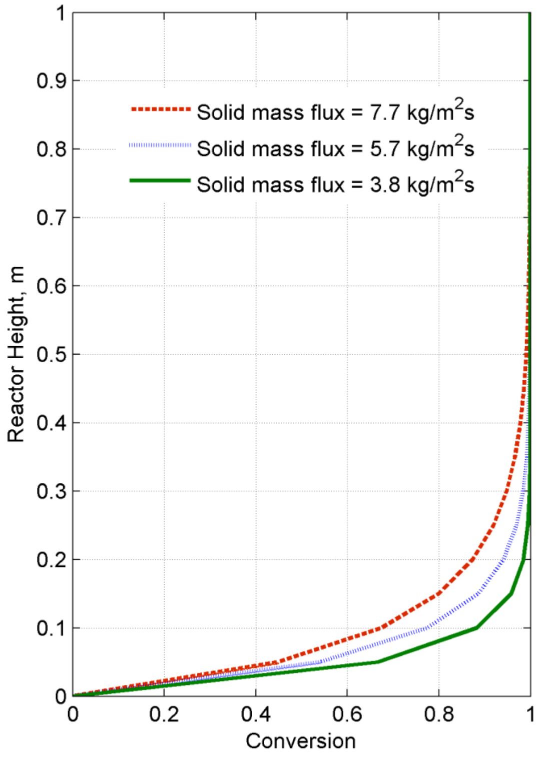

Figure 6.10 – Effect of solid input rate on overall reactor conversion.

6.4.4. Water vapour and gas flow rate profiles inside the reactor

The role of water vapour pressure inside the particle and in the surrounding bulk gas on the progress of calcination has been extensively studied in Chapters 3–5. It was concluded that effect of the surrounding vapour pressure on both reaction progress and mechanism is insignificant as long as the water vapour pressure is less than 15 atm, as was shown in Figure 3.8. However, the vapour content in a FBR is of interest for the treatment of the effluent gas and also for the heat balance inside the reactor. In addition, it could be worthwhile to estimate the maximum vapour pressure exerted by the water vapour under different operating conditions. A comprehensive model must involve the mass balance of the air and water vapour species along with the main reactant(s) and product(s). Figure 6.11 shows how the water vapour builds up inside the reactor due to vapour production from the reacting particles. The profile of the total volumetric flow rate of the gas passing through the reactor, Figure 6.12, shows a considerable decrease in the lower part of the FBR, which is due to the large temperature drop of the inlet gas (Figure 6.8a). The production of water vapour due to the calcination reaction causes an increase in the overall molar gas flow rate inside the bed, and this counteracts the effect of the reduced temperature on the volumetric flow rate to some extent.

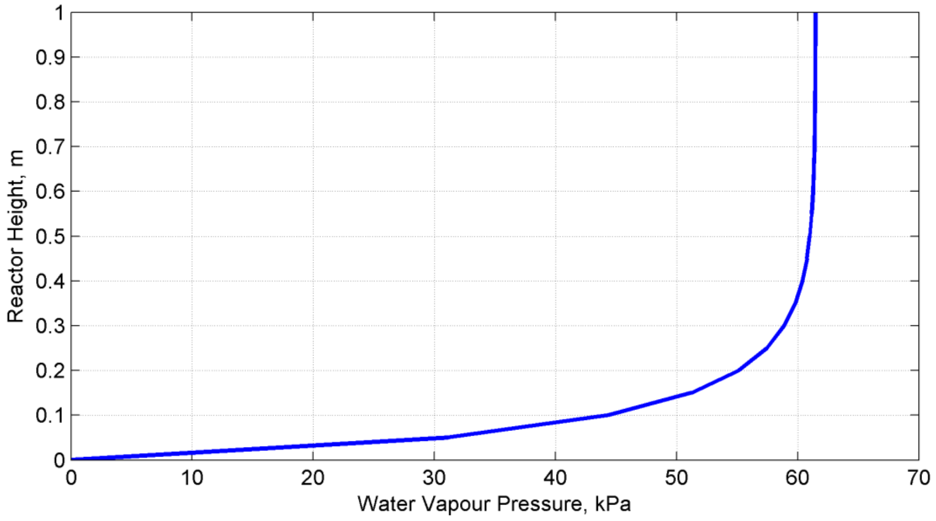

Figure 6.11 – Water vapour pressure build-up inside the reactor.

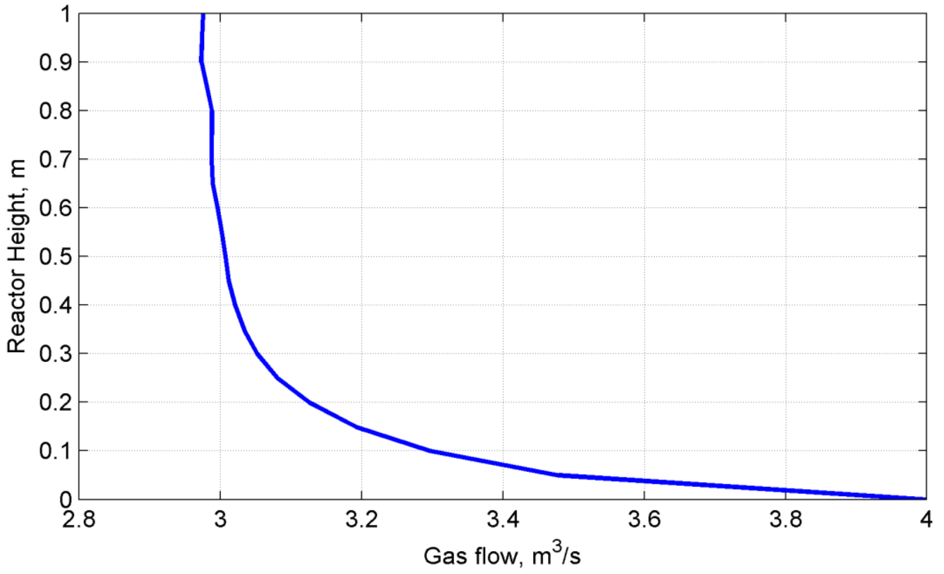

Figure 6.12 – Overall gas (air + water vapour) volumetric flow rate inside the reactor.

6.4.5. Time scales of the multi-scale model

The importance of time scale diversity can be clarified by focusing on different concepts at different scales. In the case of gibbsite calcination for instance, the process vessel could have a characteristic time of several minutes (the residence time in the reactor) and the reaction might be completed for a single particle within a similar time, e.g. a hundred seconds. In contrast, the gas pressure inside a single particle may change within a fraction of a second. This does not present particular modelling challenges, but it makes the set of equations stiff, slightly complicating the solution.

This example shows how investigation and control of product quality characteristics such as porosity of the product, which is certainly affected by the internal gas pressure history, must allow for information communication between two different time scales in the model (Figure 2.2). Further inclusion of a model for the meso scale would make the simulation more realistic by allowing for more details of the gas and solid flow patterns, such as cluster formation in CFBs (Table 2.1). Nevertheless it must be noted that adding another scale, with its own model elements, would definitely increase computational time and costs. Accordingly, goal-oriented management of the time and length scales included in the model plays a leading role in the model's success.

In this chapter the connection between the time scale diversity at the particle scale and reactor scale has been implemented via consideration of the residence time distribution for the reactor and the changes that each particle experiences in response to its reaction environment. The multi-scale concept offers a very interesting area for further research: monitoring the process performance and product quality over different time scales.

6.5. Summary

In this chapter a simplified reactor scale model is presented and combined with a particle scale model to illustrate the multi-scale modelling methodology for a FBR. In spite of the simple structure of the proposed model, the main features of a gibbsite calciner are reasonably captured. Gas and solid temperature profiles, trends in overall gas flow rate and water vapour pressure inside the bed, alumina and gibbsite concentration profiles, and effects of the solid throughput rate on the reactor performance are predicted and explained based on the proposed model.

The spatially distributed, particle scale model developed in Chapter 3 was employed in this chapter. This was due to the potential of the distributed model to handle more species in future studies, which will be important for gaining the greatest benefit from the multi-scale modelling approach. However, the simple shrinking core model and multi-stage, multi reaction shrinking core model, which were developed in Chapters 4 and 5 respectively, could also be applied to multi-scale modelling work using a similar approach.

The multi-scale model was solved numerically through an iterative procedure that alternated between solving particle scale and reactor scale models. An iterative method was chosen to ease the model solution as the variables at the two scales have complicated interactions. The key variable that complicates the model solution is the temperature of the gas at the reactor scale: it affects the conversion history at the particle scale by changing one of the boundary conditions and is in turn affected by the extent of particle reaction through the overall energy balance at the reactor scale.

Nomenclature

A	Reactor cross section area, [m^2]
C_p	Molar heat capacity, [J/mol.K]
C_{Air}	Air concentration, [mol/m^3]
C_{Al}	Alumina concentration, [mol/m^3]
C_G	Gibbsite concentration, [mol/m^3]
C_W	Water vapour concentration, [mol/m^3]
C_{Wb}	Water vapour concentration in bubble phase, [mol/m^3]
C_{We}	Water vapour concentration in emulsion phase, [mol/m^3]
d_b	Bubble diameter, [m]
D_{bm}	Maximum bubble diameter, [m]
D_t	Reactor diameter, [m]
$E(t)$	Residence time distribution function, [1/s]
H	Reactor height, [m]
ΔH	Enthalpy of reaction, [J/mol]

h	Heat transfer coefficient, [W/m^2 K]
K_{cb}	Cloud-to-bubble gas interchange coefficient, [1/s]
K_{eb}	Emulsion-to-bubble gas interchange coefficient, [1/s]
K_{ec}	Emulsion-to-cloud gas interchange coefficient, [1/s]
n	Number of CSTRs, [–]
R^*	Overall reaction rate, [mol/m^3 s]
$\dot{S}$	Solid volumetric flow rate, [m^3/s]
T	Gas temperature, [K]
T_0	Initial hot gas temperature, [K]
T_p	Average particle temperature, [K]
T_{p0}	Initial particle temperature, [K]
U_0	Superficial gas velocity, [m/s]
u_{br}	Bubble rise velocity, [m/s]
U_b	Bubble velocity, [m/s]
U_e	Emulsion velocity, [m/s]
U_{mf}	Minimum fluidization velocity, [m/s]
V_R	Reactor volume, [m^3]
$\overline{X}$	Average conversion in a single CSTR, [–]
$X(t)$	Conversion as a function of time in a single particle, [–]
$\dot{Y}$	Gas volumetric flow rate, [m^3/s]

Greek symbols

α	Stoichiometric coefficient: moles of alumina produced / moles of gibbsite consumed, [–]
γ_M	Parameter in Horio and Nonaka (1987) correlation, [–]
δ	Bubble fraction, [–]
ε	Bed voidage, [–]
ε_{mf}	Bed voidage at minimum fluidization velocity, [–]
θ	Dimensionless time, [–]
μ_g	Gas viscosity, [Pa s]
ρ	Solid (gibbsite) density, [kg/m^3]
τ	Average residence time, [s]
τ_i	Average residence time in a single CSTR, [s]

ω	Stoichiometric coefficient: moles of water produced / moles of gibbsite consumed, [–]

References

Behjat, Y., Shahhosseini, S., & Hashemabadi, S. H. 2008. CFD modeling of hydrodynamic and heat transfer in fluidized bed reactors. *International Communications in Heat and Mass Transfer*. 35, 357–368.

Beyer, H. K., Borbély, G., Miasnikov, & P. Rózsa, P. 1989. A new potential large-scale application of zeolites as fire-retardant material, in: Karge, H. G., Weitkamp, J. (Eds.), *Zeolites as Catalysts, Sorbents, and Detergent Builders: Applications and Innovations*, Elsevier, Amsterdam, pp. 635–644.

Braatz, R. D., Alkire, R. C., Rusli, E., & Drews, T. O. 2004. Multiscale systems engineering with applications to chemical reaction processes. *Chemical Engineering Science*. 59, 5623–5628.

Breault, R. W. 2006. A review of gas–solid dispersion and mass transfer coefficient correlations in circulating fluidized beds. *Powder Technology*. 163, 9–17.

Breault, R. W., & Guenther, C. P. 2009. Mass transfer in the core-annular and fast fluidization flow regimes of a CFB. *Powder Technology*. 190, 385–389.

Curtis, J. S., & van Wachem, B. 2004. Modeling particle-laden flows: A research outlook. *AIChE Journal*. 50, 2638–2645.

Deen, N. G., van Sint Annaland, M., van der Hoef, M. A., & Kuipers, J. A. M. 2007. Review of discrete particle modeling of fluidized beds. *Chemical Engineering Science*. 62, 28–44.

Dong, W., Wang, W., & Li, J. 2008. A multiscale mass transfer model for gas–solid riser flows: Part 1 — Sub-grid model and simple tests. *Chemical Engineering Science*. 63, 2798–2810.

Fogler, H. S., 2008. *Elements of Chemical Reaction Engineering*, fourth ed., Pearson Education International: USA.

Horio, M., & Nonaka, A. 1987. A generalized bubble diameter correlation for gas-solid fluidized beds. *AIChE Journal*. 33, 1865–1872.

Kunii, D., & Levenspiel, O. 1991. *Fluidization Engineering*, second ed., Butterworth-Heinemann, Boston, pp. 268–271.

Marsh, C. 2009. CFD Modelling of alumina calciner furnaces. In: *Seventh International Conference on CFD in the Minerals and Process Industries*, Melbourne, Australia, 9–11 December 2009.

McAuley, K. B., Talbot, J. P., & Harris, T. J. 1994. A comparison of two-phase and well-mixed models for fluidized-bed polyethylene reactors. *Chemical Engineering Science*. 49, 2035–2045.

Mostoufi, N., Cui, H., & Chaouki, J. 2001. A comparison of two- and single-phase models for fluidized-bed reactors. *Industrial and Engineering Chemistry Research*. 40, 5526–5532.

Schmidt, H. W. 1996. Alumina calcination with the advanced circulating fluidized bed technology: A design with increased efficiency combined with operating flexibility. *TMS Annual Meeting* 7th February 1996.

van der Hoef, M. A., van Sint Annaland, M., & Kuipers, J. A. M. 2005. Computational fluid dynamics for dense gas-solid fluidized beds: A multi-scale modeling strategy. *China Particuology*. 3, 69–77.

Wang, L., Yang, N., & Li, J. 2005. Multi-scale mass transfer model for gas-solid two-phase flow. *Chemical Engineering Communications*. 192, 1636–1654.

7

Conclusion and future work

Multi-scale modelling of a fluidized bed reactor for the calcination, or thermal dehydration, of gibbsite to alumina has been studied both conceptually and from first principles in this thesis. A conceptual multi-scale model was envisioned, then three alternative particle scale models were developed and finally one of them was linked with a simple reactor scale model to create a multi-scale model.

In Chapter 2 a conceptual framework was proposed for a multi-scale model to predict the performance of fluidized bed reactors used for gibbsite calcination. The aim of the conceptual model was to relate product quality parameters, such as particle size and chemical composition, with calciner design and operating conditions. It hypothesised linking together a single-particle reaction model, a meso-scale model describing fluidized bed hydrodynamics, and a vessel-scale model. This framework depicted the scales, mechanisms and potential models needed, as well as commenting on the important variables at each scale.

Particle scale modelling was then focussed upon using a variety of methodologies.

A model that coupled dynamic, 1-D spatially-distributed mass and energy balances with appropriate thermal transformation kinetics was developed in Chapter 3. The model, which predicts radially distributed gibbsite and water concentrations, and the temperature profile inside a particle, was validated against laboratory gibbsite calcination data in the temperature range 873 to 923 K. A feature of gibbsite calcination, which was noted in experimental studies in the literature, is that the water vapour that is produced during the reaction actually lowers the reaction rate.

For the first time, the evolution of temperature and internal pressure in a gibbsite particle undergoing thermal dehydration was predicted by a mathematical model. The water vapour pressure at the centre of a dehydrating gibbsite particle can reach values in the order of 100 atm, which can help explain the occurrence of particle fracture and the possibility of forming a boehmite phase. The assumed effective diffusion coefficient has a strong influence on the model prediction; the lower the effective diffusivity, the higher the value of the maximum particle internal pressure. The model prediction was shown to be very sensitive to the heat transfer coefficient, effective diffusivity, particle size and external pressure, but relatively less sensitive to the external mass transfer coefficient and particle thermal conductivity. The model results suggest that gibbsite particles undergoing calcination are spatially uniform in terms of temperature, and are insensitive to the external mass transfer environment.

In Chapter 4, an alternative approach was taken to modelling calcination and similar solid-to-gas thermal decomposition reactions at the particle scale. This was motivated partly by the desire to have a model that was solved more quickly than the distributed model of Chapter 3. The model was based on the unreacted shrinking core approach. A new variation of the shrinking core model was developed for solid decomposition reactions in which the product gas species reduces the reaction rate. Shrinking core models reported in the literature previously cannot be directly applied to such cases as they include gas-phase reactants in their stoichiometry and reaction rate equations. The new model predicts particle conversion and temperature as functions of time. For the isothermal case, the numerical solution of the unreacted shrinking core model has been validated against a newly-developed analytical solution. For non-isothermal conditions, the shrinking core model results closely match those from the distributed model created in Chapter 3. The non-isothermal unreacted shrinking core model is simpler and easier to solve than the partial differential-algebraic distributed model. Computational efficiency is relevant in multi-scale modelling since the small-scale model may be run very many times during a multi-scale simulation.

As before, the new shrinking core model was applied to gibbsite calcination, both to verify the model and to investigate its behaviour through a sensitivity study. Using literature experimental data, the gibbsite dehydration rate parameters were estimated over a wide temperature range, from 490 to 923 K. The order of the reaction rate with respect to water vapour concentration was found to be $n = -1$. The inhibiting effect of the water vapour concentration (negative n) leads to good agreement with experimental data, and yields an activation energy that is consistent with literature values. Estimated values of the activation energy and Arrhenius pre-exponential coefficients are reported separately for low and high temperature ranges.

Chapter 5 extended the shrinking core model developed in Chapter 4 by allowing for the formation of another solid species. Thus, a multi-stage, multi-reaction, non-isothermal shrinking core model was created for gas-solid decomposition reactions in which the produced gas inhibits the reaction and in which a solid intermediate product forms. The model has three stages and accounts for transitions in the reaction pathways. It consists of a set of ordinary differential and algebraic equations that were solved numerically. The model results display good agreement with experimental data for the calcination of gibbsite to alumina with boehmite as an intermediate product. This extended model shows a significant improvement compared to the single-stage, single-reaction model of Chapter 4. The predicted temperature history is consistent with trends observed in experimental studies. Different plateaux in the temperature history can be attributed to different reaction pathways and the model may help in detecting the occurrence of various pathways in particle temperature data. The effect of particle size and heating rate on the formation of the intermediate product was investigated and the results are in agreement with practical observations.

In Chapter 6, a simplified reactor scale model was presented and combined with one of the particle scale models to illustrate multi-scale modelling for a fluidized bed reactor. The reactor scale model consisted of material and energy balances over a series of connected well mixed volumes and allowed for a distribution of solid residence times, but did not explicitly account for the reactor hydrodynamics. In spite of the simple structure of the proposed multi-scale model, the main features of a gibbsite calciner are reasonably captured. Gas and solid temperature profiles, trends in the total gas flow rate and water vapour pressure inside the bed, alumina and gibbsite concentration profiles, and effects of the solid throughput rate on the reactor performance are predicted and explained based on the proposed model. One of the main challenges in formulating the multi-scale model was ensuring the correct transfer of information between the particle scale and reactor scale models.

The spatially distributed particle scale model developed in Chapter 3 was used in this multi-scale model. This was due to potential of the distributed model to handle more species in future studies, which is important for gaining the greatest benefit from a multi-scale approach. However, the simple shrinking core model and multi-stage, multi-reaction shrinking core model, which were developed in Chapters 4 and 5 respectively, could also be used in multi-scale modelling by following a similar approach.

This study has revealed a range of future research issues that may be of interest to scientist and engineers:

- The conceptual multi-scale modelling framework that was described in the second chapter could be enhanced to become a more comprehensive modelling roadmap. Among the possible enhancements is linking the Design of Experiments (DOE) to the framework. Currently, performing DOE based on a multi-scale model and DOE for multi-scale model validation are both in their infancy, and there is wide scope for potential research to be done in this area. In addition, consideration of product quality parameters within the conceptual framework will help make future modelling endeavours more goal-oriented.

- Modelling at the particle scale was performed via different modelling approaches in the thesis. However, there are other modelling possibilities at this scale. For instance, the “grain model” has not been tested for gibbsite calcination.

- With regards to the distributed particle scale model, the inclusion of more species should be considered in future work. For gibbsite calcination, these species are different phases of alumina. Further, more detailed investigation of the profiles inside a particle may help explain more of the issues experienced in industry. For instance, the profile of water vapour pressure inside the particle may be able to explain particle fracture and the porosity distribution during the calcination process.

- Modelling at the particle scale would be enhanced by considering product quality-related parameters. For instance, the development particle scale models for the prediction of porosity and specific surface area, as well as mechanical properties of the product, would be valuable additions. These kinds of model can enrich a multi-scale modelling effort by aligning the modelling goal towards "product design". To address this goal properly, however, good collaboration between experimental and modelling researchers is needed. There are many gaps in the experimental literature on particle scale gibbsite calcination, particularly in terms of the spatial distribution of solid phases inside a particle as a function of reaction progress. These experimental studies could be directed using enhanced models that have a special focus on predicting product quality.

- The reactor scale offers considerable and interesting research potential for future work. Some of the improvement of predictions at the reactor scale would depend on modelling enhancements at the particle scale. However, considerable progress could be made at the reactor scale for calcination by taking inspiration from fluidized bed reactor modelling performed in other industries. Improved hydrodynamic predictions for calciners, and linking reaction with hydrodynamics, can open new doors for the exploration of calciner behaviour. For this purpose, use of a traditional process simulator like Aspen Plus is an interesting possibility, as solid process multi-scale modelling has apparently not been dealt with in this kind of simulator before. A separate calcination process model linked to the simulator as a user defined module is a potential project for the future.
- Development of a model library at different scales, according to the conceptual framework of Chapter 2, is a possibility that would give scientists and engineers flexibility and assistance in future multi-scale modelling efforts. Some elements of this library have been created in this thesis.

In addition to the issues mentioned above, Chapter 2 includes some further research possibilities for gibbsite calcination and the multi-scale modelling of calciners.